AUA 2026 Washington, DC

Advancing Precision Therapy: A 3D Metastasis-on-Chip Platform for Therapeutic Target Discovery in Prostate Cancer

M. Haack[1,2], J. Stein[2], A. Neuhäusler[2], SD. Markowitsch[1], J. Dietz[2], U. Ritz[3], A. Haferkamp[1], A. Blaeser[2]

[1]Johannes Gutenberg University Medical Center, Department of Urology and Paediatric Urology, Mainz, Germany
[2]Technical University of Darmstadt, Institute for BioMedical Printing Technology, Darmstadt, Germany
[3]Johannes Gutenberg University Medical Center, Department of Orthopaedics and Traumatology, Mainz, Germany

INTRODUCTION

Bone is the predominant site of metastasis in advanced prostate cancer (PCa), frequently leading to complications such as fractures and severe pain. The CXCR4/CXCL12 axis plays a critical role in PCa cell homing to bone. However, the underlining mechanisms of early bone metastasis are still unclear. Conventional 2D cultures and animal models are limited in their ability to replicate human bone microenvironment and observe early colonization by disseminated tumor cells. Therefore, physiologically relevant in vitro systems are essential for investigating tumor-bone interactions and evaluating therapeutic targets.

RESULTS

PCa cells successfully invaded and colonized the 3D-bone-scaffold forming micro-metastasis of approximately 500µm in diameter after 3d (D-F).

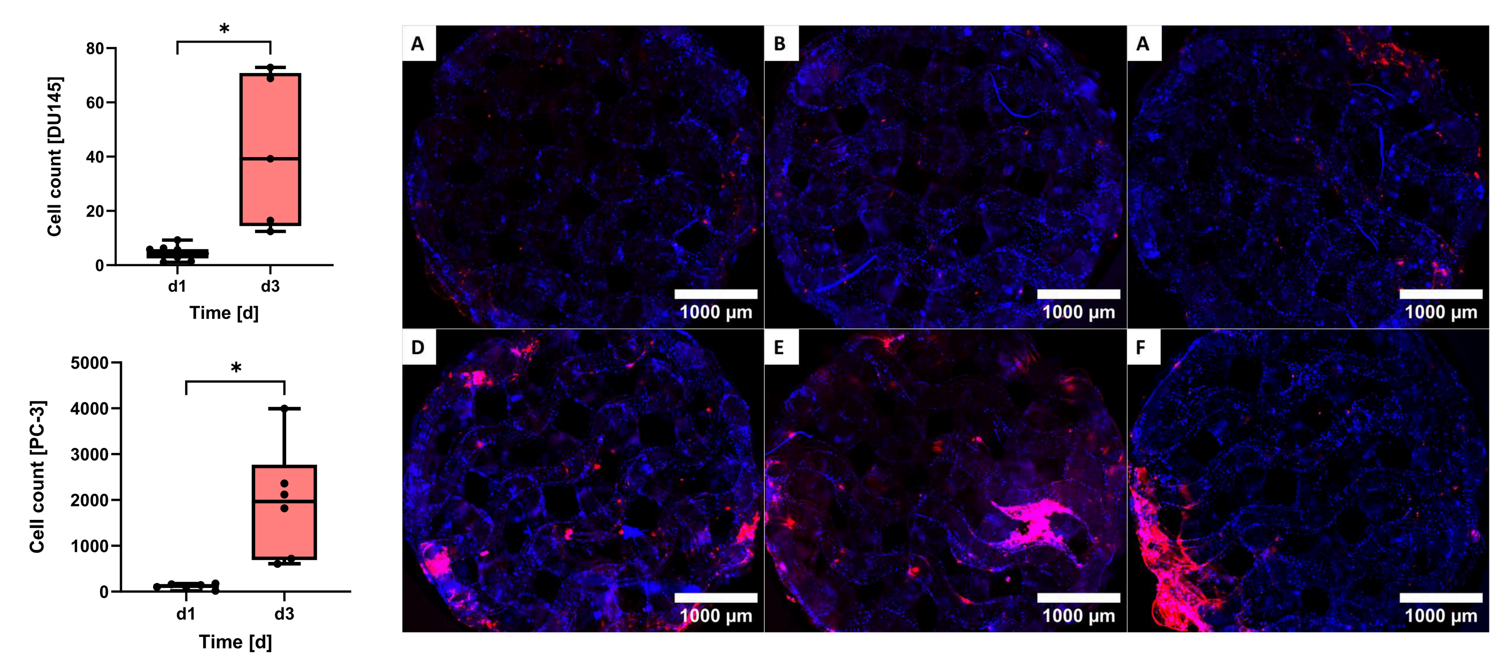

Antagonization of CXCR4 with Plerixafor (AMD3100) successfully reduced PCa cell invasion into the 3D-bone-scaffold after 24h under dynamic culture conditions.

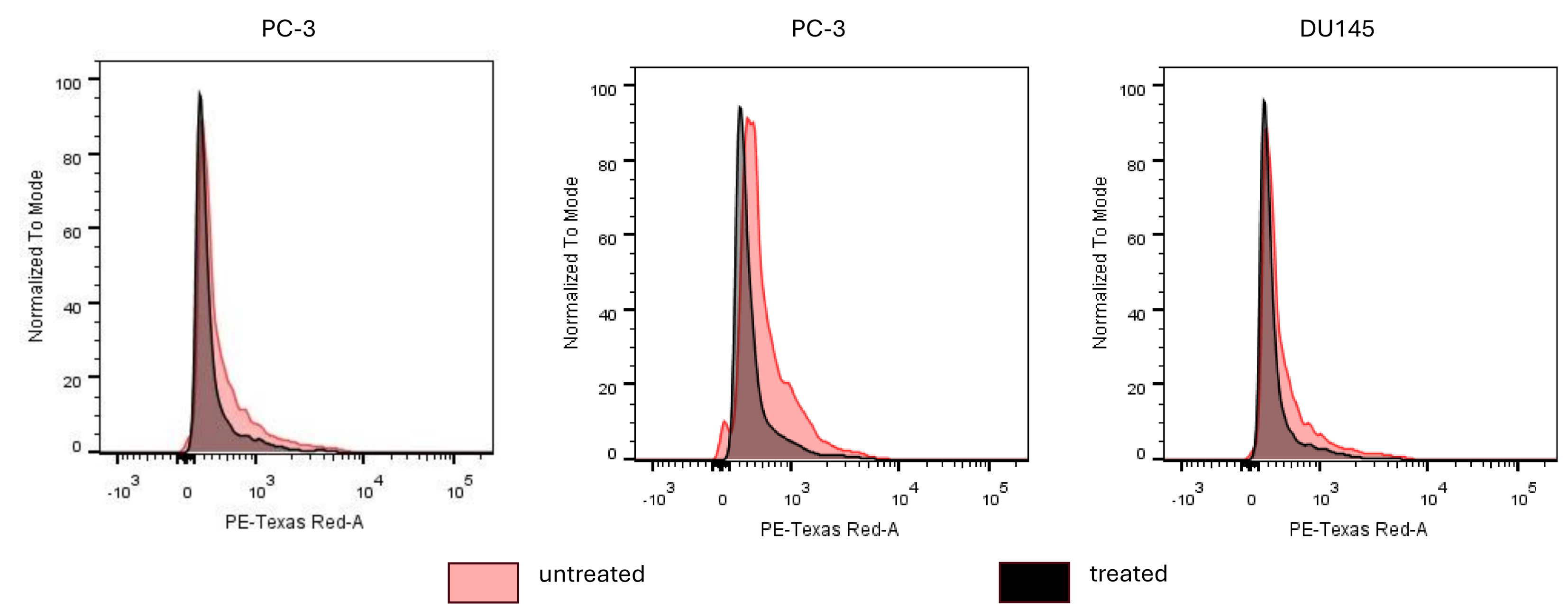

METHODS

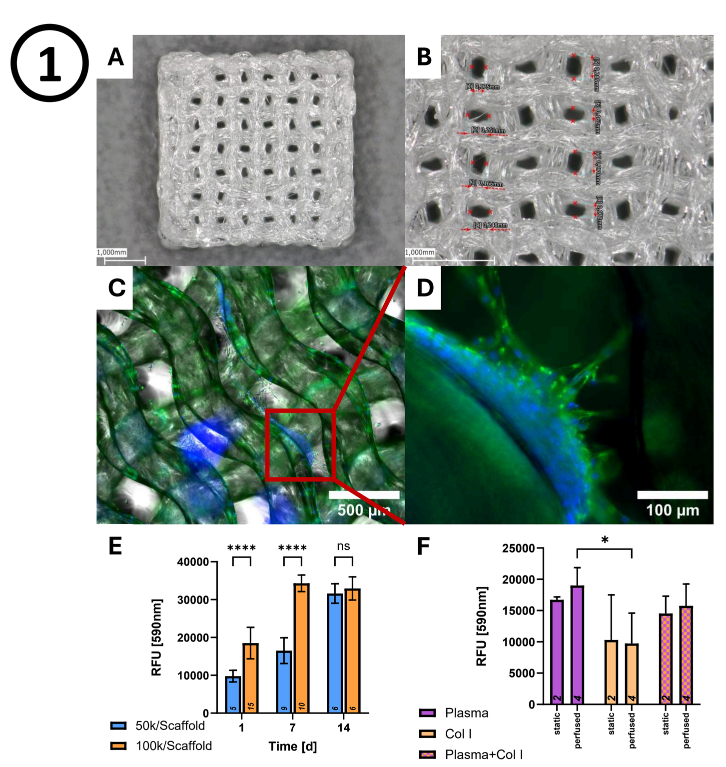

Osteoblasts adhered and proliferated sufficiently on FFF-printed PLA-scaffolds (A-D). Maximum confluency was reached after 14d, regardless of initial seeding concentration (E). O_2 plasma treatment increased adhesion under dynamic conditions compared to collagen-I or both (F).

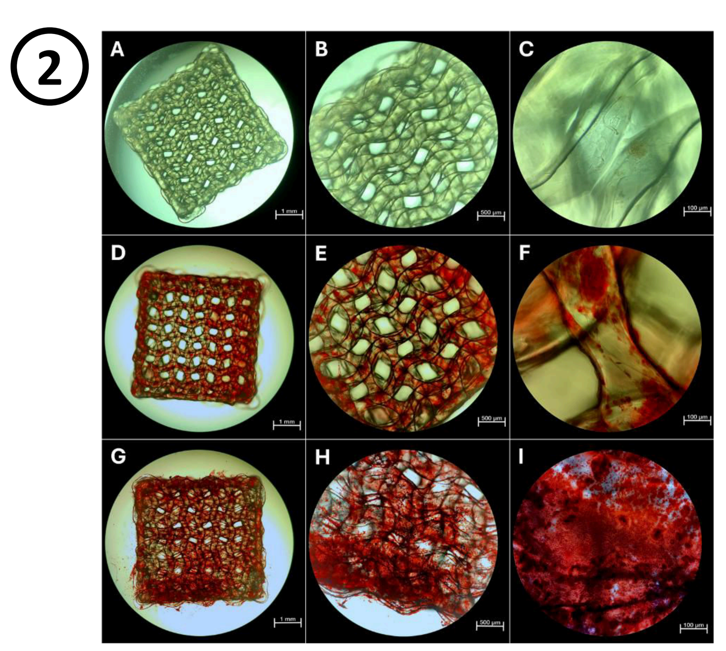

Sufficient matrix mineralization was achieved with common osteogenic media supplements over a period of three weeks (D-F). Without supplements PLA-scaffolds did not induce matrix mineralization (A-C). Bone formation was more pronounced in higher passages (G-I).

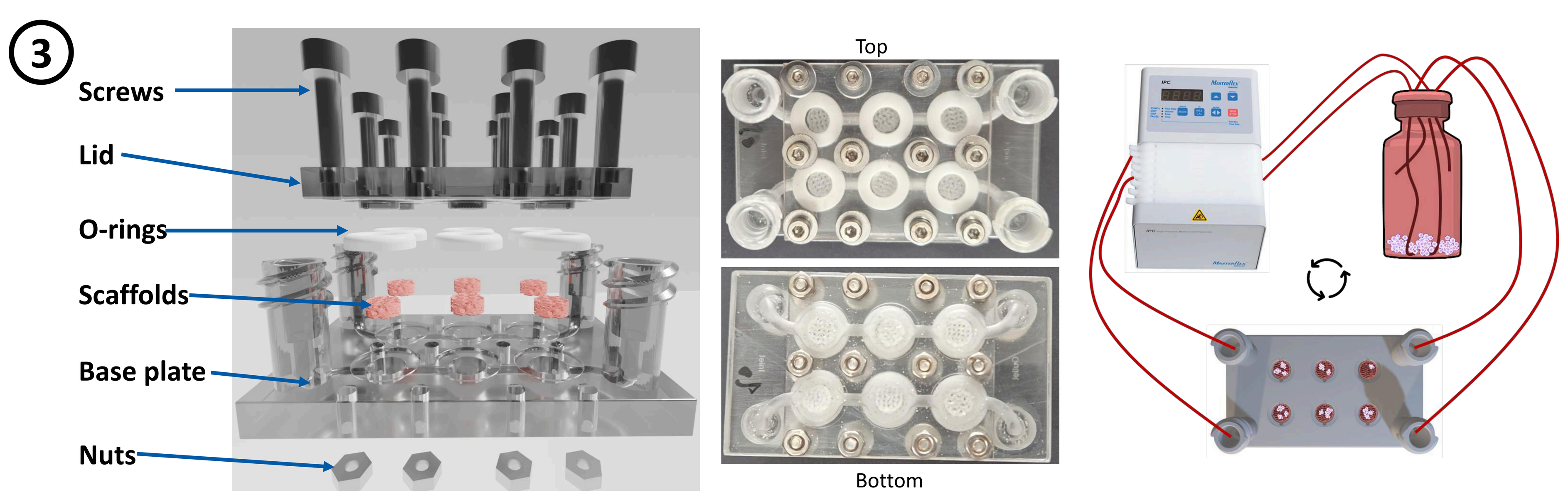

DLP-printed microfluidic devices consisted of a base plate containing two perfusion lines, each with three culture chambers, and two Luer-lock connectors (inlet/outlet). A screw-on lid with silicone O-rings ensured a watertight seal. A peristaltic perfusion pump provided continuous media flow and circulation of PCa cells.

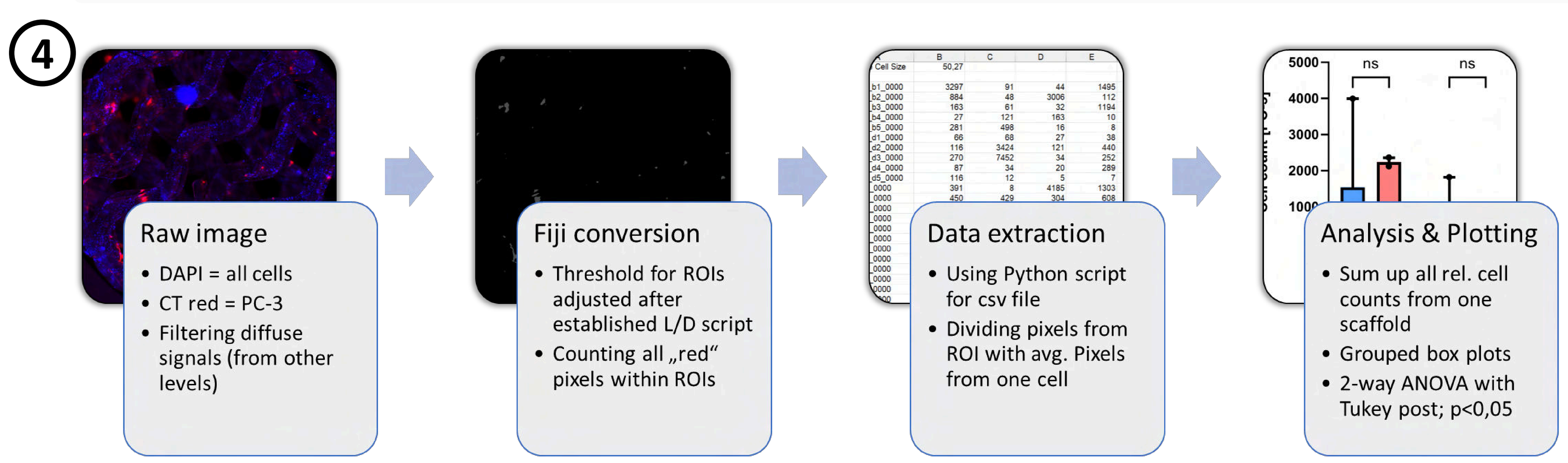

Quantification of fluorescently labeled tumor cells using an automated Fiji script.

CONCLUSIONS

- This microfluidic bone-metastasis-on-chip platform replicates early PCa-colonization, enabling direct visualization of invasion, clustering, and micro-metastasis formation.
- CXCR4 blockade successfully suppresses metastatic seeding, reducing invasion by 30% and thereby underscoring the CXCR4/CXCL12 axis as a critical driver of early PCa-metastasis.
- This Platform provides a scalable preclinical testbed for dissecting metastatic mechanisms and evaluating targeted anti-metastatic therapies.

DISCLOSURES

The project was funded by Ferdinand Eisenberger Research Grant by the German Society of Urology (HaM1/FE-24) and Monika Kutzner Foundation.

DGU Deutsche Gesellschaft für Urologie e.V.

MONIKA KUTZNER STIFTUNG

Reduction of serum PAI-1 and improvement in endothelial function by a nitric oxide generating nutraceutical: an open-label clinical trial

David Geffen School of Medicine

UCLA Health

Sriram V. Eleswarapu, MD, PhD

Division of Andrology, Department of Urology, David Geffen School of Medicine, University of California, Los Angeles

Nitric oxide (NO)

Simple gas signaling molecule

Produced by nitric oxide synthases (NOS)

Lipid soluble → membrane permeable

Degraded within seconds in tissues

Regulates vascular tone, platelet inhibition, neurotransmission through the NOS-NO-soluble guanylyl cyclase (sGC)-cGMP pathway

Concept applied in urology to treat erectile dysfunction through PDE-5i

This NO-to-cGMP biology underlies endothelial health and longevity

Endothelial NO production declines by 50% by age 45

Can we overcome deficient endothelial NO production?

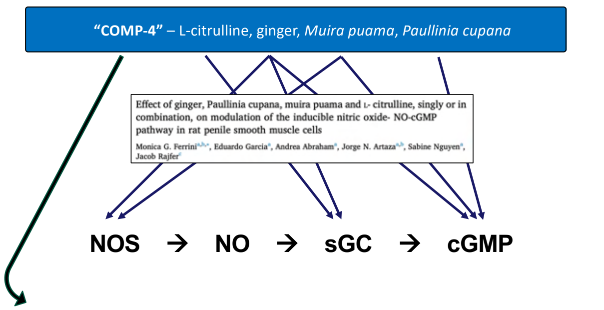

COMP-4 protects endothelial cells through NO pathway

(Adapted from our group's prior work: Ferrini et al., *PLoS ONE* 2025)

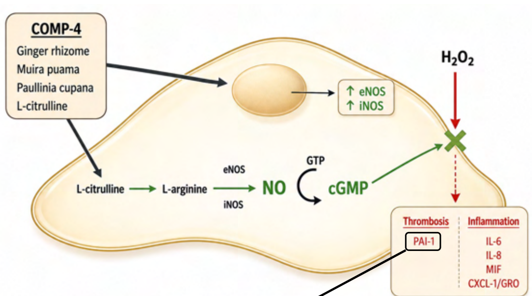

PAI-1 (aka SERPINE1) may be a target for intervention

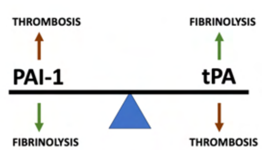

Study Design

Objective:	Evaluate COMP-4 effects on endothelial function and PAI-1 in healthy young adults
Design:	Single-arm, open-label clinical trial
Enrollment:	Men and women 18-40 years old
Intervention:	Two weeks of oral COMP-4 (two pills twice a day)
Assessment:	Pre-treatment and post-treatment arterial flow-mediated dilation and PAI-1

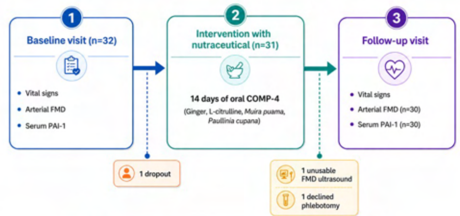

Arterial flow-mediated dilation (FMD)

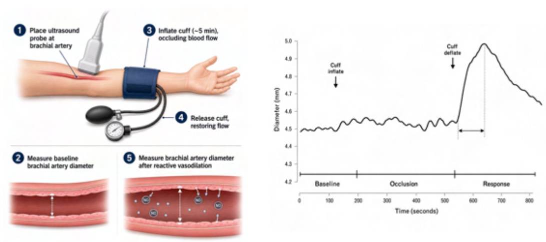

Arterial FMD increased 37% (p=0.0025)

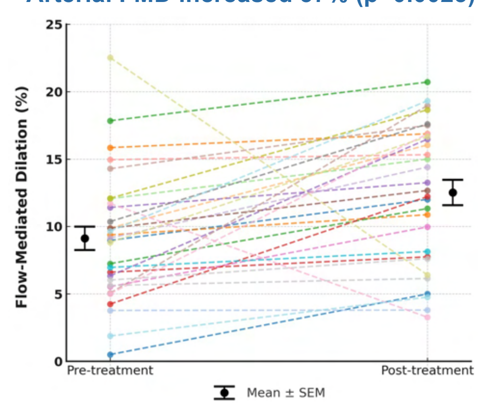

Serum PAI-1 decreased 36% (p<0.001)

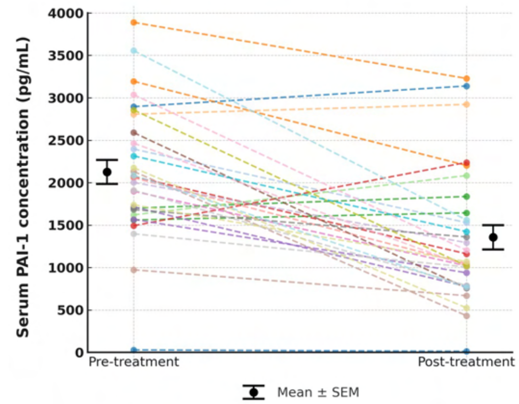

Clinical significance and next steps

COMP-4 improves FMD in healthy young subjects

We know that for every 1% increase in FMD → 8-13% reduction in cardiovascular events

COMP-4 reduces PAI-1 in healthy young subjects

PAI-1 is a key marker of cardiovascular risk and vascular aging

No current pharmaceutical options to target PAI-1 safely (toxicity among candidate drugs)

Follow-up trial is now under way with expanded population

Participants of all ages (instead of young subjects)

Six-week treatment duration (instead of two weeks)

Interface of urology, vascular biology, and longevity

NO foundation → translational target

We are performing mechanistically informed clinical trials

In vitro, COMP-4 activates NO-to-cGMP pathway, reduces PAI-1, mediates inflammation

In vivo, COMP-4 increases FMD and reduces PAI-1 after 14 days

There is a broad clinical horizon for intervening on the NO-to-cGMP pathway

Motivates investigations to optimize NO bioavailability and PDE-5i responsiveness

Explore targets for senotherapeutic development

Collaborators & Team

UCLA Andrology: Jacob Rajfer, MD; Istvan Kovanecz, PhD; Thiago Furtado, MD; Reza Kianian, MD; Ha-Jung Kim

UCLA Urology Clinical Trials: Nazy Zomorodian, RN, MSN, CUNP; Randy Caliliw

UCLA Radiology: Kate Franey; Steven Raman, MD

UCLA School of Nursing: Ossanna Amran; Mary Rezk-Hanna, MSN, PhD

Charles Drew University School of Medicine: Monica Ferrini, PhD

AUA 2026
Washington, DC

Feasibility and acceptability of a prospective remote pilot study for assessment of environmental exposures and male fertility

Tristan M. Nicholson,[1,2] Ingrid Robertson,[3] Liddy Boland,[4] Damon W. Chan,[3] Maximilian S. Jentzsch,[1] Christine Loftus,[2] Thomas J. Walsh,[1] Charles H. Muller,[1] Catherine J. Karr,[2,5] James Smith,[6,7] Krystal Pollitt,[4] John K. Amory,[8] Ashleigh B. Theberge[1,3]

Departments of [1]Urology, [2]Environmental & Occupational Health Sciences, [3]Chemistry, [5]Pediatrics and [8]Medicine, University of Washington, Seattle, WA, [4]Yale School of Public Health, New Haven, CT, [6]Department of Urology, University of California, San Francisco, CA, [7]Fellow Health, Inc., San Leandro, CA.

INTRODUCTION

There is emerging evidence that links wildfire smoke exposure to declines in sperm parameters in retrospective analyses. To better understand the impact of airborne environmental exposures on male fertility, we designed the homeSPERM pilot study, a prospective cohort study including biospecimen collection (blood and semen), measurement of airborne environmental exposures, and questionnaires. Our objectives were to:

1. Demonstrate feasibility and acceptability of serial biospecimen collection and exposure assessment among reproductive aged men.
2. Compare the research participant experience with in-person versus remote biospecimen collection.
3. Characterize participant-level airborne exposures pertinent for male fertility.

METHODS

Study Overview

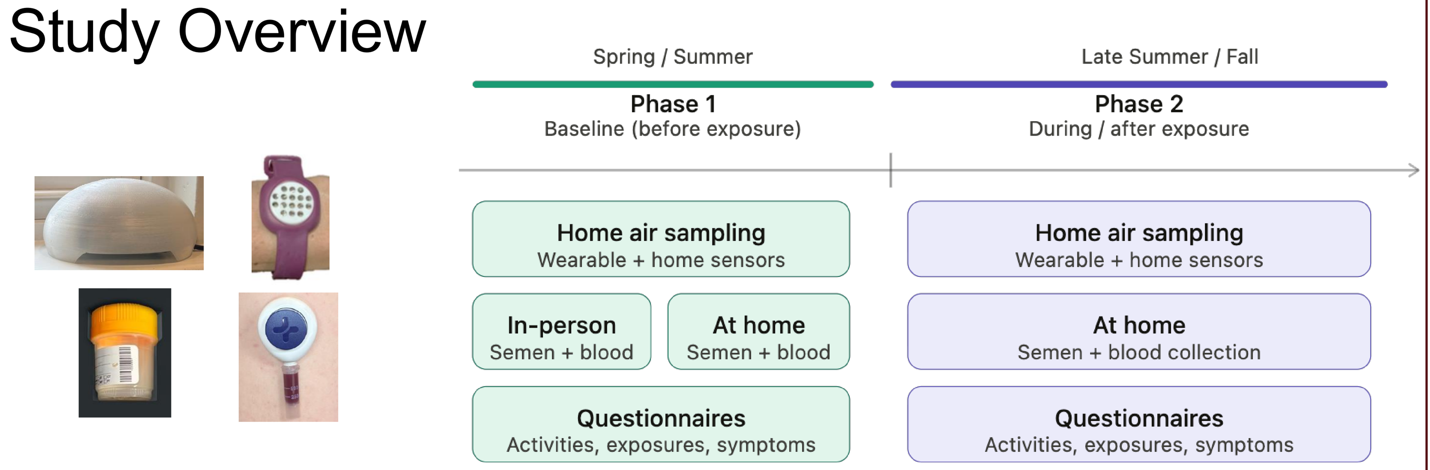

RESULTS

Recruitment & Enrollment

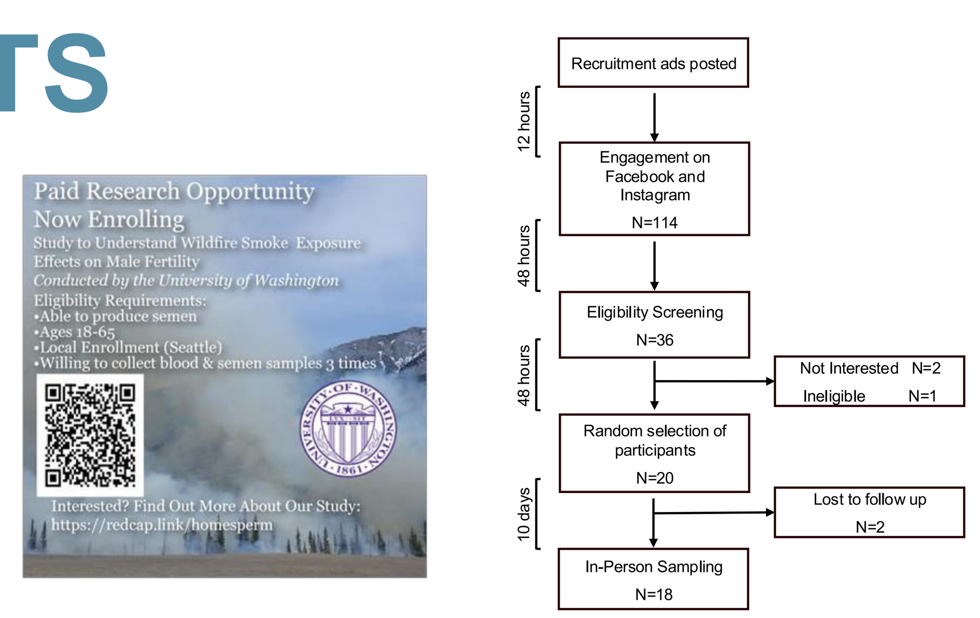

Figure 1. Example digital recruitment ad and timeline of recruitment and enrollment activities.

RESULTS

Study Cohort

Characteristic	Full cohort (n = 18)	FreshAir Wristband subsample (n = 9)
Demographics		
Age (years), mean ± SD	32.6 ± 7.5	31.3 ± 7.2
White, non-hispanic, n (%)	7 (39%)	5 (55%)
Asian, non-hispanic, n (%)	8 (44%)	3 (33%)
Other/multiracial	3(17%)	1 (11%)
Substance use		
Current smoker (cigarettes, joints, blunts), n (%)	4 (22%)	2 (22%)
Current THC use, n (%)	7 (39%)	3 (33%)
Secondhand smoke exposure, n (%)	6 (33%)	4 (44%)
Exposure behaviors		
Uses a gas stove indoors, n (%)	7 (39%)	3 (33%)
Used a propane or charcoal barbeque, n (%)	4 (22%)	1 (11%)
Attended a bonfire, n (%)	7 (39%)	2 (22%)
When the Purple Air sensor changes color I… (n=17)		
Close windows/doors only, n (%)	7 (41%)	2 (29%)
Turn on an air purifier, wear an N95 mask, and avoid using the gas stove, n (%)	1 (6%)	0 (0%)
Wear a surgical or cloth mask	0 (0%)	0 (0%)
Avoid exercising	0 (0%)	0 (0%)
Other	1 (6%)	1 (14%)
Make no changes	9 (53%)	4 (57%)

Abbreviations: SD, standard deviation; THC, delta-9-tetrahydrocannabinol.

Acceptability of Semen Collection

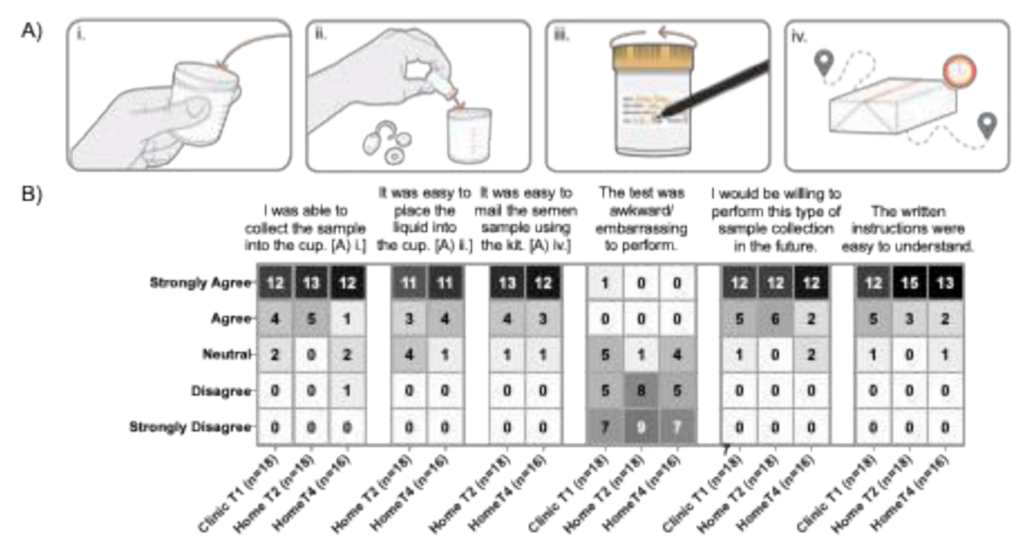

Acceptability of Blood Collection

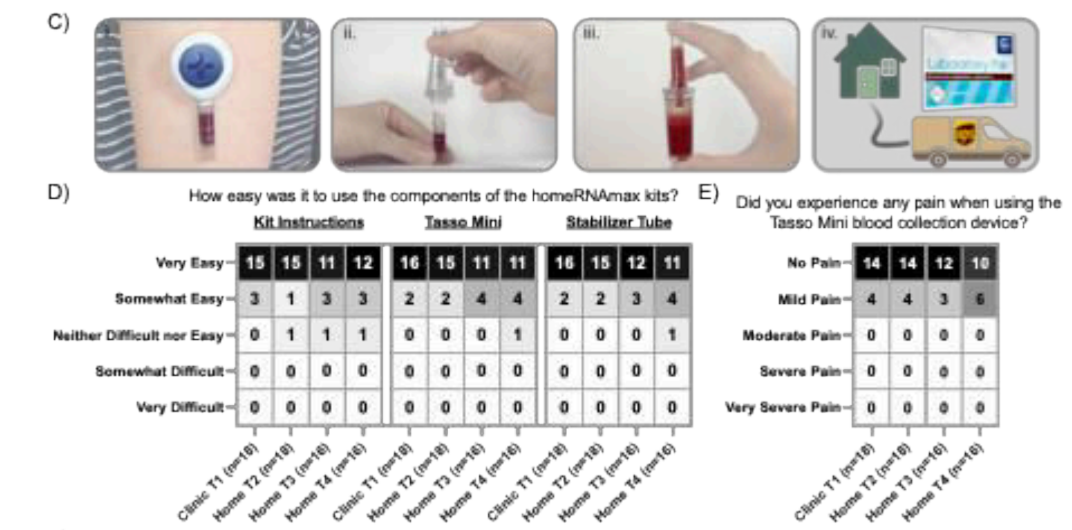

Figure 2. Participant experiences with study biosampling activities. A. Participant instructions for use of Fellow semen collection kit. B. Participant ratings of semen sampling experience. C. Participant instructions for use of Tasso Mini blood collection device with homeRNAmax kits. D. Participant ratings of blood sampling experience.

Semen Parameters

Semen Parameter	Semen Analysis #1 Mean (SD)	Semen Analysis #2 Mean (SD)	WHO 2021 (6th) Ed Lower 5th Percentile Mean (95% CI)
Volume (mL)	3.2 (2.0)	3.3 (1.9)	1.4 (1.3-1.5)
Count (10^6 cells)	167.4 (129.0)	216.3 (214.0)	39 (35-40)
Concentration (10^6 cells per mL)	60 (48)	62 (45)	73.0*
Morphology (% normal)	6 (2)	8 (3)	4 (3.9-4)
Progressive Motility (%)	37 (15)	47 (18)	30 (29-31)
Total Motile Count (10^6 cells)	72.3 (96.9)	74.9 (103.0)	Not Included

Abbreviations: SD, standard deviation; CI, confidence interval; WHO, World Health Organization.

End of Study: 15/16 participants indicated that remote sampling (Semen and Blood) would be significantly easier compared to in clinic collection

Participant Fine Particulate Matter ($PM_{2.5}$)

Purple Air Sensor (Indoor)

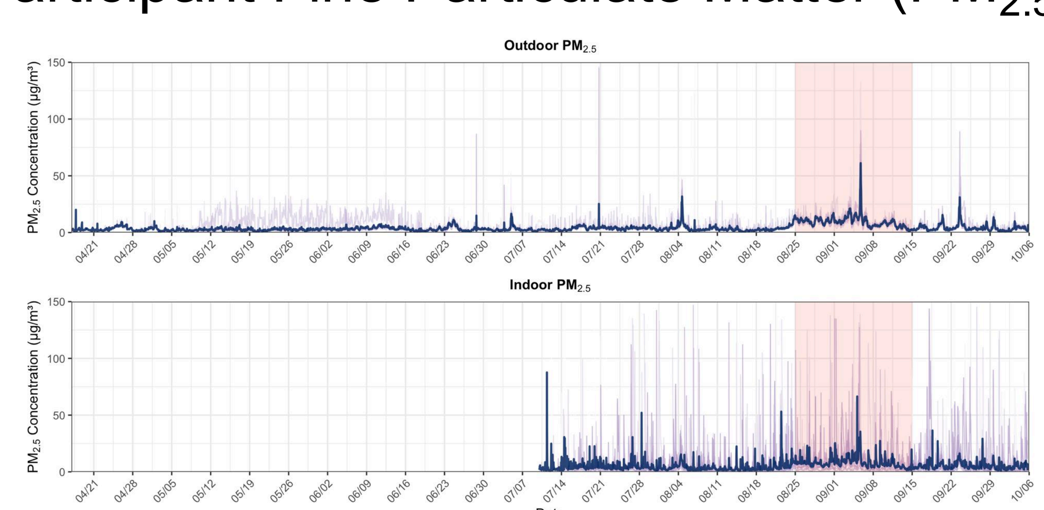

Figure 3. Indoor and outdoor $PM_{2.5}$ mass concentrations for all participants across the study period (April–October 2025). The blue line represents the average $PM_{2.5}$ concentration across all participants. Red shading indicates the Bear Gulch wildfire smoke event (August 25 – September 15, 2025).

Compounds Detected with Wearable Passive Sensors

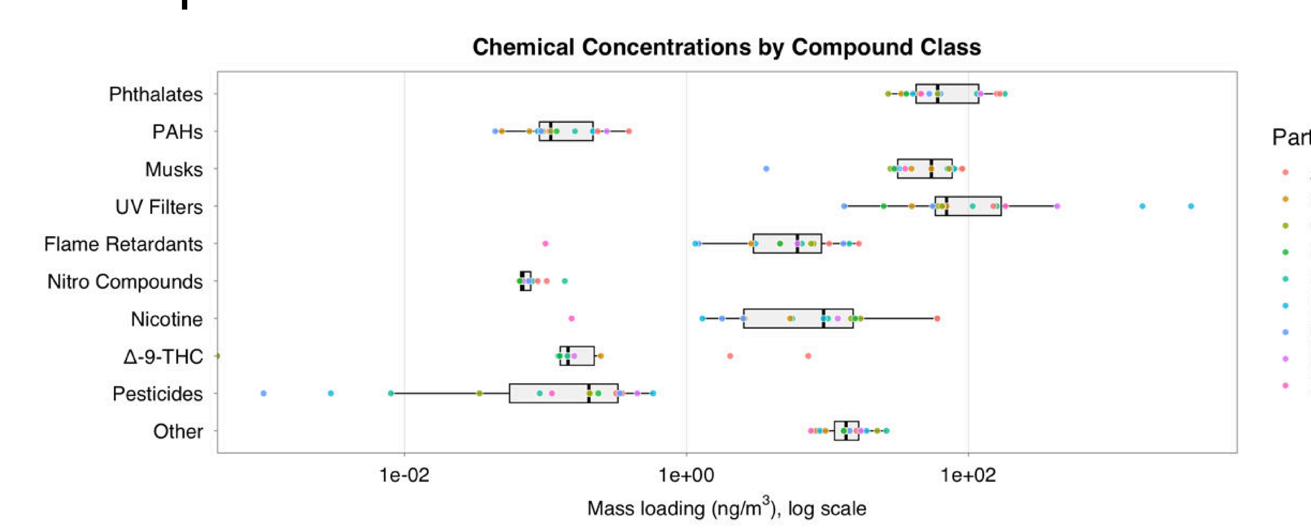

FreshAir Wristband

Figure 4. Mass loading in ng/m³ on participant FreshAir wristbands grouped by compound classification. Abbreviations: PAHs, Polycyclic Aromatic Hydrocarbons, THC, delta-9-tetrahydrocannabinol

CONCLUSIONS

1. We demonstrate feasible enrollment and study activity completion for community dwelling reproductive aged men in our prospective pilot study.

2. Remote and in person research activities are acceptable to participants, but participants preferred remote/at home biosampling.

3. Remote airborne exposure sampling with outdoor, indoor and wearable passive sensors captures a breadth of participant-level exposures pertinent to male fertility.

4. Future work will expand to diverse geographic contexts and larger, more representative samples.

ACKNOWLEDGEMENTS

Pediatric and Reproductive Environmental Health K12 Scholar Program (K12ES033584)

DISCLOSURES

Tasso, Inc (Immediate Family Member)
Company Officer
Direct Stockholder
Fellow, Inc (Research Collaboration)
Purchase kits for research

AUA 2026
Washington, DC

Redefining Sperm Search and Morphology with Artificial Intelligence driven Imaging Cytometry

Blair Stocks, MD, PhD, Aidan Boyne, BS, Katelynn Salmon, BS, Amelia Oppenheimer, BA, Taylor Kohn, MD, M Phil, Mohit Khera, MD, MBA, MPH, and Larry Lipshultz, MD

Baylor College of Medicine
SCOTT DEPARTMENT OF UROLOGY
MALE REPRODUCTIVE MEDICINE & SURGERY

INTRODUCTION

- Azoospermia leads to invasive surgical retrieval with limited success (30–50%), while isolated teratozoospermia has poor reproducibility and unclear prognostic value.
- Current methods of semen analyses lack sensitive, objective, and scalable tools.
- There exists a need to develop a means to identify sperm in azoospermic patients and better define morphology in an unbiased, timely, comprehensive, and accurate manner.

HYPOTHESIS

- High-throughput imaging cytometry paired with Artificial Intelligence (AI) driven image analysis represents an unpresented approach to redefine rare sperm search and morphologic assessment for the infertile male.

METHODS & PLATFORMS

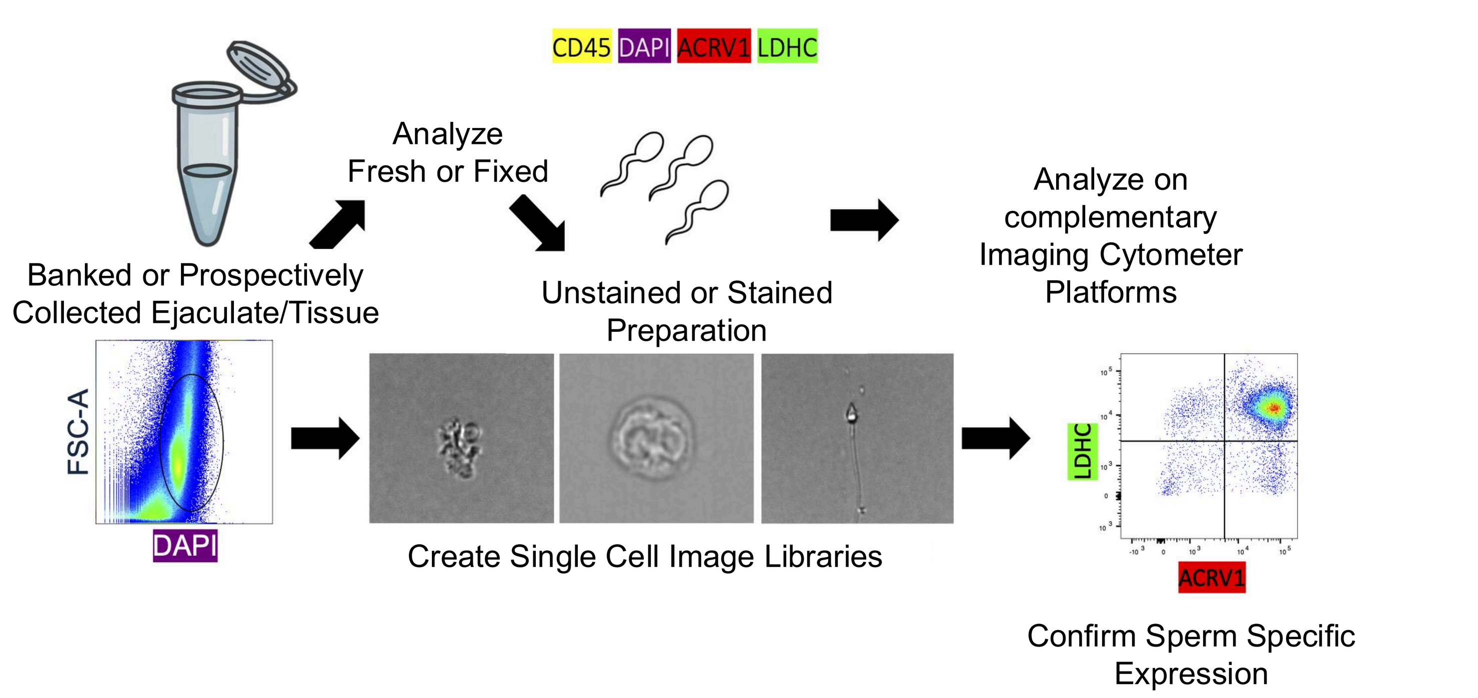

Experimental Workflow. Ejaculate and testicular tissue samples are identified as remnant samples from our biobank (IRB H-47408) or prospectively collected after informed consent (IRB H-57193). Samples are analyzed either fresh or after fixation/permeabilization. Samples are then left unstained or stained with fluorescently tagged antibodies targeted to sperm specific proteins. Samples are then analyzed on one of the three imaging cytometers (below) and data stored. Images are then analyzed using proprietary software or self-programmed platforms.

ImageStream

Attune Cytpix

A8/S8 Spectral

RESULTS AND ONGOING WORK

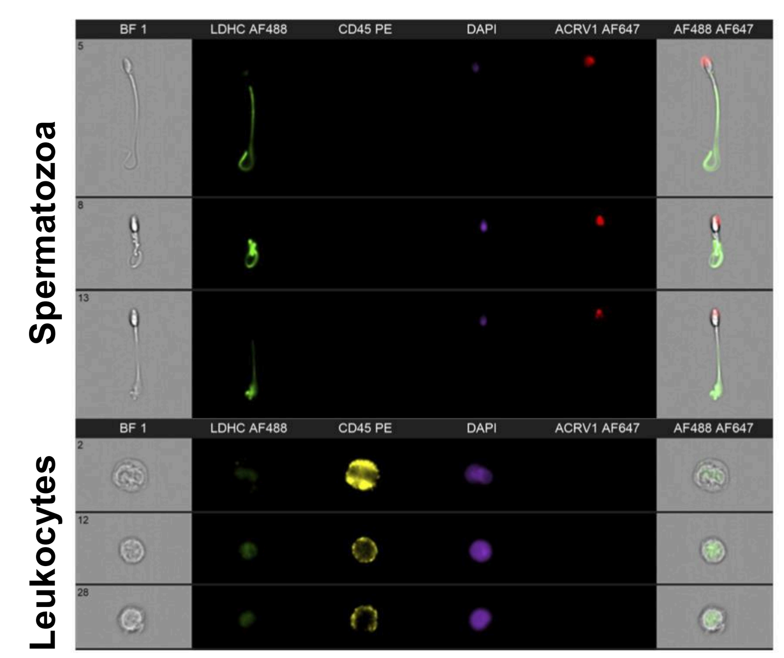

Figure 1. Curation of "Ground Truth" image libraries of spermatozoa with sperm specific markers using the ImageStream platform. While low-throughput (5 events/second), this platform generates brightfield/fluorescent overlays at 60x resolution (0.3um/pixel) with 12 fluorescent channels. Here, spermatozoa express Lactate Dehydrogenase C (LDHC) along their tails and Acrosomal Vesicle Protein 1 (ACRV1) on their heads. Contaminating leukocytes lack expression of sperm specific markers and express CD45. Current efforts are underway incorporating additional sperm specific markers including DPEP3, IZUMO1, and others. Libraries will be curated from normospermic fertile controls as well as infertile males of various etiologies (idiopathic, oligoasthenoterato (OATS), crypto, etc.).

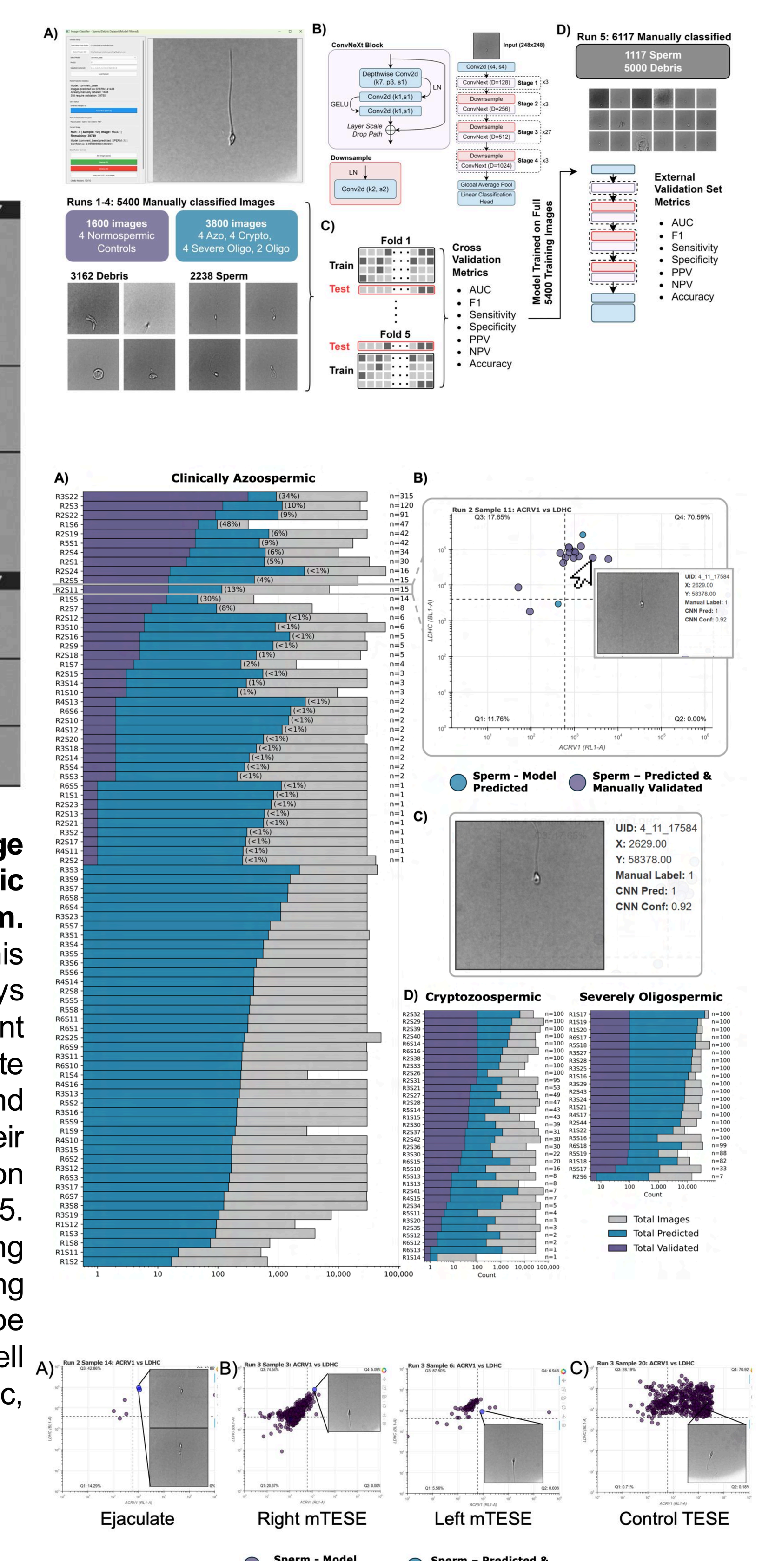

Figure 2. AI-based sperm detection model development, validation, and detection of ultra-rare sperm in clinically azoospermic samples using the Attune Cytpix.

Top Panel. A) Manual annotation interface used to classify images as sperm or debris, generating labeled datasets for training from initial acquisition runs. B) ConvNeXt architecture for binary classification, incorporating patch-based image embedding followed by hierarchical feature extraction and a fully connected output layer. C) Five-fold cross-validation framework with balanced training sets and non-overlapping validation subsets to ensure robust model performance. D) Independent test set validation using images from a separate acquisition run not included in training.

Middle Panel. A) Model application to clinically azoospermic samples demonstrating total images acquired, model-predicted sperm, and manually verified sperm counts. B) Representative co-expression of sperm-specific markers ACRV1 and LDHC confirming biological validity of detected cells. C) Graphical user interface enabling visualization and interrogation of individual cell images alongside marker expression. D) Model performance in cryptozoospermic and severely oligospermic samples, with comparison of total images, model predictions, and manual verification.

Bottom Panel. CNN-based sperm detection identifies rare, manually validated sperm in an azoospermic ejaculate (A) and corresponding negative mTESE samples (B), with comparison to a control TESE specimen from a post-vas individual (C).

These data were recently published (*Stocks, et al. Fert Stert, In Press, 2026*).

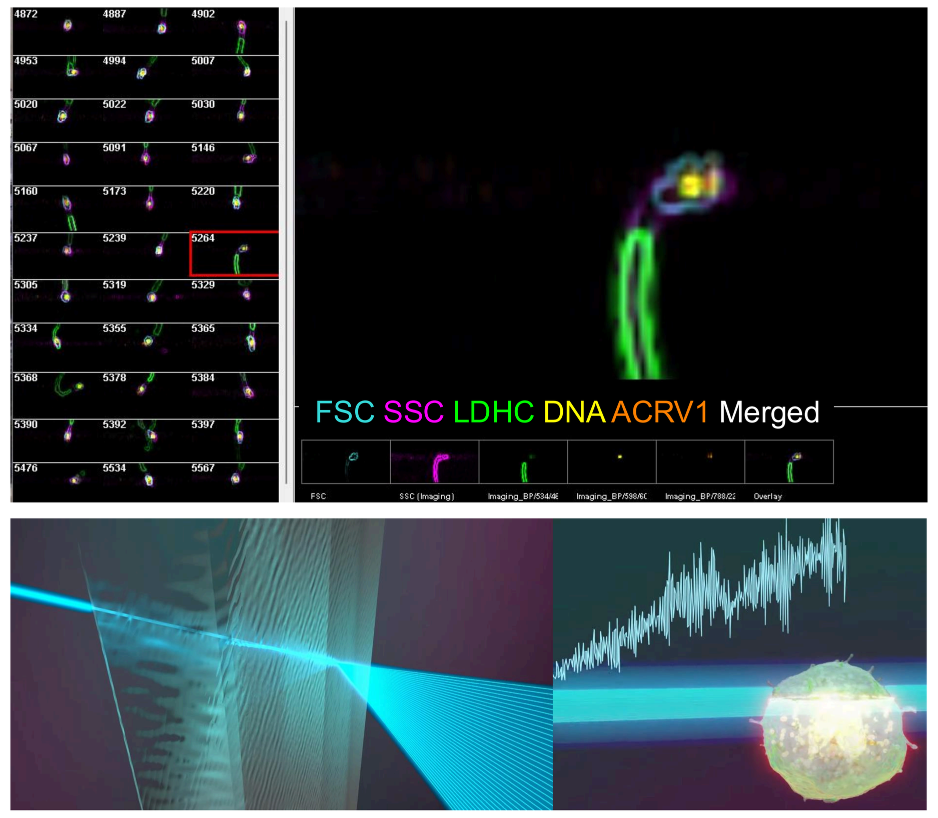

Figure 3. A8/S8 Spectral Cytometry for real-time, nondestructive analysis and sorting of spermatozoa. Reconstructed image of spermatozoa using CellView™ Image Technology on A8 Spectral Cytometer (top). CellView™ reconstructs images of cellular events in real time in a non-destructive means using forward scatter (FSC), side scatter (SSC), and light loss parameters collected off the blue (488nm) laser line which is split by a prism (bottom). Simultaneously, any fluorophore excited by the 488nm laser can be mapped onto this reconstructed image (~1-1.5um/pixel resolution). This platform can not only analyze cells, but sort individual cells at tested rates of 750-1000 cells per second.

https://www.bdbiosciences.com/en-us/learn/applications/cell-view-image-technology?tab=Technology

CONCLUSIONS

- While significant preclinical testing and validation will be required prior to clinical use, advanced imaging flow cytometry and sorting, paired with Artificial Intelligence (AI) driven image analysis, may represent a novel means to 1) identify and collect ultra-rare sperm in ejaculate or mTESE samples of azoospermic patients for use in IVF/ICSI and 2) redefine sperm morphology through whole-ejaculate analysis via supervised and unsupervised image analysis.

ACKNOWLEDGEMENTS

- Internal BCM seed funding was used to support this project. This project was also supported by the Cytometry and Cell Sorting Core at BCM with funding from the CPRIT Core Facility Support Award (CPRIT-RP180672), the NIH (P30 CA125123 and S10 RR024574) and the assistance of Joel M. Sederstrom.

DISCLOSURES

None

CONTACT

blair.stocks@bcm.edu

Artificial Intelligence-Enhanced Augmented Reality for Precision Robotic Prostatectomy

AUA 2026
Washington, DC

Daniele Amparore, Enrico Checcucci, Sabrina De Cillis, Pietro Piazzolla, Cristian Fiori, Francesco Porpiglia

Department of Oncology, University of Turin, Orbassano, Italy
Division of Urology, Department of Surgery, Candiolo Cancer Institute FPO-IRCCS, Candiolo, Italy

INTRODUCTION

- Positive surgical margins (**PSMs**) remain a **major challenge during** nerve-sparing robotic radical prostatectomy (**RARP**)
- Standard surgery relies on cognitive interpretation of MRI
- Artificial intelligence (**AI**) + 3D augmented reality (**3D-AR**) may **improve real-time tumor localization** & surgical precision
- **Aim** → to evaluate whether **AI-enhanced 3D-AR guidance improves onco & functional outcomes** during RARP

METHODS

- Prospective **multicenter RCT** (NCT06318559) including 133 patients with PCa and **MRI evidence of extracapsular extension (ECE) or bulging**
- Patients were randomized 2:1 to:
  - **Standard MRI-guided nerve-sparing RARP** (n=84)
  - **AI-enhanced 3D-AR–guided RARP** (n=49)
- In the 3D-AR group, preoperative mpMRI images converted into patient-specific 3D models
- An **AI-based** convolutional neural network (CNN) enabled **automatic real-time overlay** of the virtual model onto the surgical field using catheter-based anatomical alignment
- **Selective biopsies** at the preserved ipsilateral NVB were performed:
  - **Cognitively** in the MRI group
  - **Under AI-AR guidance** in the 3D group

- **Primary endpoint**: PSM rate
- **Secondary endpoints**:
  - Continence (0/safety pad)
  - Potency recovery (IIEF5>17)
  - Postoperative radiotherapy
  - Biochemical recurrence (BCR)

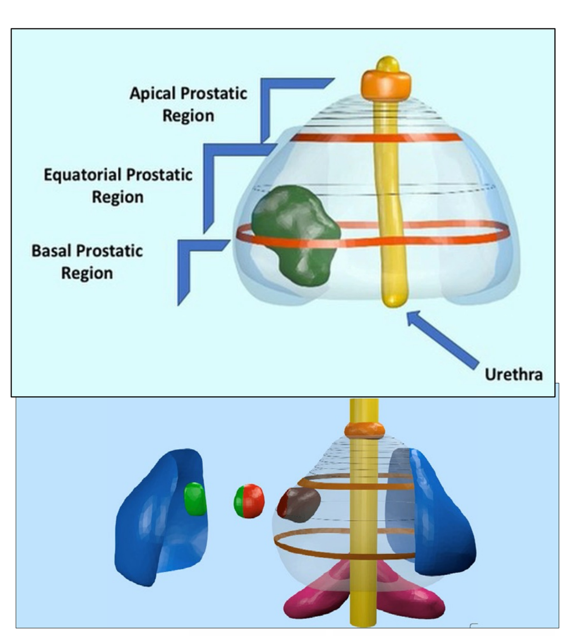

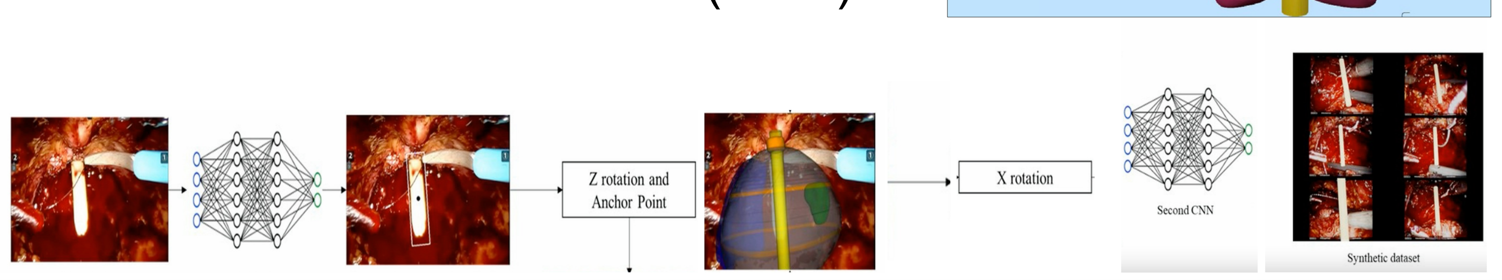

Patient characteristics	3D-AR group (49 pz)	MRI group (84 pz)
Age (yr), median (IQR)	68 (61–72)	69 (64–73)
BMI, median (IQR)	26 (25–29)	26 (24–28)
PSA (ng/ml), median (IQR)	7.8 (6.4–11.4)	7.7 (5.2–10)
Positive DRE, *n* (%)	20/49 (41)	40/84 (48)
IIEF-5 score, median (IQR)	17 (13–21)	17 (12–22)
Prostate volume (ml), median (IQR)[a]	39 (27–54)	40 (30–53)
Lesion volume (mm), median (IQR)	10 (4.9–23)	6.1 (1.2–5)
PIRADS score, *n/N* (%)		
3	2/49 (4.1)	6/84 (7.1)
4	16/49 (33)	32/84 (38)
5	31/49 (63)	46/84 (55)
MRI lesion characteristics, *n/N* (%)		
ECE	22/49 (45)	27/84 (32)
Bulging	27/49 (55)	57/84 (68)
GS, median (IQR)	7 (7–8)	7 (7–7)

Intra- and perioperative findings	3D-AR group	MRI group	*p* value
Operative time (min), mean (SD)	135 (120–142)	127 (118–133)	0.08
Time for excisional biopsy (min), mean (SD)	4 (2.5–4.7)	3 (2.0–3.8)	0.1
Blood loss (ml), mean (SD)	442 (347–548)	476 (350–584)	0.3
Nerve sparing, *n/N* (%)			0.6
Full NS	10/49 (20)	13/84 (16)	
Partial NS	32/49 (65)	55/84 (66)	
Minimal NS	7/49 (14)	16/84 (19)	
Postoperative surgery-related complications, *n/N* (%)	1/49 (2)	7/84 (8.3)	0.1
Postoperative Clavien III–V complications, *n* (%)	0 (0)	1 (1.2)	0.4
Catheterization time (min), median (IQR)	5 (4–6)	5 (4–6)	0.5
Hospital stay (d), median (IQR)	5 (4–6)	5 (4–6)	0.4
Urinary continence, defined as “social continence”, *n/N* (%)			
1 wk after catheter removal	32/49 (66)	57/84 (68)	0.8
1 mo after surgery	35/49 (71)	63/84 (75)	0.6
3 mo after surgery	38/44 (86)	65/74 (88)	0.8
6 mo after surgery	34/37 (92)	55 /60 (92)	0.9
12 mo after surgery	30/32 (94)	39/55 (75)	0.03
Urinary continence, defined as “total continence”, *n/N* (%)			
1 wk after catheter removal	22/49 (45)	48/84 (57)	0.3
1 mo after surgery	28/49 (57)	40/84 (48)	0.5
3 mo after surgery	35/44 (80)	57/74 (77)	0.7
6 mo after surgery	34/37 (92)	54/60 (90)	0.7
12 mo after surgery	29/32 (91)	39/55 (71)	0.03
Potency rate, *n/N* (%)			
1 mo after surgery	10/49 (20)	18/84 (21)	0.9
3 mo after surgery	19/44 (43)	39/74 (53)	0.5
6 mo after surgery	14/37 (38)	31/60 (52)	0.2
12 mo after surgery	13/32 (41)	22/55 (40)	0.2
Postoperative radiotherapy, *n/N* (%)			
Overall	8/45 (18)	27/78 (35)	0.046
Salvage RT	6/34 (18)	8/53 (15)	0.7
Biochemical recurrence at 12th month, *n/N* (%)	6/34 (18)	8/53 (15)	0.7

Pathological data	3D-AR group (49)	MRI group (84)	*p* value
Prostate volume (ml), median (IQR)	32 (27–48)	35 (27–48)	0.7
Tumor volume (ml), median (IQR)	3.7 (2.6–6)	3.8 (2.3–6)	0.8
Pathological stage, *n/N* (%)			
pT2	40/49 (82)	69/84 (82)	0.3
pT3	9/49 (18)	15 (18)	
Gleason score, *n/N* (%)			
2–6	2/49 (4.1)	2/84 (2.4)	0.2
7	32/49 (65)	67/84 (80)	
8–10	15/49 (31)	15/84 (18)	

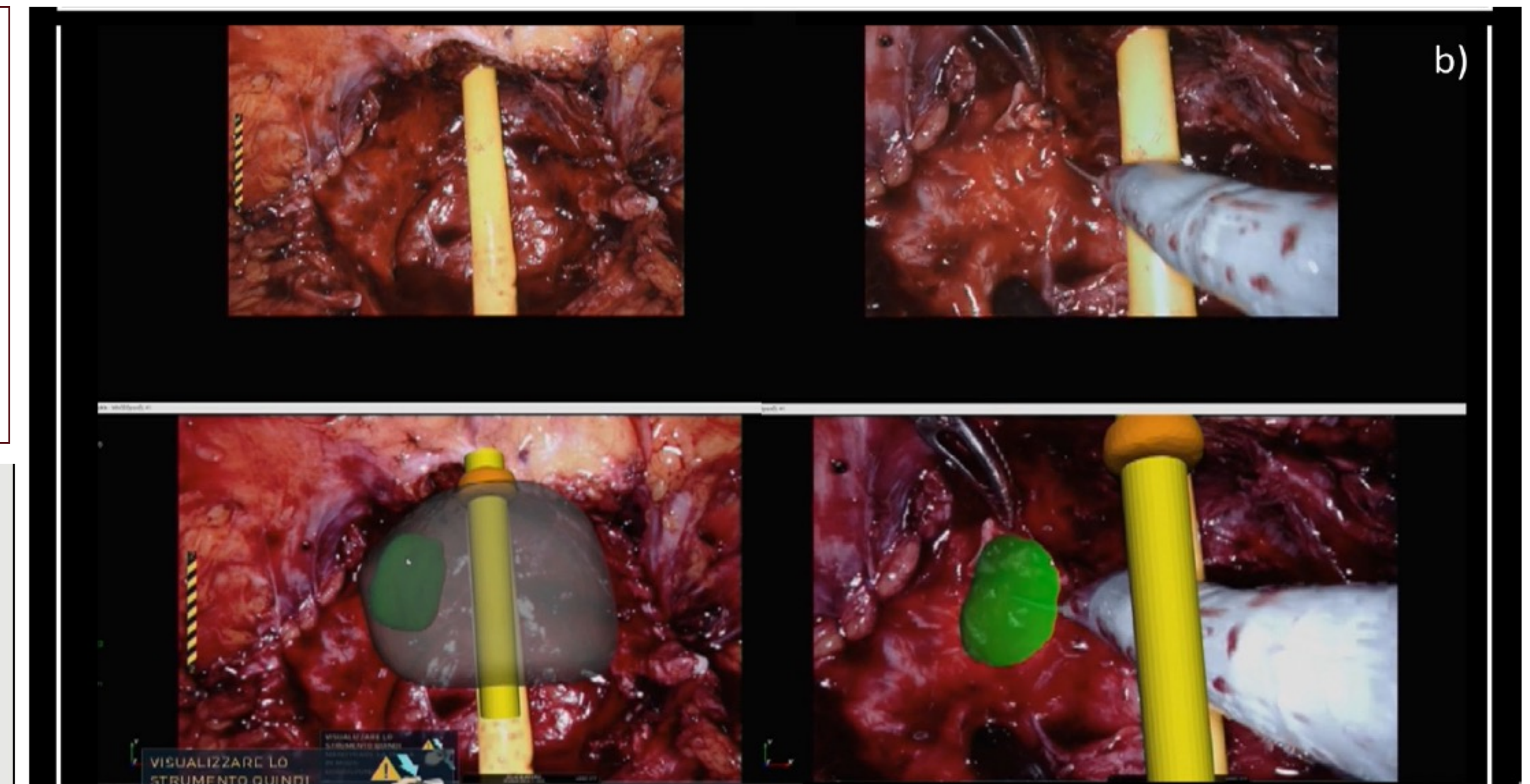

RESULTS

- Baseline characteristics comparable
- no differences in operative time, blood loss, hospital stay, or complications
- Surface PSMs were similar (47% vs 45%, p=0.8)
- **3D-AR guided biopsies** identified **more positive NVB lesions** (52% vs 13%, p=0.001), **reducing final NVB-level PSMs** (22% vs 39%, p=0.047)
- The **3D-AR** group showed **improved continence recovery at 12 months** (Social continence: 94% vs 75% - Total continence: 91% vs 71%; p=0.03)
- Potency recovery and BCR rates were comparable, while **postoperative radiotherapy was lower in the AR group** (18% vs 35%, p=0.046)

	Patient (*n*)			PSM[b]			NVB Bx+[c]			PSMs on NVB after excisional biopsy[d]		
	MRI group	3D-AR group	*p* value	MRI group	3D-AR group	*p* value	MRI group	3D-AR group	*p* value	MRI group	3D-AR group	*p* value
Overall	84	49	–	38/84 (45)	23/49 (47)	0.8	5/38 (13)	12/23 (52)	0.001	33/84 (39)	11/49 (22)	0.047

AR = augmented reality; 3D = three dimensional; MRI = magnetic resonance imaging; NVB = neurovascular bundle; NVB Bx+ = positive neurovascular bundle biopsy; PSM = positive surgical margin.

[a] Data are presented as *n/N* (%), unless otherwise indicated.
[b] The presence of PSMs at the level of prostate surface.
[c] The positivity of excisional biopsy at the level of NVB.
[d] The presence of residual cancer cells on the level of NVB.

CONCLUSIONS

- AI-enhanced **3D augmented reality significantly reduced final NVB-level positive surgical margins** (22% vs 39%) during nerve-sparing robotic prostatectomy, improving continence recovery, reducing postoperative radiotherapy

Retinoic Acid Signaling and Immune Microenvironment Signatures Drive Response to Enfortumab Vedotin and NECTIN4 CAR-T therapy

University of California San Francisco

AUA 2026

Tamilla Nechiporuk, Brendan L Raizenne MD, Sha Zhu, Yuxin Yang, Shivani Saxena, Elizabeth Yip, Kevin Chang, William Dougherty, Jun Zhu, Rosalie Nolley, Imene Boukhalfa Ep Hanafi, Rhea Master, Sima P. Porten, Terence Friedlander, Vadim S. Koshkin, David Quigley, Franklin Huang MD PhD, Jonathan Chou, and Carissa E. Chu
University of California, San Francisco, CA, USA

ABSTRACT

Urothelial carcinoma (UC) remains a leading cause of cancer mortality, with limited durable responses in the metastatic setting. Enfortumab vedotin (EV), a NECTIN4 targeting antibody drug conjugate (ADC), has improved outcomes, yet therapeutic response critically depends on **NECTIN4 (gene: *NECTIN4*) localization at the plasma membrane.** While NECTIN4 expression is enriched in luminal bladder cancer subtypes, the mechanisms regulating its cell-surface availability remain poorly understood.

We performed a **genome-wide CRISPR interference (CRISPRi) FACS-based screen** to identify regulators of surface NECTIN4 expression. We uncover opposing roles for cell differentiation programs, with **luminal pathways acting as positive regulators** and **basal/EMT-associated programs as negative regulators** of Nectin-4 surface expression. Notably, **retinoic acid (RA) signaling emerged as a central regulator**, increasing both total and surface NECTIN4 as part of a luminal differentiation program. Pharmacologic activation of RA signaling sensitized bladder cancer cells to NECTIN4 directed therapies, including EV and CAR T cells. EV and EV-resistant cells employed canonical EMT program that was reversed in the presence of RA.

Furthermore, spatial single cell-profiling of a tumor microarray of patients treated with EV revealed responders to EV possess **a pre-existing immune activated niche** enriched in antigen presentation and T-cell co-stimulation. As expected, luminal urothelial cancer cells were associated with response.

Together, these findings establish a model in which **differentiation state regulates NECTIN4 availability and sensitivity to targeted therapies** and identify a novel biomarker strongly associated with response.

Introduction/Methods: Enfortumab vedotin (EV) is a NECTIN4 targeting antibody drug conjugate (ADC) approved as a frontline therapy for advanced and metastatic bladder cancer in combination with pembrolizumab. Clinical response to EV depends on **NECTIN4 localization at the plasma membrane**, frequently disrupted in non-responsive and resistant tumors. NECTIN4 expression is enriched in luminal bladder cancer subtypes, suggesting that differentiation state influences therapeutic efficacy.

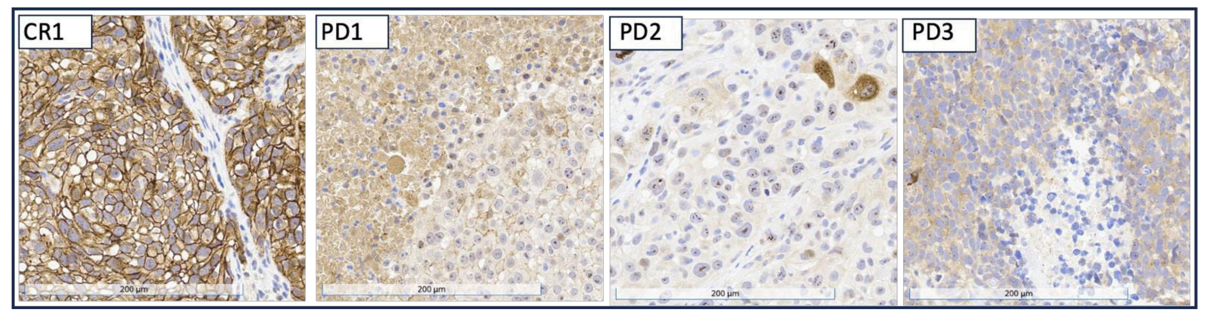

Figure 1. NECTIN4 immunohistochemistry of tumors from patients with metastatic bladder cancer treated with EV monotherapy. Complete response (CR), progressive disease (PD).

To define mechanisms regulating NECTIN4 cell-surface expression and identify strategies to enhance NECTIN4-targeted therapies, we performed a **genome-wide CRISPRi FACS-based screen**. This approach identified regulators of high and low surface NECTIN4, revealing pathways linked to **luminal differentiation (positive regulators)** and **basal/EMT programs (negative regulators)** in bladder epithelium.

Figure 2. FACS-based CRISPRi screen identifies top positive and negative regulators of Nectin-4 expression

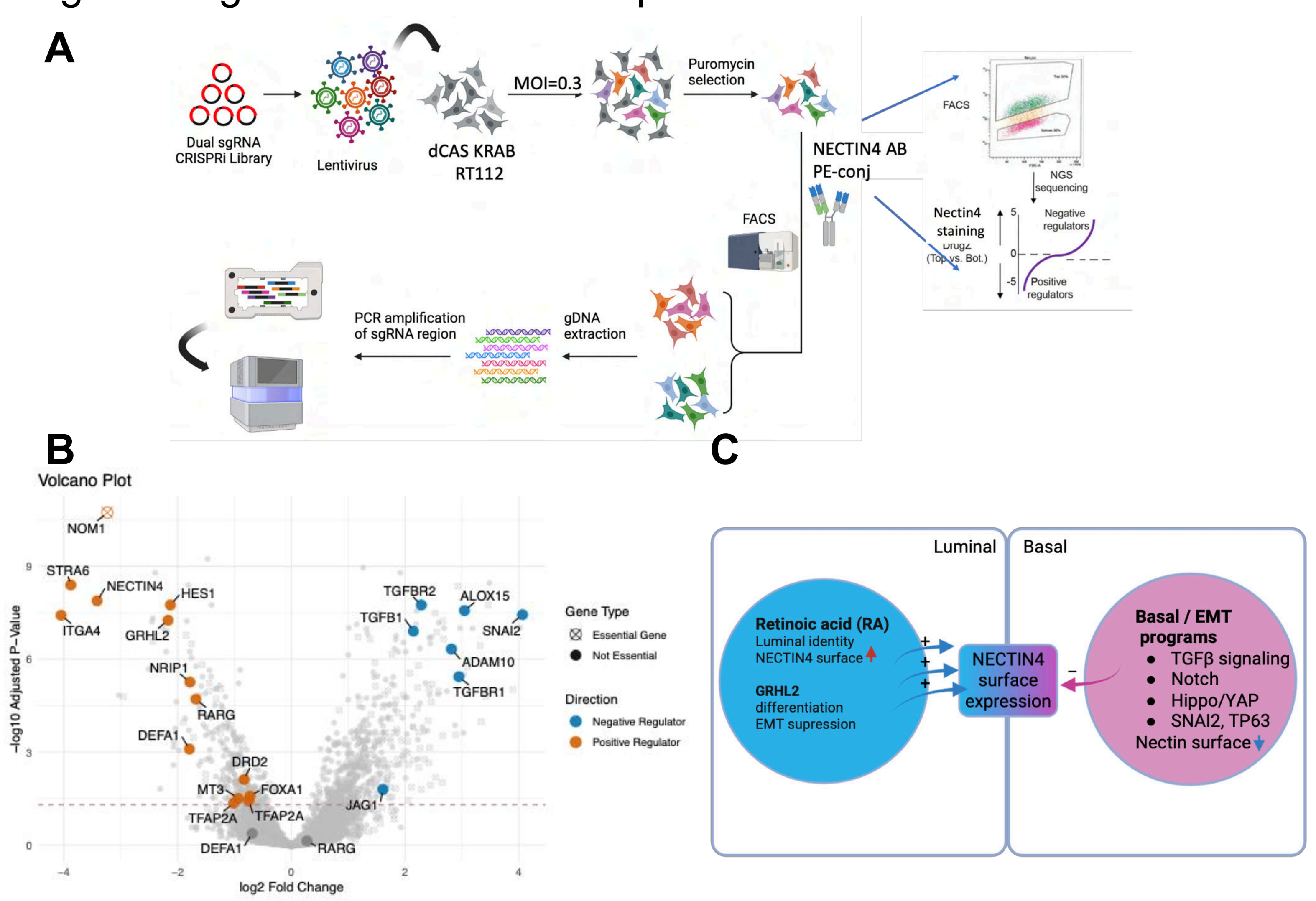

(A) Schematic of CRISPRi FACS-based screen for regulators of surface NECTIN4 expression. (B) Volcano plot of positive and negative regulators of surface NECTIN4 in CRISPRi screen. (C) Pathways controlling NECTIN4 surface expression. Luminal differentiation pathways as positive regulators and basal/epithelial-mesenchymal transition (EMT)-associated programs as negative regulators.

Figure 3. Validation of screen hits across multiple BC cell lines

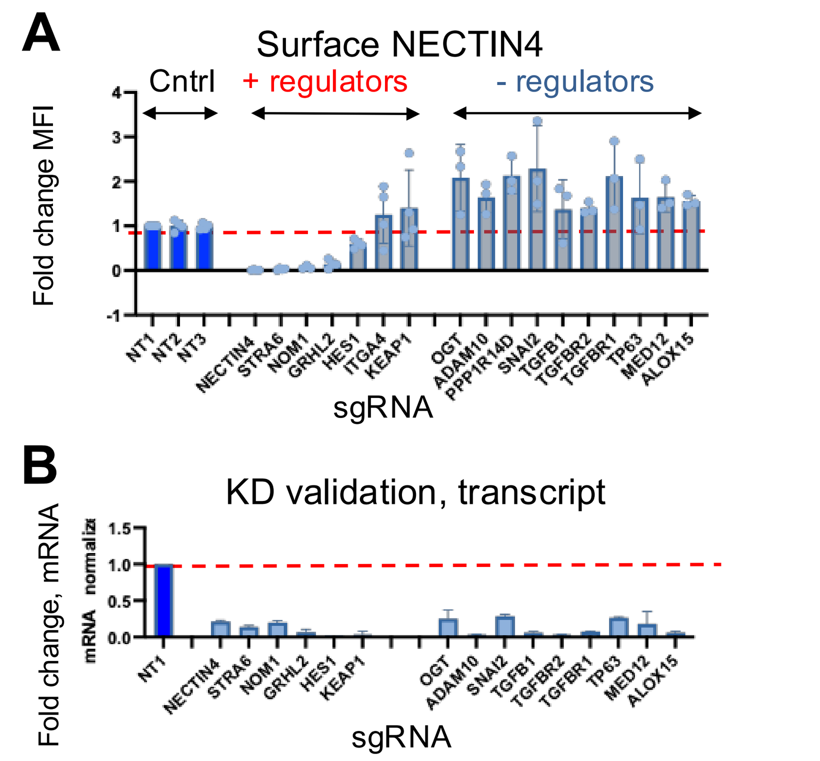

(A) Flow cytometry with individual genes KD for NECTIN4 surface expression (B) validation at the mRNA level.

Gene	regulator	RT112	UMUC14	UMUC1
STRA6	Positive	+	+	+
NOM1	Positive	+	+	+
GRHL2	Positive	+	-	+
HES1	Positive	+	+	+
KEAP1	Positive	-	-	n/a
ITGA4	Positive	+/-	+	+
NECTIN4	Positive	+	+	+
TP63	Negative	+	n/a	+
SNAI2	Negative	+	+	-
MED12	Negative	+	-	n/a
ALOX15	Negative	+	+	-
TGFBR1	Negative	+	-	+
TGFBR2	Negative	+	+	-
OGT	Negative	+	+	+
ADAM10	Negative	+	+	+
TGFB1	Negative	+	+	-
PPP1R14D	Negative	+	+	n/a

Table 1. Validation of NECTIN4 CRISPRi screen hits in luminal bladder cancer cell lines

Figure 4. Retinoic acid is a central regulator NECTIN4 surface/total protein expression and can increase surface NECTIN4 and can enhance sensitivity to EV and CAR-T therapy

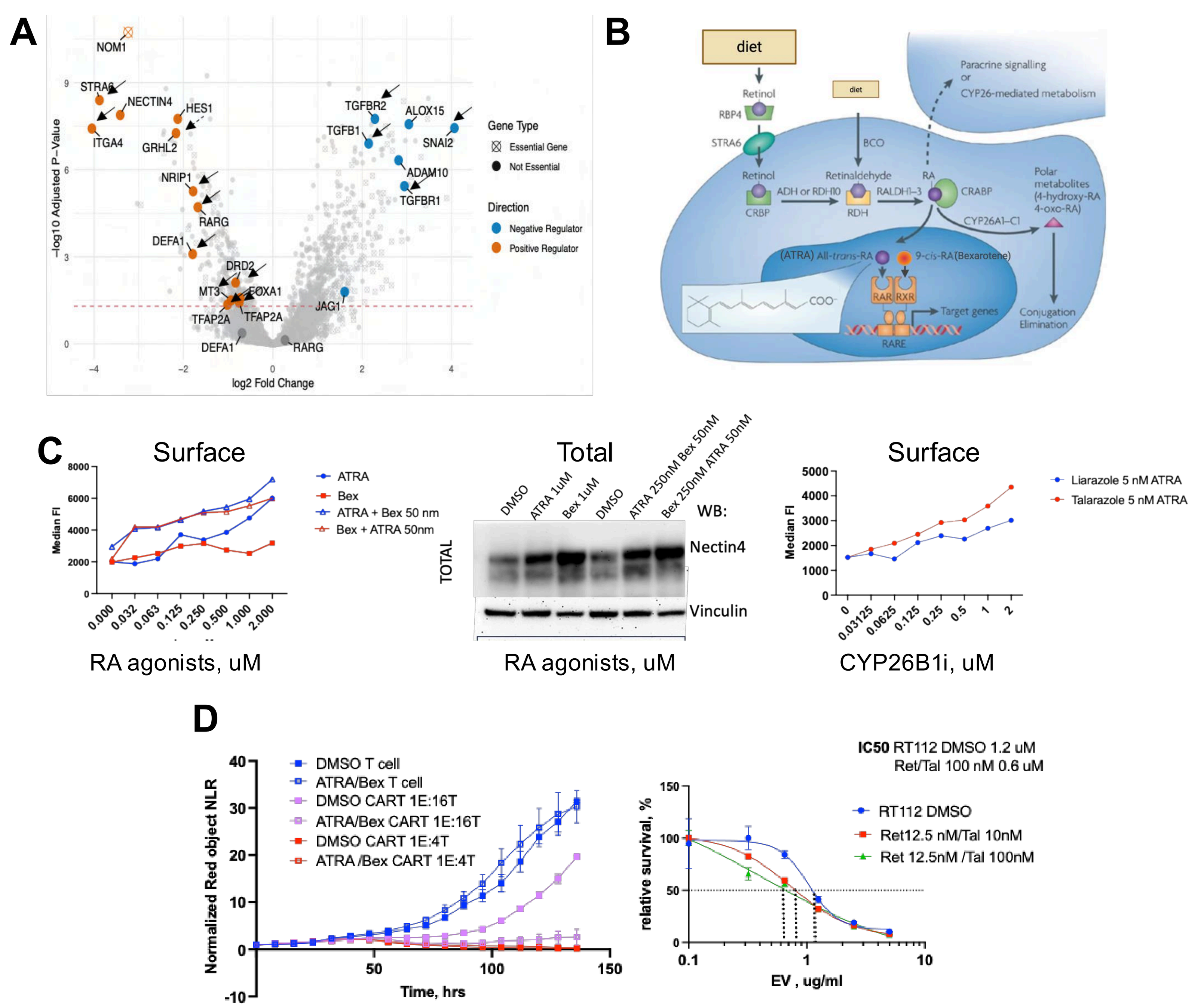

(A) Members of the RA signaling are significantly enriched in CRISPR screen hits. (B) Retinoic acid signaling pathway in bladder cancer (adapted from Niederreither and Dolle, Nat Gen Review 2008, Vol 9). (C) Concordance between surface and total NECTIN4 protein change induced by RA agonists ATRA/Bex and inhibitors of RA oxidation (CYP26B1i, liarozole and talarozole) showing increased surface and total NECTIN4. (D) Combination of ATRA 125 nM/Bex 50nM ATRA or retinol with talarozole enhance efficacy of NECTIN4 CAR T and EV.

Figure 5. RT112 EV-resistant cell lines (EVR) downregulate surface NECTIN4 and can be re-sensitized to EV with retinol and talarozole

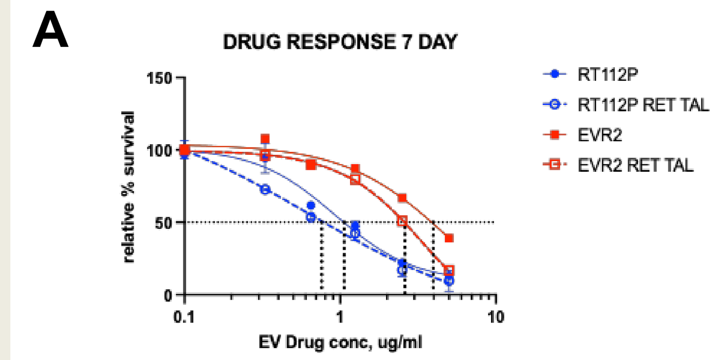

B

IC50, uM	RT112	EVR1	EVR2	EVR4	EVR10
DMSO	1.1	1.8	4	2.5	1.9
Retinol 250 nM Talarazole 100nM	0.75	1.8	2.5	1.1	1.9

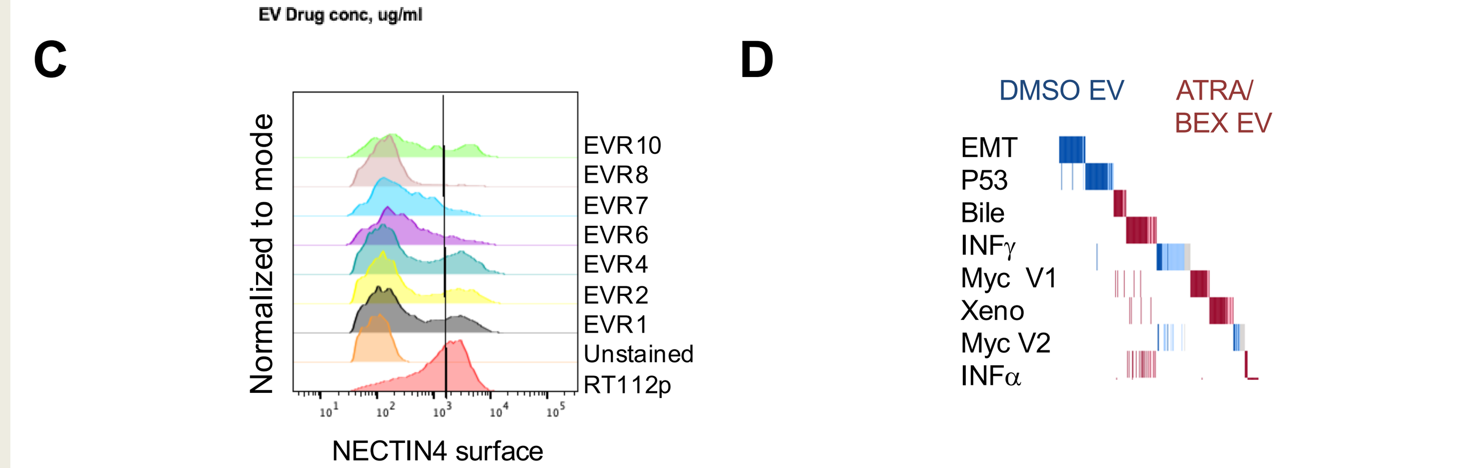

(A,B) EV sensitivity in representative EVR2 cell line and corresponding IC50 values. (C) Staining for surface NECTIN4 in EVR lines. (D) EV treatment induces EMT/P53 pathway genes that is prevented when cotreated with ATRA/Bex

Figure 6. Single-cell spatial transcriptomics identifies pre-existing spatial neighborhood “16” strongly associated with response to EV

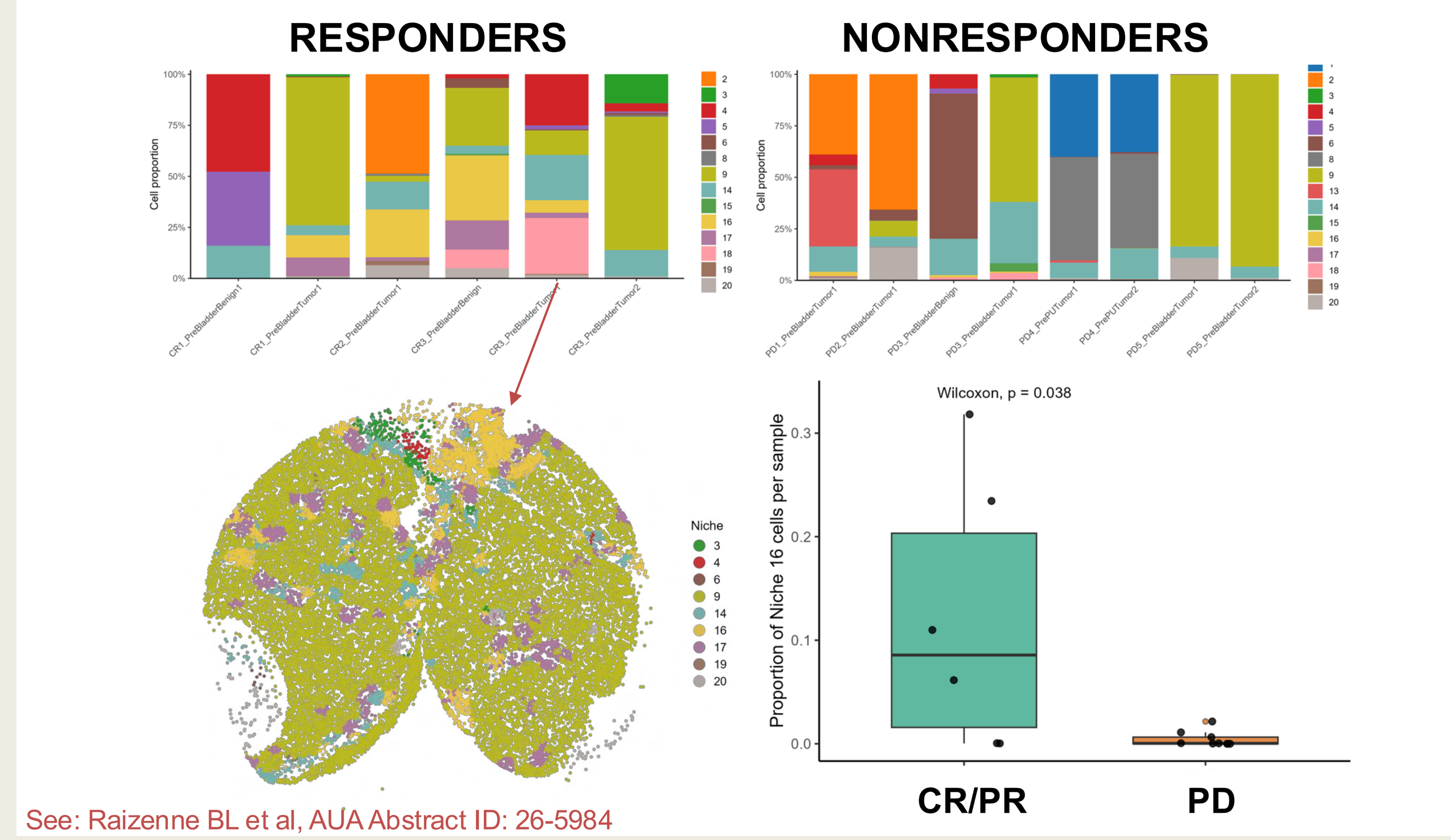

See: Raizenne BL et al, AUA Abstract ID: 26-5984

CONCLUSIONS

- A genome-wide CRISPRi screen identifies luminal differentiation programs as positive regulators and basal/EMT programs as negative regulators of NECTIN4 cell-surface expression.
- Retinoic acid (RA) signaling is a central positive regulator of NECTIN4 surface abundance. RA agonists and CYP26B1 inhibition reproduce this effect and enhance sensitivity to EV and NECTIN4 CAR T therapy
- These findings define a model in which luminal differentiation state and repression of EMT program regulate NECTIN4 surface expression.
- Spatial single cell-profiling revealed that patients responding to enfortumab vedotin ± pembrolizumab possess a pre-existing immune activated niche enriched in antigen presentation and T-cell co-stimulation.

Prostate MRI Utilization and Risk Calculators to Improve the Quality of Prostate Cancer Detection

Hiten D. Patel

1. Department of Urology, Feinberg School of Medicine, Northwestern University, Chicago, IL. 2. Surgery Service, Jesse Brown VA Medical Center, Chicago, IL. 3. Center of Innovation for Complex Chronic Healthcare, Edward Hines Jr. VA Hospital, Hines, IL.

Background

- Magnetic resonance imaging (MRI) reduces overdiagnosis of low-risk prostate cancer (PCa) while maintaining or increasing detection of high-risk PCa.
- Prostate MRI utilization in practice has not been well characterized, especially for higher risk populations such as Veterans and Black men.
- In addition, MRI-based risk calculators may replace traditional PCa risk prediction tools (e.g. PCPT, PBCG).
- Aims:

  (1) Characterize trends and disparities in prostate MRI use across the Veterans Health Administration (VHA)
  (2) Develop and compare MRI-based risk calculators to inform strategies to improve MRI implementation into practice

Methods

- **Prostate MRI Use Analysis**
  - VHA Corporate Data Warehouse: biopsy-naïve, elevated PSA (diagnosis code), prostate biopsy (2015-2023)
    - Multivariable mixed-effects logistic regression performed with VHA site as a random effect
  - TriNetX: biopsy-naïve, elevated PSA (4+), prostate biopsy (2016-2025)
    - Propensity score matched (PSM) analyses across PSA strata
- **MRI-Based Risk Calculators**
  - PLUM (Loyola University, N=1,010): MRI cohort
    - Validation sets: North American (UAB, N=371), European (NTNU, N=303)
  - mynMRIsk (Northwestern University, N=1,494): advanced serum biomarker (Prostate Health Index (PHI)) + MRI cohort
  - Primary Outcome: clinically significant PCa (csPCa) defined as grade group 2 (GG2) or higher

Prostate MRI Use

- **VHA (N=120,105)**
  - 2015-2023: 2% to 41%
  - Lower for Black (2023: 37% vs. 44%) and rural (2023: 35% vs. 43%) Veterans
- **TriNetX (N=33,017)**
  - 2016-2025: 14% to 53%
  - Lower for Black patients across PSA strata on PSM analyses

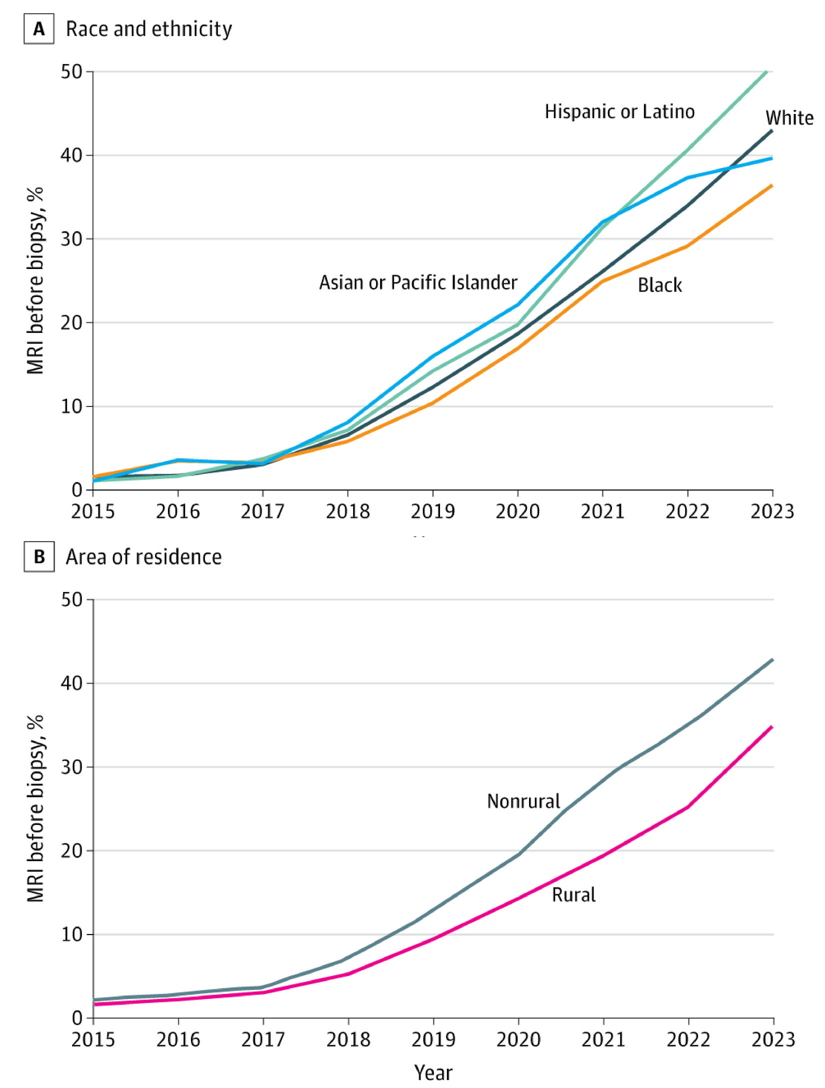

Figure 1 (left). Prostate MRI utilization by (A) race and (B) rural/urban location. VHA 2015-2023.

Figure 2 (right). (A) Prostate MRI utilization by race among patients receiving first-time biopsy (N=33,017). (B) Among all patients with a first-time PSA value of 4+ (N=550,352), the rate of biopsy remained stable (~6%) over time while prostate MRI use increased (2.6% to 9.3%). The rate of negative biopsy was lower for MRI (30%) relative to the non-MRI (45%) biopsy pathway based on PCa diagnosis within 1 year. TriNetX 2016-2025.

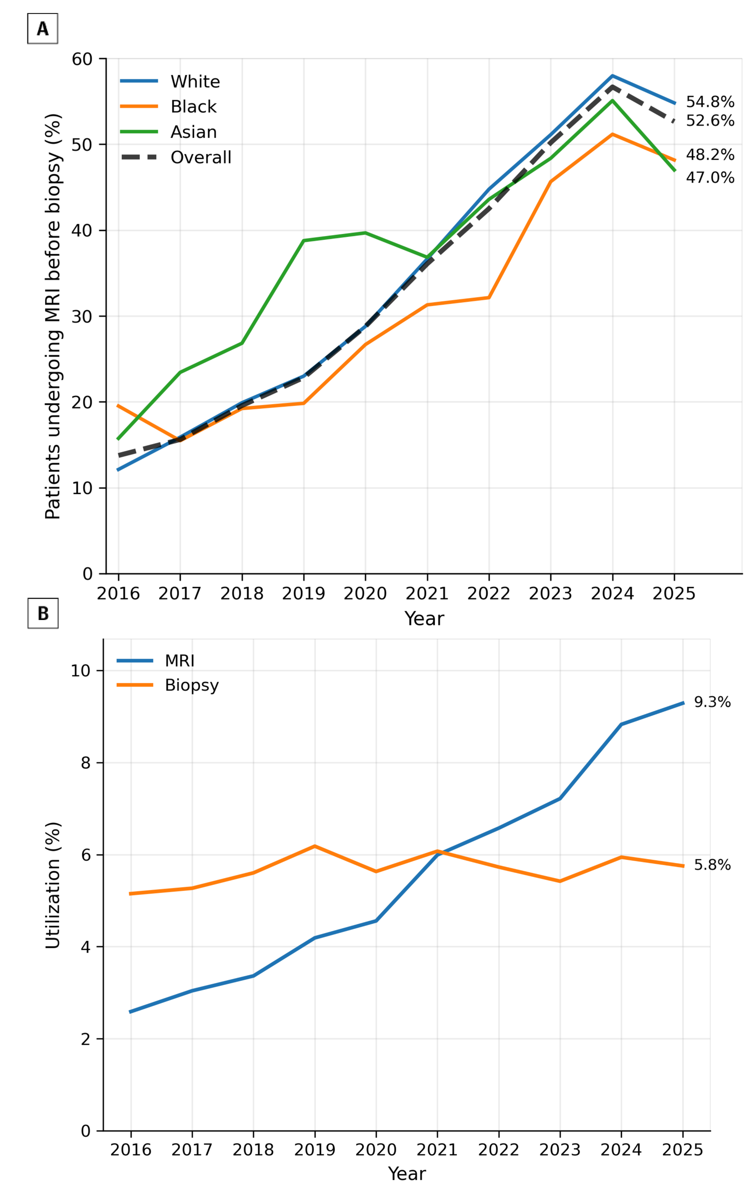

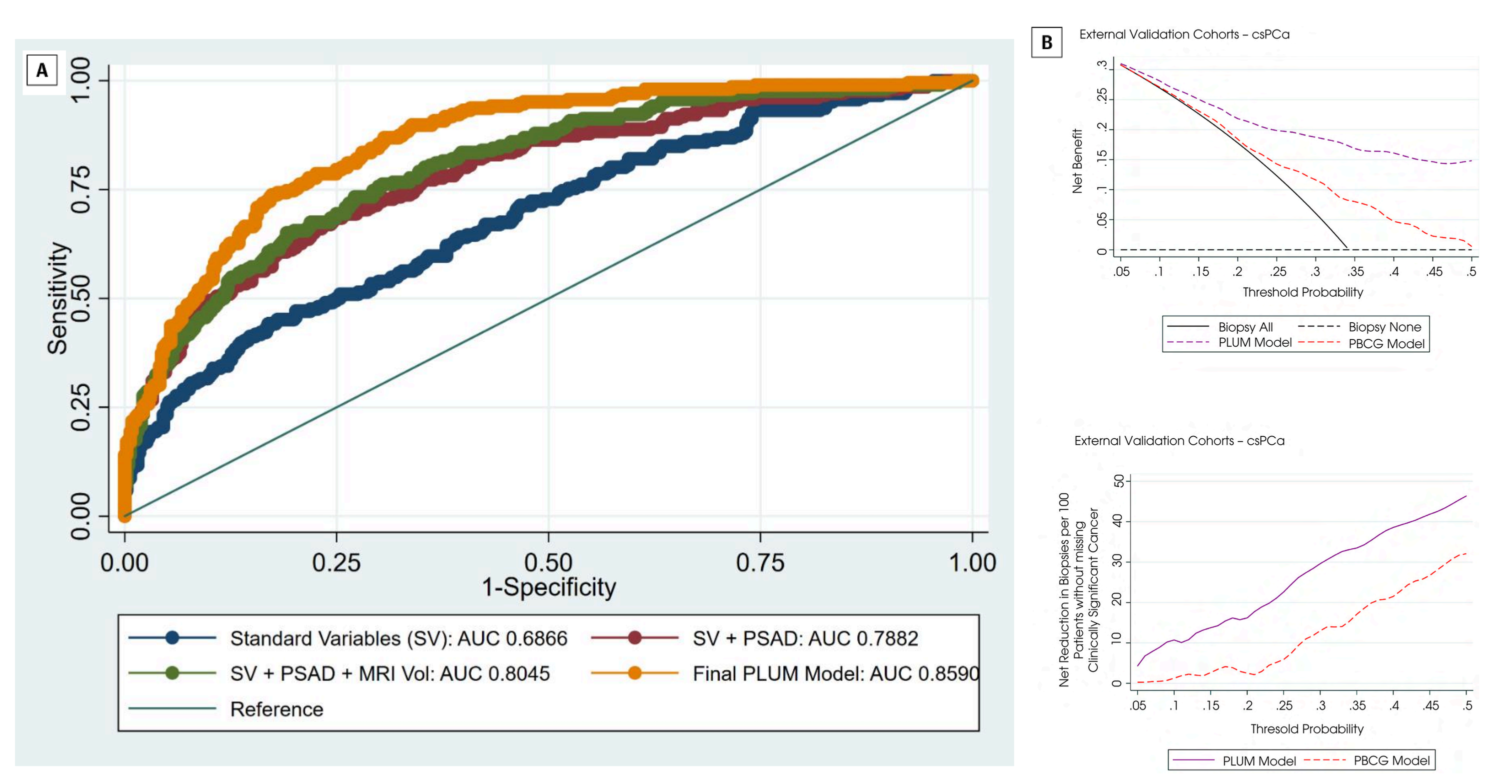

Figure 3 (left). (A) Receiver operating characteristics for development of the PLUM (Prospective Loyola University Multiparametric MRI Cohort) risk calculator. (B) Decision curve analysis comparing PLUM and PBCG for csPCa (GG2+) thresholds for biopsy to calculate net benefit and effective reduction is biopsies without missing csPCa.

Table . AUC Estimates Based on Receiver Operating Curves for the 4 Selected Models in the North American, European, and PHI Advanced Serum Biomarker Cohorts

	Cohort, AUC (95% CI)		
Model	North American	European	PHI
PLUM	0.85 (0.80-0.89)	0.90 (0.86-0.93)	0.82 (0.80-0.84)
RPCRC-MRI	0.83 (0.78-0.87)	0.90 (0.86-0.93)	0.79 (0.77-0.81)
UCLA-Cornell	0.83 (0.80-0.88)	0.90 (0.86-0.93)	0.83 (0.81-0.85)
Van Leeuwen	0.83 (0.79-0.88)	0.90 (0.87-0.93)	0.80 (0.78-0.82)

Table (left). Discrimination was largely comparable across models in the North American and Europea validation cohorts. However, PLUM and RPCRC-MRI were best calibrated. Notably, all models were prone to underestimation in the cohort using an advanced serum biomarker (PHI). PLUM also outperformed the Stanford model (84.1% vs 81.1%, p=0.002).

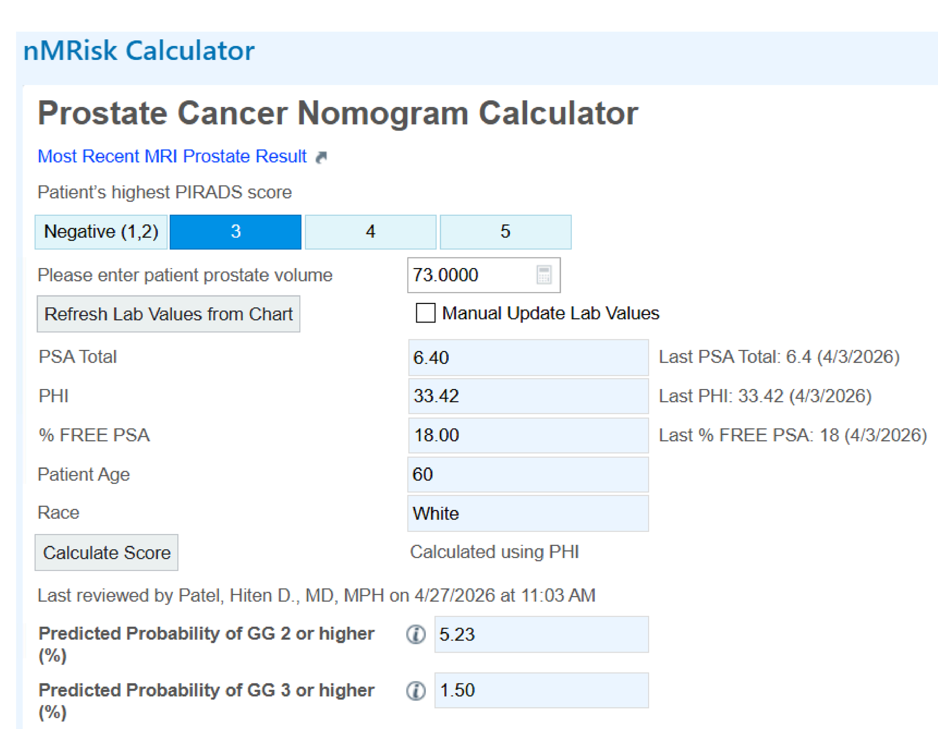

Figure 4 (left). The mynMRIsk calculator was integrated as an EMR-based tool in EPIC at Northwestern Medicine. Patient age, race, and biomarker values are automatically pulled by the SmartPhrase while MRI PI-RADS and volume are entered. The generated values can be inserted into clinical notes and used in shared decision-making with patients.

MRI-Based Risk Calculators

- PLUM vs PBCG
  - Development (0.86 vs 0.66) and external validation (0.84 vs. 0.66); PLUM able to avoid 41% at 7.5% csPCa cost threshold
- Comparisons of MRI-Based RCs
  - PLUM and RPCRC-MRI best calibrated in NA and EU validation sets; underestimation in PHI cohort
- **mynMRIsk Calculator**
  - Flexible biomarker (PSA, %free PSA, PHI) and MRI (multi- vs bi-parametric) options with AUCs ≥0.88 on development and validation; PHI model avoided 39.1% bx while missing 0.8% csPCa (20% GG2+ biopsy threshold)

Conclusions

- Prebiopsy prostate MRI is being increasingly utilized (>40% in VHA, >50% in TriNetX) but remains lower than ~90% use at some academic health centers.
- Despite an equal access system, disparities and site variation in MRI use were observed in the VHA which will guide implementation efforts to measure barriers and facilitators (e.g. imaging capacity, provider habits).
- Quality considerations for prostate MRI include disparate use (access), imaging quality, radiologist accuracy, and AI-integration to "raise the floor".
- MRI-based risk calculators can be developed and incorporate advanced biomarkers for use across practice settings.
- Ongoing work: Implementation efforts using risk calculators (VHA, EMR-integration, decision aids) and development of AI-augmented PCa detection algorithms (HIT-PIRADS, PI-CAI) to improve biopsy decisions (avoid unnecessary biopsies) and optimize csPCa detection.

References:

Patel HD, et al. A Prostate Biopsy Risk Calculator based on MRI: Development and Comparison of PLUM to the PBCG. BJU Int. 2023 Feb;131(2):227-235. PMID: 35733400.
Huang MM, et al. MRI Utilization Rates for Veterans at Risk of Prostate Cancer. JAMA Netw Open. 2025 Nov 3;8(11):e2543567. PMID: 41252171.
Patel HD, et al. Comparison of Magnetic Resonance Imaging-Based Risk Calculators to Predict Prostate Cancer Risk. JAMA Netw Open. 2024 Mar 4;7(3):e241516. PMID: 38451522.
Siddiqui MR, et al. Optimizing detection of clinically significant prostate cancer through nomograms incorporating mri, clinical features, and advanced serum biomarkers in biopsy naïve men. Prostate Cancer Prostatic Dis. 2023 Sep;26(3):588-595. PMID: 36973367.
Saha A et al (PI-CAI-ProCAncer-I-COMFORT-STHLM3-MRI-PRIME consortia). Scaling Artificial Intelligence for Prostate Cancer Detection on MRI towards Population-Based Screening and Primary Diagnosis in a Global, Multiethnic Population. RSNA 2025 Abstract (November 30-December 4, 2025).

Funding and acknowledgements: Funded by Prostate Cancer Foundation (24YOUN22), Department of Defense (HT9425-25-1-0498), and SWIFT grant from the Veterans Health Administration (CINCCH). Contents do not represent the views of the U.S. Department of Veterans Affairs or the United States Government.

Northwestern Medicine

NORTHWESTERN UNIVERSITY FEINBERG SCHOOL OF MEDICINE

AUA 2026 Washington, DC

IMPROVING THE DIAGNOSTIC UTILITY OF BLADDER MUCOSAL BIOPSIES IN INTERSTITIAL CYSTITIS/ BLADDER PAIN SYNDROME

Hannah Ruetten[1,2], Raymond Xu[3], Harrison Martin[1], Dylan T. Wolff[3], Rory Ritts[2], Wencheng Li[1], Kaylee Ferrara[3], Robert J Evans[3], Gopal Badlani[3], Stephen J Walker[2,3]

[1]Department of Pathology, Wake Forest University School of Medicine, [2]Wake Forest Institute for Regenerative Medicine, [3]Department of Urology, Wake Forest University School of Medicine, Winston-Salem, North Carolina, USA

BACKGROUND

Interstitial cystitis/bladder pain syndrome

- Chronic bladder/pelvic pain and lower urinary tract symptoms
- Unknown etiology
- Diagnosis of exclusion
  - Cystoscopy with or without cytology and biopsy not required for diagnosis

Current Information on biopsy report

- Inflammation
  - type: Acute, Chronic, Chronic Active
  - +/- severity
  - +/- distribution
- Mast cell count/range
  - various stains utilized
  - units variable or not provided
- +/- description of any denudation, hemorrhage, and/or edema
- +/- comment on presence of muscularis propria

Many clinicians find pathology reports do not contain helpful information for diagnosis or prognosis.

MAST CELLS AND INTERSTITIAL CYSTITIS/BLADDER PAIN SYNDROME REVISITED

Retrospective analysis of 461 diagnostic pathology reports collected from our IRB-approved prospective study of patients diagnosed with IC/BPS at the Urology Clinic at Wake Forest Baptist Hospital from October 2011 to July 2023 (IRB00018552).

Mast-cell stain	
TPSAB1	61.0%
KIT	29.3%
Toluidine blue	2.0%
Combination	3.7%
Not specified	4.1%

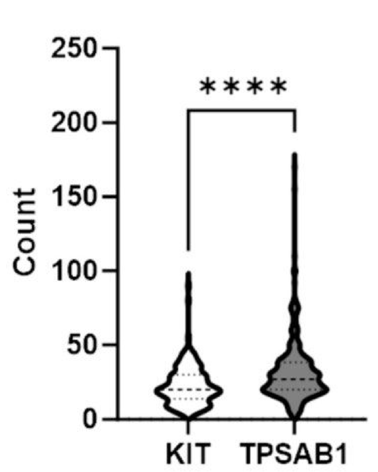

Staining strategy for mast-cell visualization differed between pathologists. This could influence clinician interpretation as counts with TPSAB1 (mast-cell tryptase) are higher than KIT (CD117).

Mast-cell count units	
HPF	84.6%
mm^2	8.5%
Unspecified	6.9%

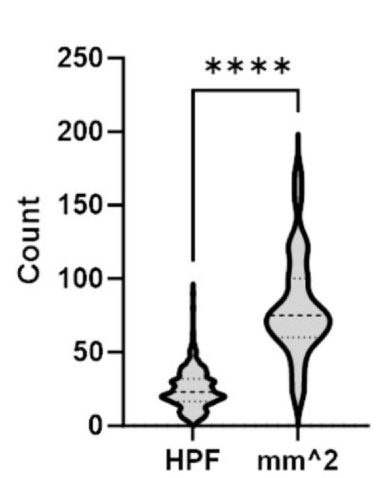

Mast-cell count was reported as a single number, range, or qualitatively with units of high-power field (HPF), mm^2, or non-specified. This could influence clinician interpretation as counts with mm^2 units will be much higher and could be misinterpreted.

There is a lack of standardization regarding histological analysis of bladder biopsies from patients with IC/BPS, leading to inconsistent data and confusion surrounding the significance of pathology report findings.
(Ruetten et al., International Urogynecology Journal, 2025)

LAMINA PROPRIA COLLAGEN ARCHITECTURE IN INTERSTITIAL CYSTITIS/BLADDER PAIN SYNDROME

Forty-four female patients were selected from Wake Forest IC/BPS registry for this study.

- non-IC/BPS controls (N=14)
- non-HL (NHL) IC/BPS patients (N=16)
- HL IC/BPS patients (N=14)

IC/BPS groups each had a roughly equal representation of low BC (LBC) and non-low BC (NLBC) patients for separate analyses.

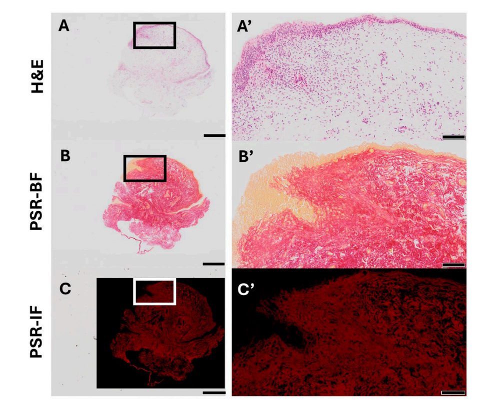

Figure 1 (left). Cold-cup mucosal bladder biopsy collagen. Representative tile scans of A) H&E, B) brightfield PSR, and C) fluorescent PSR. Scale bar is 500μm. Representative insets of A') H&E, B') brightfield PSR, and C') fluorescent PSR. Scale bar is 100μm.

HUNNER LESION

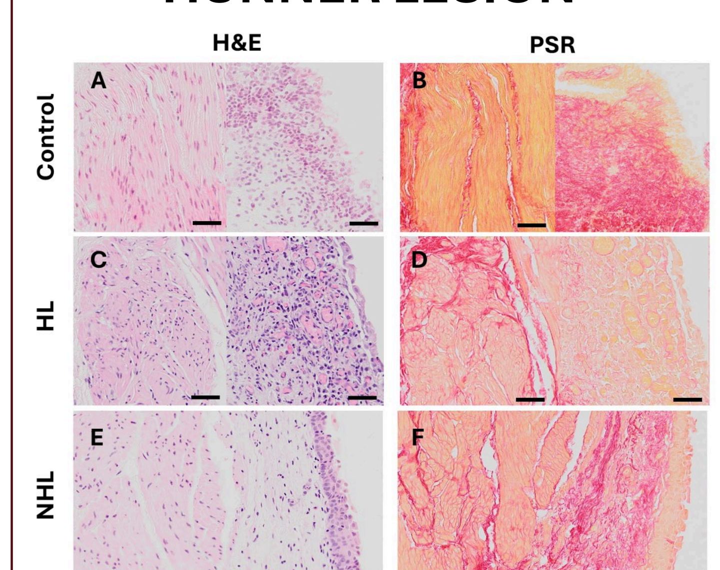

Figure 2 (left). HL patients have increased acute inflammation, more severe chronic inflammation, and increased peri-muscular collagen deposition, compared to NHL and controls. Representative images of A) H&E and B) PSR control (Acute inflammation: absent, Chronic inflammation: moderate, Peri-inflammatory collagen thinning: absent, Peri-muscular collagen disorganization: absent, Peri-muscular collagen accumulation: absent), C) H&E and D) PSR HL IC/BPS patient (Acute inflammation: present, Chronic inflammation: severe, Peri-inflammatory collagen thinning: present, Peri-muscular collagen disorganization: present, Peri-muscular collagen accumulation: present), and D) H&E and E) PSR NHL IC/BPS patient (Acute inflammation: absent, Chronic inflammation: minimal/absent, Peri-inflammatory collagen thinning: absent, Peri-muscular collagen disorganization: absent, Peri-muscular collagen accumulation: absent). Scale bar is 50μm.

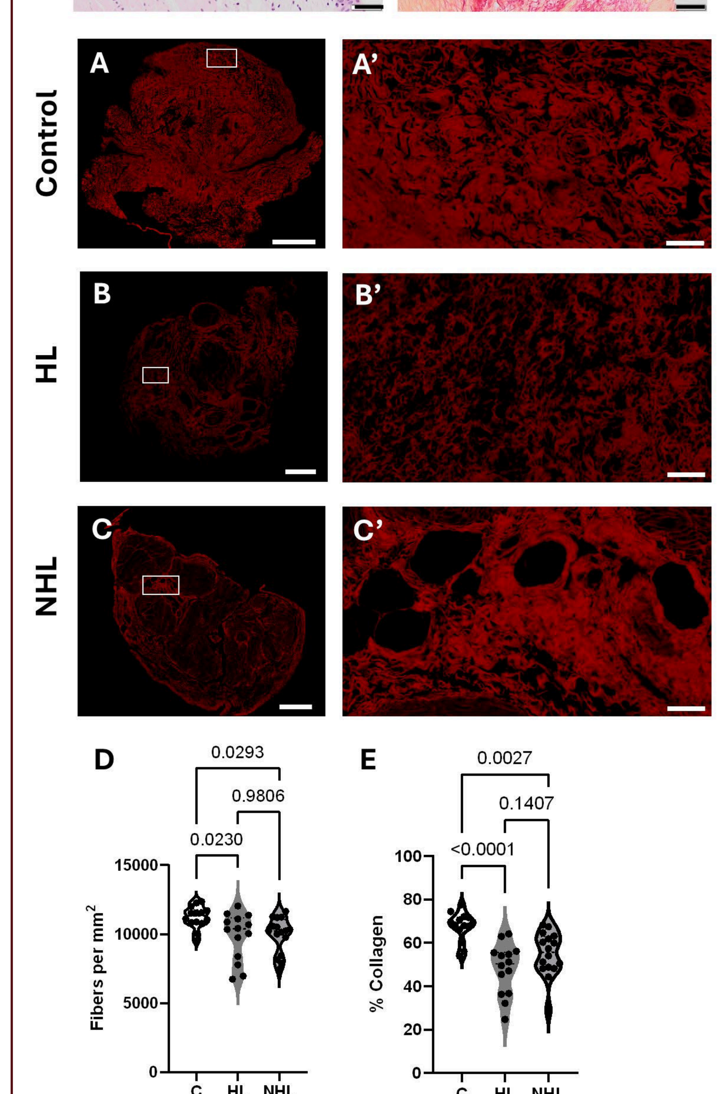

Figure 3 (left). Hunner lesion (HL) and non-Hunner lesion (NHL) patients have decreased bladder lamina propria collagen density compared to non- interstitial cystitis/ bladder pain syndrome (IC/BPS) controls Representative images of lamina propria collagen of A) controls (N=14), B) HL IC/BPS patients (N=14), and C) NHL IC/BPS patients (N=16). D) collagen fibers per mm2. E) collagen expressed as a percentage of total tissue area. Groups were compared using an ordinary one-way ANOVA followed by Tukey's multiple comparison test. A p-value less than 0.05 was considered significant. Scale bar is 50μm.

LOW BLADDER CAPACITY

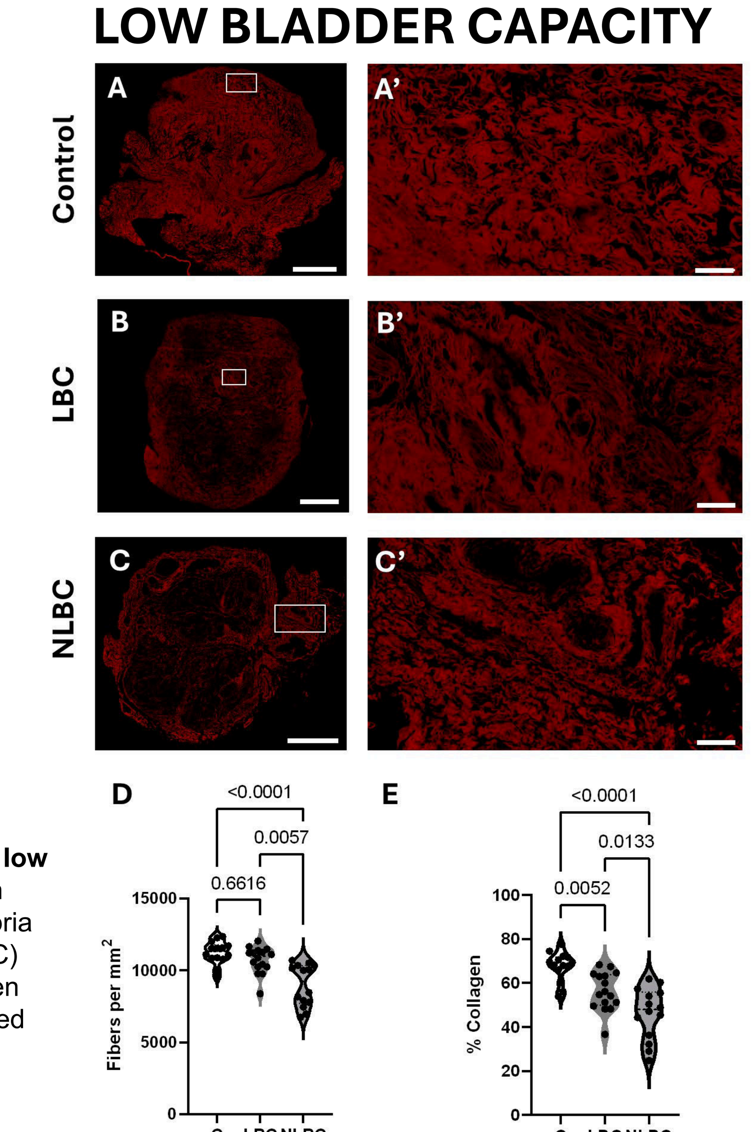

Figure 4 (right). Non-low bladder capacity (NLBC) patients have decreased bladder lamina propria collagen density compared to low bladder capacity (LBC) and non- interstitial cystitis/ bladder pain syndrome (IC/BPS) controls. Representative images of lamina propria collagen of A) controls (N=14), B) LBC IC/BPS patients (N=17), and C) NLBC IC/BPS patients (N=13). D) collagen fibers per mm^2. E) collagen expressed as a percentage of total tissue area. Groups were compared using an ordinary one-way ANOVA followed by Tukey's multiple comparison test. A p-value less than 0.05 was considered significant. Scale bar is 50μm.

These findings suggest a dynamic collagen fiber destruction and redistribution process unique to each IC/BPS subgroup, which likely contributes to the underlying pathophysiology of IC/BPS.
(Ruetten et al., Journal of Histochemistry & Cytochemistry, 2026)

REGENERATIVE CAPACITY OF THE INTERSTITIAL CYSTITIS/ BLADDER PAIN SYNDROME BLADDER

Twenty-two female patients were selected from Wake Forest IC/BPS registry for this study.

- non-IC/BPS controls (N=4)
- non-HL (NHL) IC/BPS patients (N=9)
- HL IC/BPS patients (N=9)

IC/BPS groups each had a roughly equal representation of low BC (LBC) and non-low BC (NLBC) patients for separate analyses.

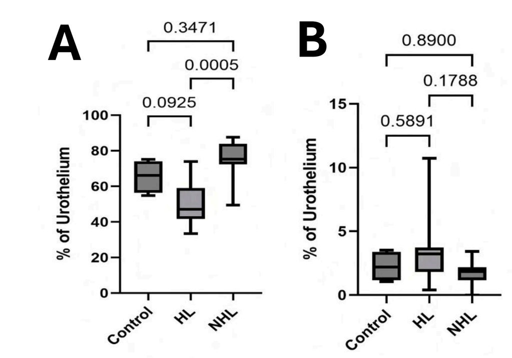

Figure 1 (left): Comparison of Hunner vs Non-Hunner lesion. Counts expressed as a percentage of overall urothelium (all CDH1+ cells). A) TP63. B) MKI67. Hunner lesion patients had a reduced %TP63 compared to non-Hunner lesion (p=0.0005) and trend toward reduction compared to control (p=0.0925). %MKI67 were similar.

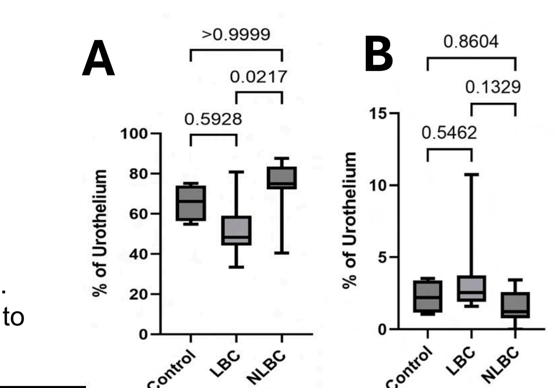

Figure 2 (right): Comparison of Low Bladder Capacity vs non-Low Bladder Capacity. Counts expressed as a percentage of overall urothelium (all CDH1+ cells). A) TP63. B) MKI67. Low bladder capacity patients had a reduced %TP63 compared to non-low bladder capacity (p=0.0217). %MKI67 were similar.

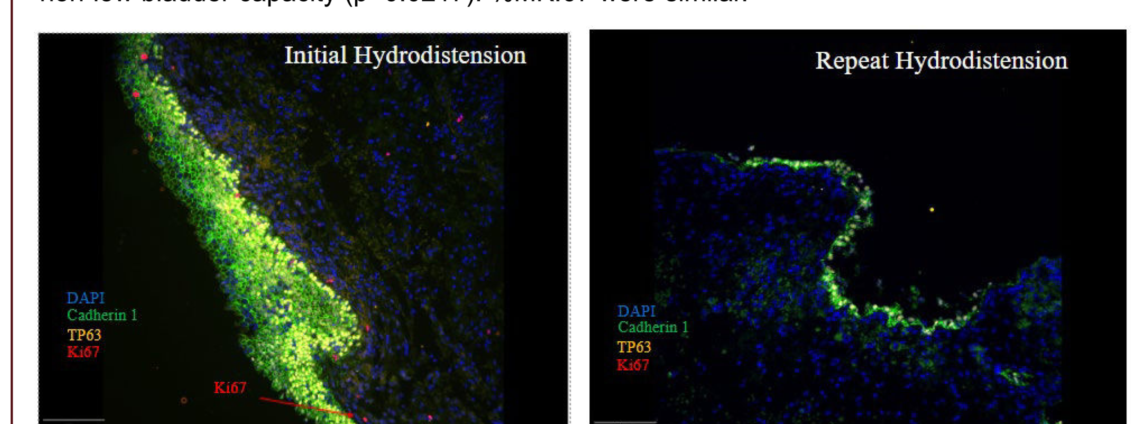

Figure 3 (left): Representative IHC image of biopsies from initial and repeat hydrodistension. CDH1 in green, TP63 in yellow, and MKI67 in red.

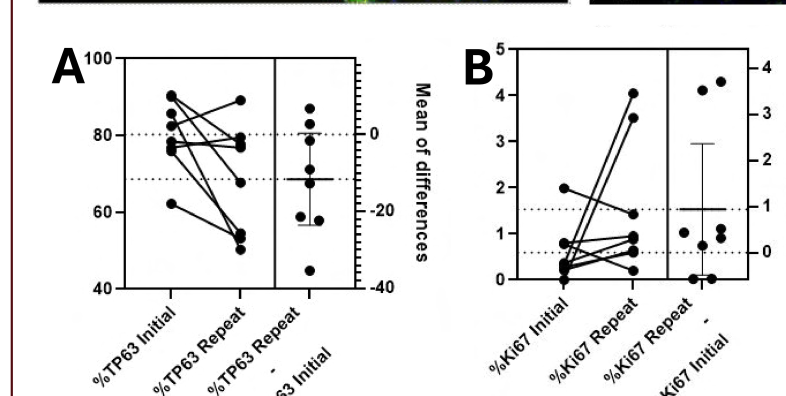

Figure 3 (left): Comparison of initial and repeat. Counts expressed as a percentage of overall urothelium (all CDH1+ cells). A) TP63. B) MKI67. Repeat biopsies had a reduced %TP63 compared to initial (11.64% decrease, p=0.05). %MKI67 were similar.
("MKI67" = "Ki67")

Some phenotypes of IC/BPS (HIC, LBC) may have a reduced bladder regenerative capacity, and this regenerative capacity may diminish overtime (repeat hydrodistension).
(Ruetten et al., unpublished)

NEXT STEPS

Through collaboration with urologists and pathologists develop a scoring guide for biopsies that includes clear findings. Perform retrospective implementation of scoring of biopsies on hundreds of patients in the Wake Forest IC/BPS registry to correlated findings with patient phenotypes, effective treatments, and disease progression. Ultimately, build a tool that pathologists can use to produce reports that can assist with clinician diagnosis, treatment selection, and monitoring for progression

ACKNOWLEDGEMENTS

These studies were partially funded by R21DK106554-01 (SJW) and 1R01DK124599-01 (SJW). Ruetten was supported by T32 OD010957 and L70 DK140978.

LinkedIn

IMPROVING QUALITY OF CARE AND PATIENT-CENTERED MANAGEMENT OF URINARY INCONTINENCE

[1]Colby Souders, [1]Abbas Bader, [2]Sweta Parija, [2]Anthony Galvez, [2]Gaurav Bhushan, [1]Richard Fantus, [2]Jejo Koola, [2]Maxwell Moore, [2]Yahir Santiago-Lastra, [2]Chaztyn Pangelia, [2]Jennifer Anger

[1] University of Kansas Medical Center [2] University of California San Diego

INTRODUCTION

- UI affects over half of women and is associated with distress, impaired quality of life, and healthcare costs.
- Despite effective non-surgical treatments, UI remains underreported, underrecognized, and undertreated in primary care.
- Baseline data demonstrate gaps in patient knowledge, provider adherence to quality indicators, and clinical management.

OBJECTIVES

- Characterize baseline UI care quality, provider/patient knowledge gaps, and patient-reported symptom burden in primary care.
- Evaluate EHR-based decision support, eConsults, and APP referral pathways to improve guideline-concordant, patient-centered UI management.

METHODS

- Conducted retrospective chart reviews of 275 patients across 91 primary care providers.
- Assessed adherence to evidence-based UI quality indicators.
- Used validated surveys to measure primary care provider UI knowledge.
- Collected patient-reported outcomes assessing UI distress, quality of life, and patient knowledge.
- Implemented clinical decision-support tools, order sets, eConsults, and APP referral pathways embedded within the EHR.

“Closing care gaps in primary care is critical to improving UI outcomes for women”

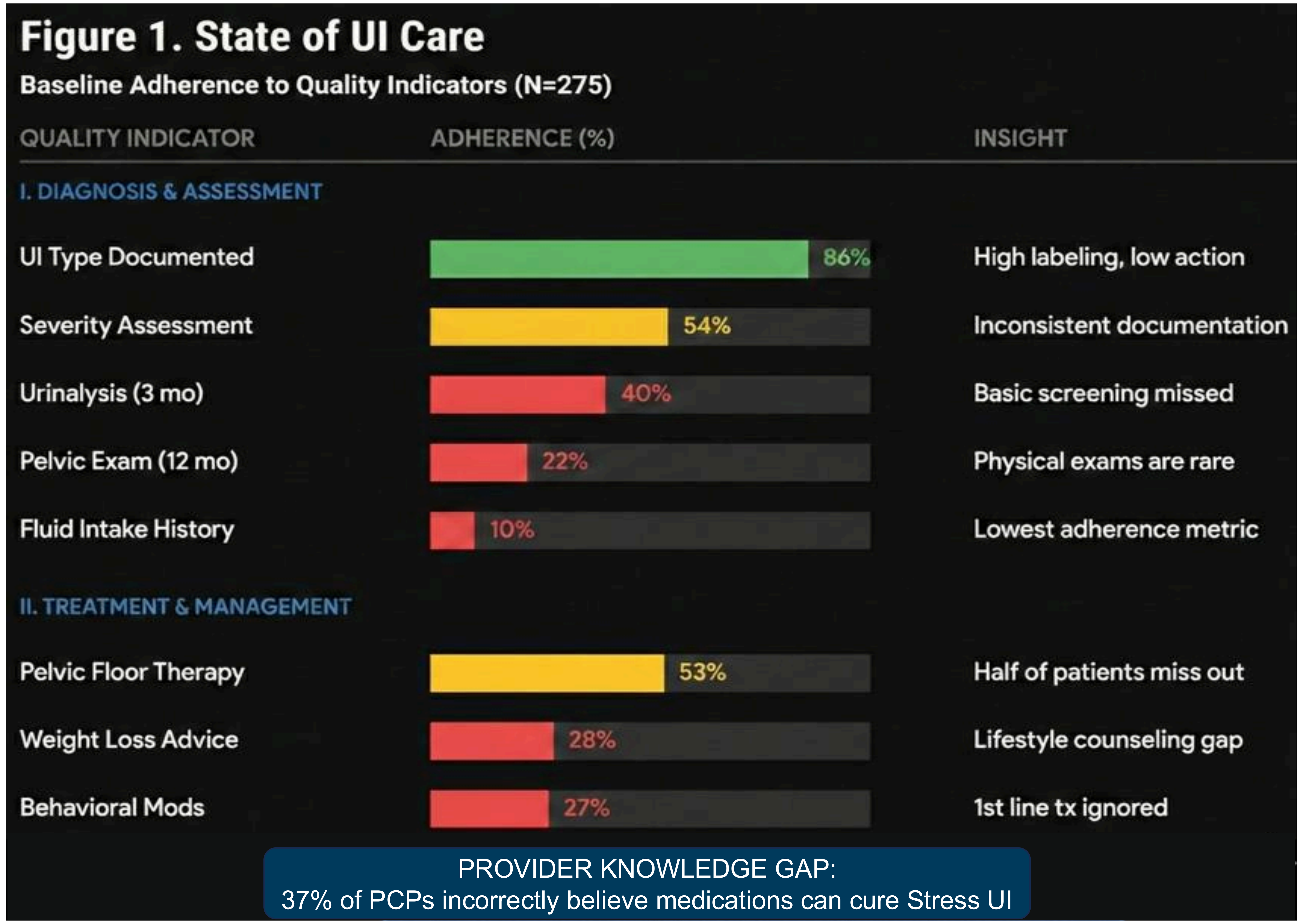

RESULTS

- Primary care providers met only 42% of expected UI quality indicators.
- Documentation of prior treatments, fluid intake, pelvic examination, and urinalysis was infrequent.
- Providers demonstrated knowledge gaps in UI subtype differentiation and management.
- Patients showed limited UI knowledge, especially regarding stress UI treatment and behavioral management of overactive bladder.
- Among screened patients, 62% reported moderate-to-severe UI distress.
- Approximately 20% reported severe impact of UI on daily living.
- Early UI-focused eConsult implementation demonstrated feasibility across multiple health systems.

CONCLUSION

- Significant provider-, patient-, and system-level gaps contribute to suboptimal UI care in primary care settings.
- Informatics-enabled tools, targeted education, and structured referral pathways may improve guideline-concordant, patient-centered UI management.
- Findings support a shift toward proactive, primary care–based UI care to improve outcomes for women affected by urinary incontinence.

FINANCIAL FUNDING

This study was funded by the Patient-Centered Outcomes Research Institute (Contract Number: UI-2021C2-23690).

AUA 2026
Washington, DC

Development of Nanoparticle-Based Magnetic Hyperthermia for Prostate Cancer

Takashi Nagai[1], Noriyasu Kawai[1], Keitaro Iida[1], Toshiki Etani[1], Taku Naiki[1], Kaname Tsutsumiuchi[2], Toyoko Imae[3], Takahiro Yasui[1]

1. Department of Nephro-urology, Nagoya City University Graduate School of Medical Sciences, Nagoya, Japan
2. College of Bioscience and Biotechnology, Chubu University, Kasugai, Aichi, Japan.
3. Graduate Institute of Applied Science and Technology, National Taiwan University of Science and Technology, Taipei, Taiwan

ABSTRACT

Treatment options for prostate cancer remain limited, underscoring the need for innovative therapeutic strategies. Our research project has focused on developing nanoparticle-based magnetic hyperthermia, which exploits the heat-generating properties of metallic nanoparticles under an alternating magnetic field. This approach enables selective heating of tumor tissues, inducing targeted cytotoxicity while minimizing collateral damage, and represents a promising alternative to conventional treatments.
To establish an effective therapeutic platform, we have developed multiple types of advanced nanoparticles, including metal–organic frameworks (MOFs), carbon nanohorns, and magnetite cationic liposomes (MCLs). These nanoparticles have demonstrated robust therapeutic performance, enabling not only magnetic hyperthermia but also chemotherapeutic delivery and photothermal or photodynamic therapy. Through these multifunctional designs, we have established a foundation for synergistic, multimodal cancer therapy capable of enhancing treatment efficacy beyond single-modality approaches.
Recently, we successfully engineered prostate-specific membrane antigen (PSMA)-targeted nanoparticles, achieving prostate cancer–specific molecular recognition and markedly improving tumor accumulation. This targeted system is expected to reduce systemic toxicity while maximizing therapeutic impact, representing a significant advancement toward clinical translation. The development of these nanoparticle platforms has been driven by strong collaboration between engineering and medical sciences, integrating materials design, surface chemistry, and cancer biology to create an ideal therapeutic architecture.
Our project represents both fundamental research in nanoparticle-based cancer treatment and a realistic pathway toward clinical application. Moreover, the versatility of MOF-, carbon-based, and MCL-derived nanoparticle systems suggests their applicability to other malignancies, expanding the potential impact of this platform across urologic and non-urologic cancers.
In summary, this multidisciplinary project bridges basic science and clinical medicine, contributing to the establishment of next-generation cancer therapies. By advancing targeted and multifunctional nanoparticles, we aim to expand treatment options for prostate cancer and nanomedicine-driven oncology.

INTRODUCTION AND OBJECTIVE

Castration-resistant prostate cancer typically exhibits a poor prognosis and limited treatment options, highlighting the urgent need for new therapies.

To address this issue, we have adopted magnetic hyperthermia for the treatment of prostate cancer by developing a novel magnetic nanoparticle.

METHODS

Development of CNH-containing magnetic nanoparticles

Combines CNH and IONP via APTES (aminopropylsilane)

CNH is treated with nitric acid to expose the -COOH group

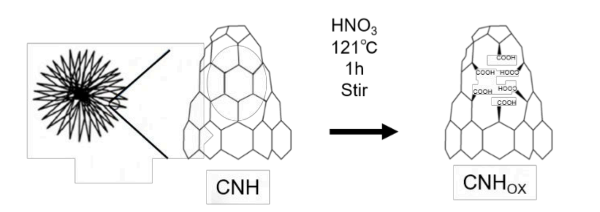

IONP and APS are combined to synthesize APS-IONP

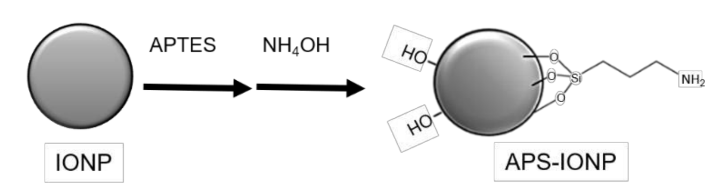

Combination of APS-IONP and CNHox to synthesize CNH-APS-IONP

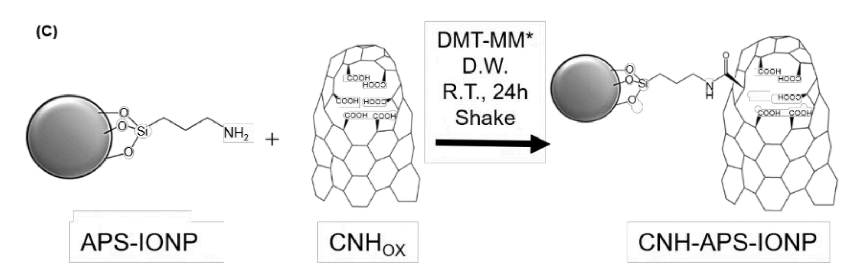

In vivo: Effects of magnetic hyperthermia using CNH-APS-IONP

Model animal: Human castration-resistant prostate cancer cell line 22Rv1 Subcutaneous transplantation model mouse

Heating method: Magnetic hyperthermiaControl (n=6), Nanoparticle injection (n=6), Nanoparticle injection + magnetic field irradiation (n=6)

(a) CNH-APS-IONP were injected locally around the tumor
(b) Heating by coiled AC magnetic field irradiation for 2 days
(Tumor temperature was measured using infrared thermography)
(c) Tumor size was measured 7 days after the hyperthermia treatment.

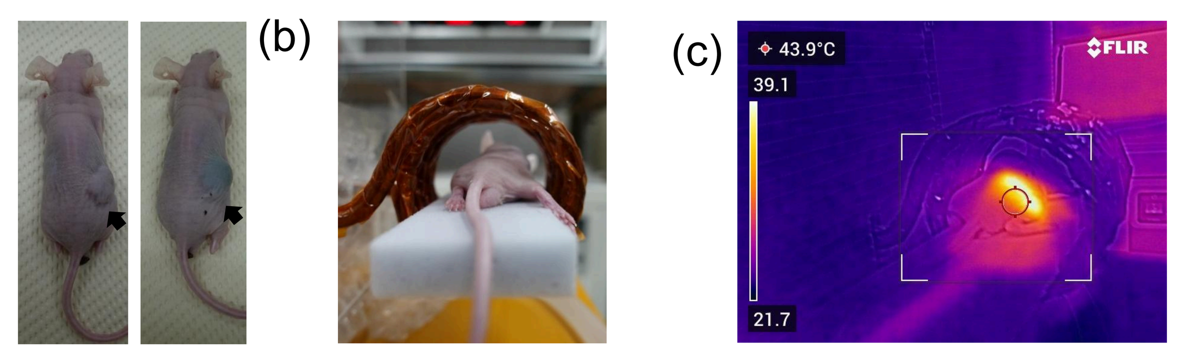

Ki-67 labeling index was used as an immunohistological test to evaluate proliferative potential.

In vitro: Molecular design of antibody-conjugated magnetic nanoparticles using a PSMA-targeting ligand

・A peptide-like small molecule in which the α-amino groups of Glu and Lys are linked via a urea bond
・Reported to exhibit high affinity for PSMA (prostate-specific membrane antigen)

Polyglycerol-coated IONP (PG-IONP)

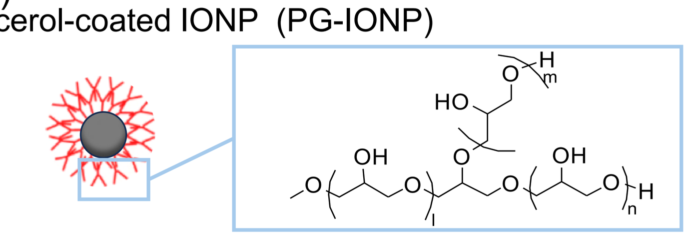

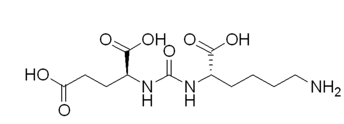

GUL (Glu-Urea-Lys)

N-(2-Aminoethyl) maleimide (AEM)

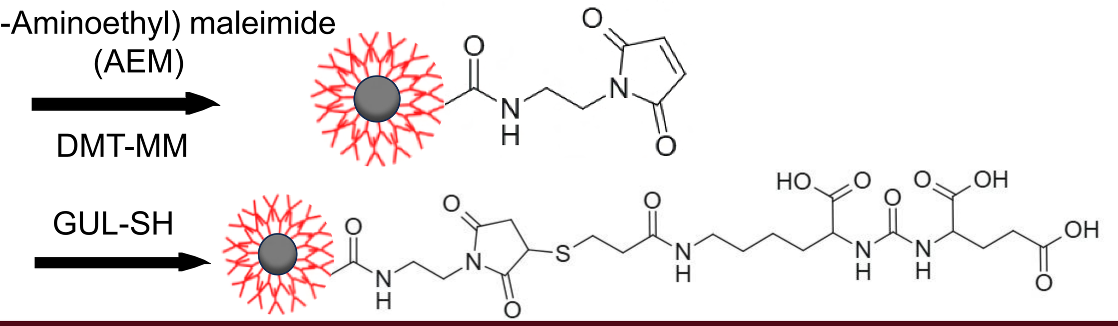

RESULTS

Characterization of CNH-APS-IONP

Measurement of nanoparticle size by dynamic light scattering

Sample	Particle size*
CNHox	213 ± 24 nm
IONP	79 ± 38 nm
CNH-APS-IONP	238 ± 67 nm

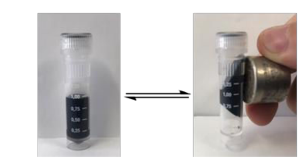

*Mean ± SD

Infrared absorption spectroscopy

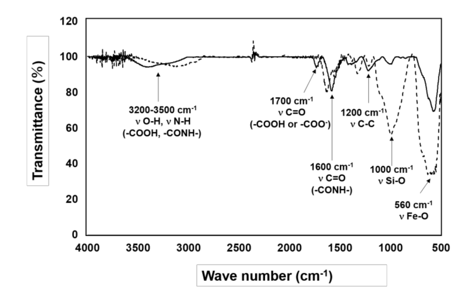

TEM and energy dispersive X-ray analysis (Bars: 100 nm)

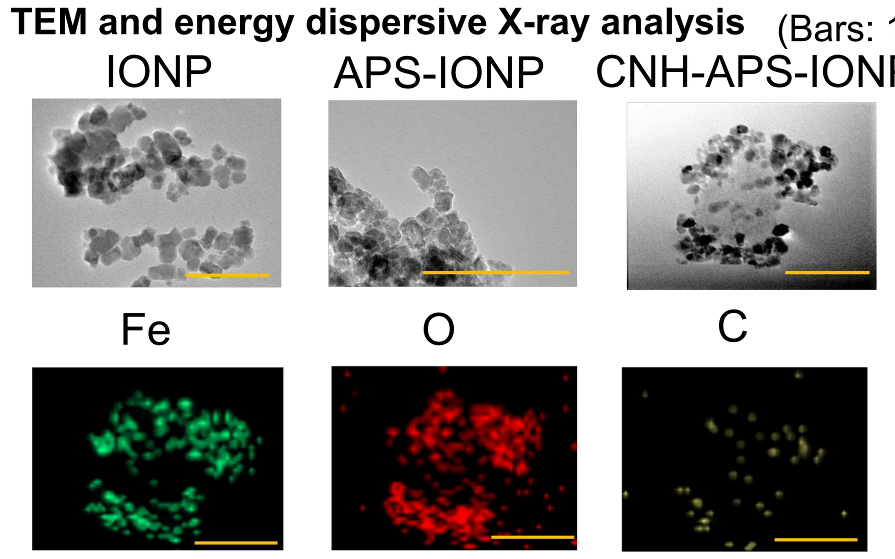

Thermotherapy Effects

Tumor and rectal temperature under AMF

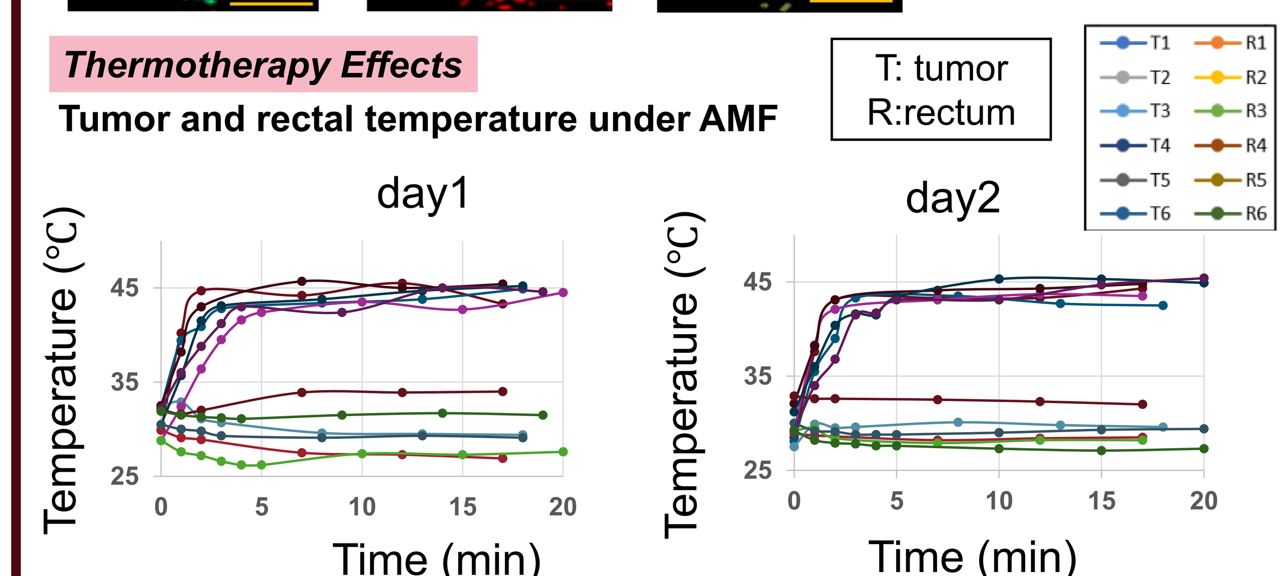

Course of tumor size in each group

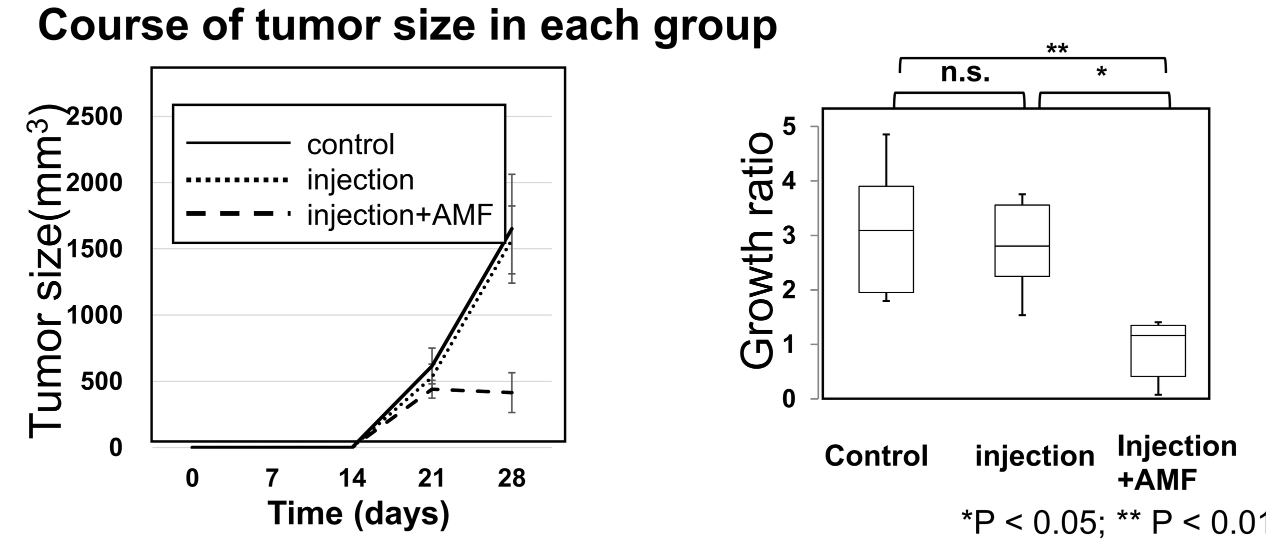

*P < 0.05; ** P < 0.01
(Kruskal-Wallis test)

RESULTS

Pathological features

<H-E staining>

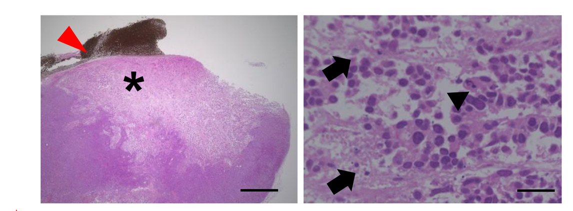

CNH-APS-IONP
* Tumor Regression Site (Bar: 1000 μm)
pyknosis
nuclear rupture (Bar: 25 μm)

<Ki-67staining>

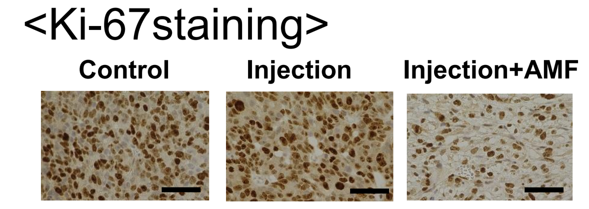

(Bar: 50 μm)

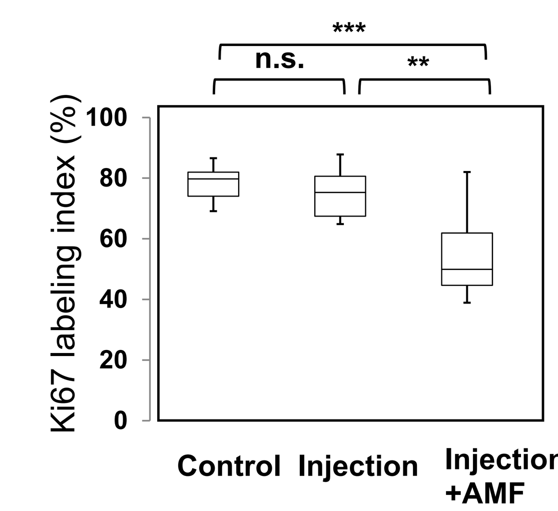

P < 0.01;* P < 0.001
(Kruskal-Wallis test)

Synthesis of GUL ^{13}C-NMR

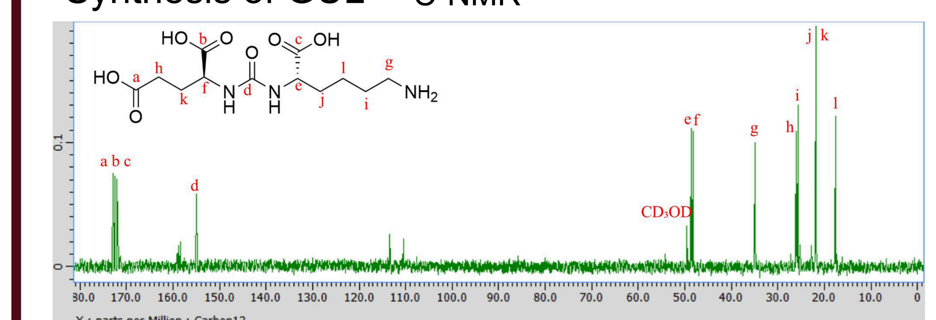

Introduction of a thiol group LC-MS/MS

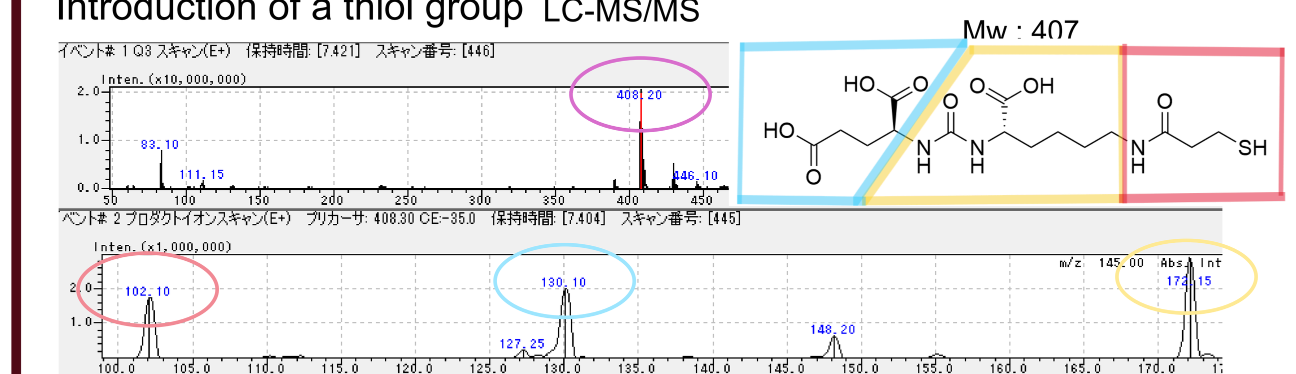

Calculation of the loading amount of GUL-conjugated PG-IONPs

Sample	Lys conc., ppm	Conjugated GUL, ligand/IONP	Corrected values of conjugated GUL[a], ligand/IONP
GUL + PG-IONP mixture	0.050 ± 0.030	870 ± 520	0
GUL-AEM-PG-IONP-2000	0.17 ± 0.04	3000 ± 700	2100 ± 700
GUL-AEM-PG-IONP-300	0.068 ± 0.020	1200 ± 400	300 ± 400

[a] Corrected by subtracting GUL adsorption (GUL + PG-IONP mixture) values.

DISCUSSION AND CONCLUSION

・CNH is reported to have low toxicity and is useful as a drug carrier, suggesting its potential as a nanoparticle that can be used in hyperthermia.
・However, the nanoparticles did not bind or accumulate specifically to prostate cancer, and the treatment of prostate cancer with multifocal lesions is a challenge.
・We have succeeded in developing nanoparticles that can generate heat under an alternating magnetic field and contain an anticancer drug, and we would like to apply them to prostate cancer in the future.
・Furthermore, GUL, which exhibits prostate cancer cell–targeting properties, was selected as a ligand to guide PG-IONPs to tumor sites, and we successfully prepared GUL-conjugated PG-IONPs.

Funding: NIDDK: K12 -DK111011-06 (Sarma PI) NIDDK R01 SUITOR 1R01DK144017-01 (Ippolito PI)

UROLOGY

Barriers, Decision-Making & Utilization of Minimally Invasive Therapies for Overactive Bladder

Bridging Patient, Clinician, and Policy Perspectives

Giulia M. Ippolito, MD, MS · *University of Michigan, Department of Urology, Ann Arbor, Michigan*

Background

- Overactive bladder (OAB) is a chronic syndrome marked by urinary urgency with or without urgency urinary incontinence, frequency, and nocturia.
- OAB symptoms affect up to 43% of adults, but despite high prevalence, OAB remains undertreated.
- **The 2024 AUA/SUFU Guideline found no evidence supporting traditional step therapy approaches but rather emphasizes shared decision-making (SDM) and individualized care.**
- **A critical gap exists to define effective strategies to provide patient centered and personalized care in OAB in the post-step therapy era.**

Aims: To facilitate **personalized, patient centered care** for patients with **Overactive Bladder** through **health services research**

1. Identify, quantify and decrease barriers to diagnosis and treatment
2. Enhance patient and clinician education and decision making through evidence-based medicine

Methods

1. Decision-making dynamics (Sitto et al. 2024)

Sequential explanatory mixed-methods study with surveys and semi-structured interviews of patients with OAB (n=20) and physicians treating OAB (n=12). Inductive/deductive coding to thematic saturation; integration with Health Belief and Ecological models.

2. Population-level Minimally Invasive Therapy (MIT) uptake (Li et al, under review. , AUA #26-3009)

Retrospective claims analysis of the LUGPA database and University of Michigan (UM) database.

LUGPA: 41 independent community urology practices, 2020–2023. Cohort is 419,041 patients

UM: Tertiary Care Academic Hospital. 2012-2021. 5300 patients

Patients with ICD-10 OAB diagnosis (N32.81, N39.41, N39.46) included; neurogenic, retention, and malignancy excluded. Kaplan-Meier and Cox proportional-hazards models for time to first MIT (CPT 64561, 64566, 64581, 64585, 64590, 52287). with diagnosis of OAB in 41 practices.

3. Therapeutic trajectories (Zheng et al., Under review)

Single-institution retrospective cohort. Idiopathic OAB patients receiving an index minimally invasive therapy (MIT); 3-year follow-up for additional therapy. Multivariable logistic regression for predictors of additional therapy. Single-institution OAB cohort post-MIT

Results:

1. Decision-making dynamics (Sitto et al. 2024)

Theme	Representative patient quotes	Representative physician quotes
Frustration with inaccessibility of OAB treatments	We have a $40 copay each time we go [to physical therapy]. Don't waste two years of somebody's life suffering while you are testing different medications."…	I would [start third-line therapy right away] if I could. I'm limited by insurance companies. Some patients, they say, "Okay, let's do Botox," or, "let's do the neuromodulator." If they're completely treatment naïve, then we have to go through at least one, if not two, medications by insurance criteria.
Discordant perception of patient education	When you start to talk in medical terms, I tell them, you know, you have to talk on my level. You know, talk English. And a lot of times they can do it. And a lot of times, I don't know, they just get frustrated too, I guess.	I used to go through, in depth, everything for third line with them. I don't always have time for that anymore, so I'll just set the stage as a, "We'll try this. If it doesn't work, I have other options," and then save third-line counseling for the next visit.
Diverging acceptability of expected outcomes	Yeah. I thought I was going to be healed. I thought I would be cured, I thought I wouldn't have… I didn't think I would be where I'm at today. Just 50% better doesn't seem like good enough to me.	I tell them, "Success means that these people who had it, their urinary leakage or urgency improved so much that they thought it was a success, and they'd recommend it to other people." I really, really stress, for all of them, that the goal is a 60% improvement in symptoms.
Lack of insight into other parties' decisional priorities and control preferences	I should have gotten in there and read more. Instead of relying so much on the doctor. You know, it was like, if he said jump, I would jump. I should have taken matters into my own hands, maybe, and gotten through this process faster. I will always keep bringing it up and asking if there is anything new on the market. And always having a discussion around it, to make sure I'm not missing something.	[I] just have a general idea of how risky it is for them to have Botox, and how likely that they will have retention. I use that to also steer patients one way or another. We say all the options are appropriate for someone, but usually I think depending on the symptoms the patient has and the clinical history, I don't think all the options are equally good for any patients. There's usually one option that I think it's a little bit better.

Most Common Factors driving OAB decision making:

Patients (n=20)	Physicians (n=12)
1 Invasiveness	1 Safety / contraindications
2 Efficacy	2 Cost & insurance
3 Risks / side effects	3 Convenience
4 Cost & insurance	4 Patient decisional priorities
5 Convenience	5 Symptom severity
6 Doctor recommendation	6 Invasiveness
7 Addressing root cause	7 Efficacy

2. Predictors of MIT uptake (Li et al)

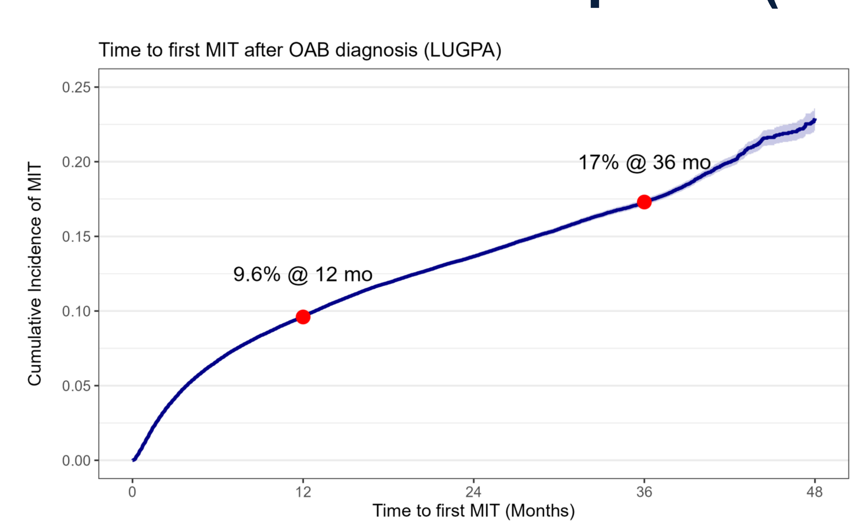

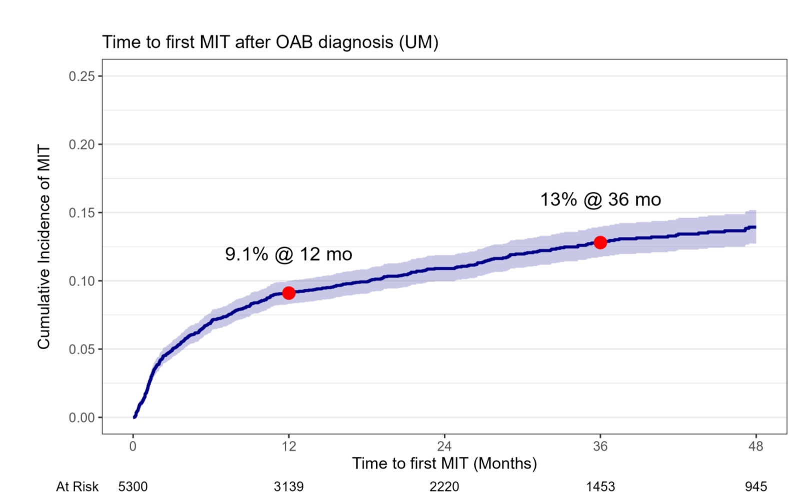

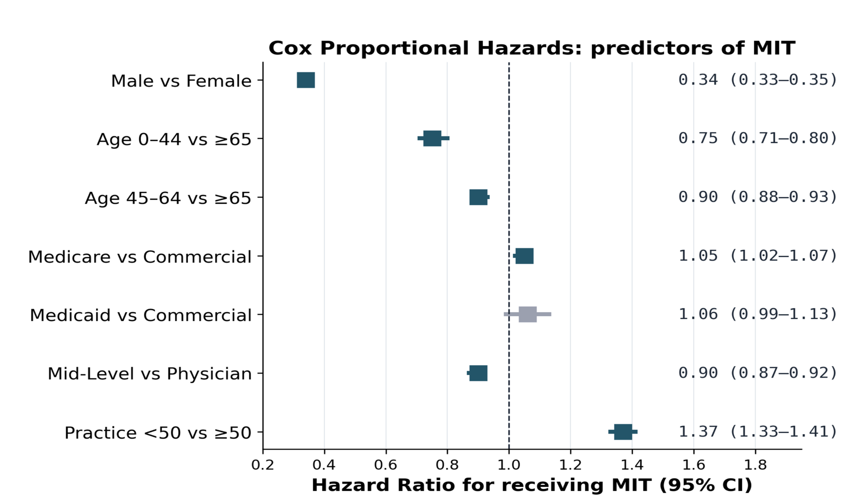

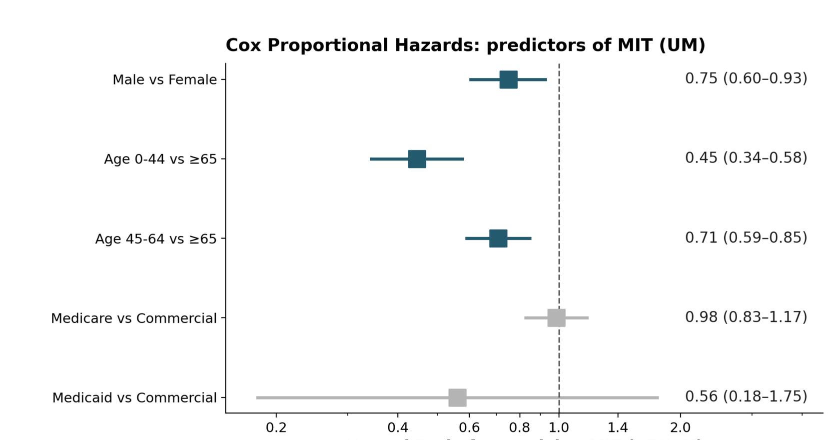

3. Therapeutic Trajectories (Zheng et al.)

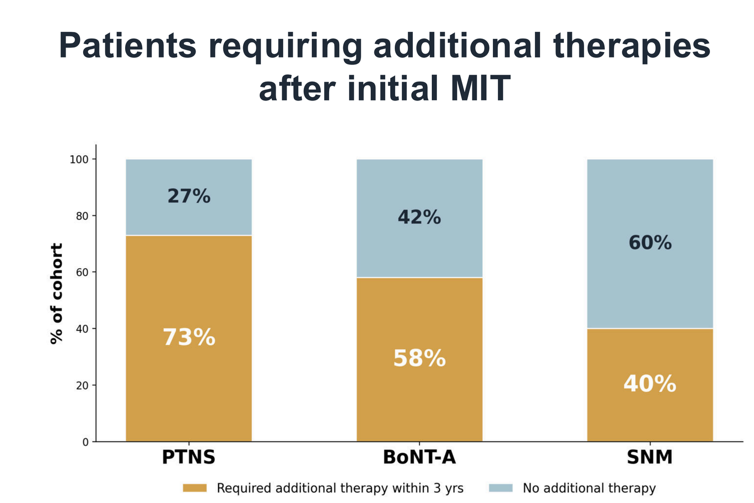

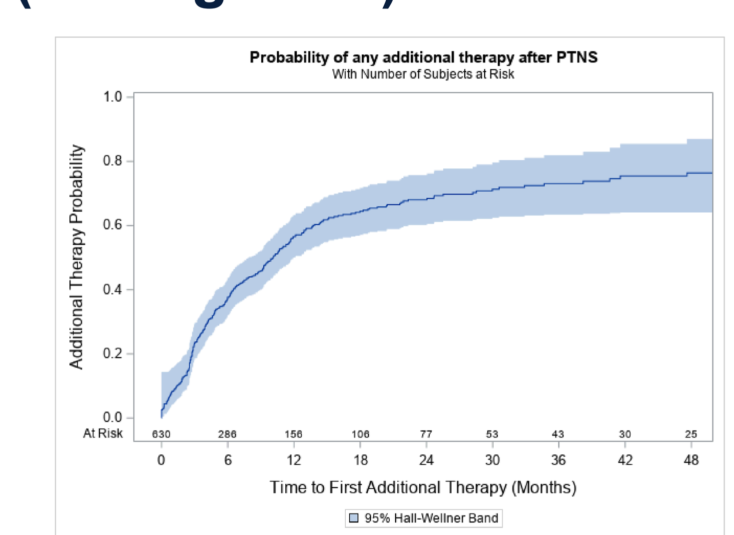

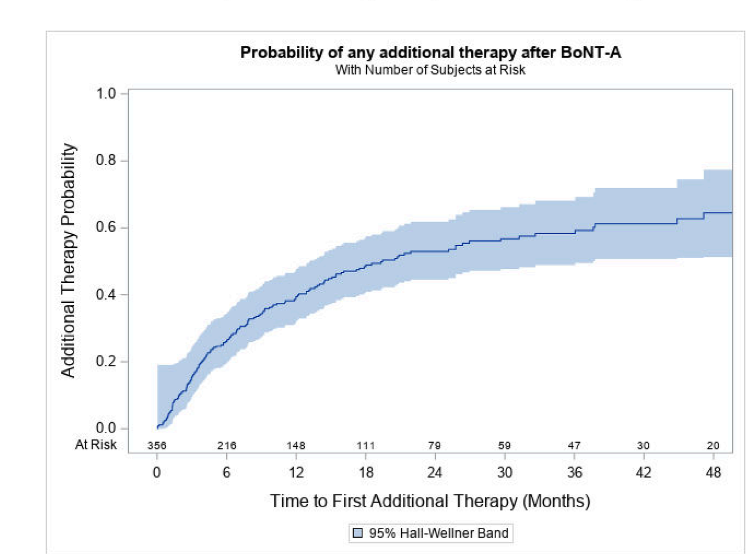

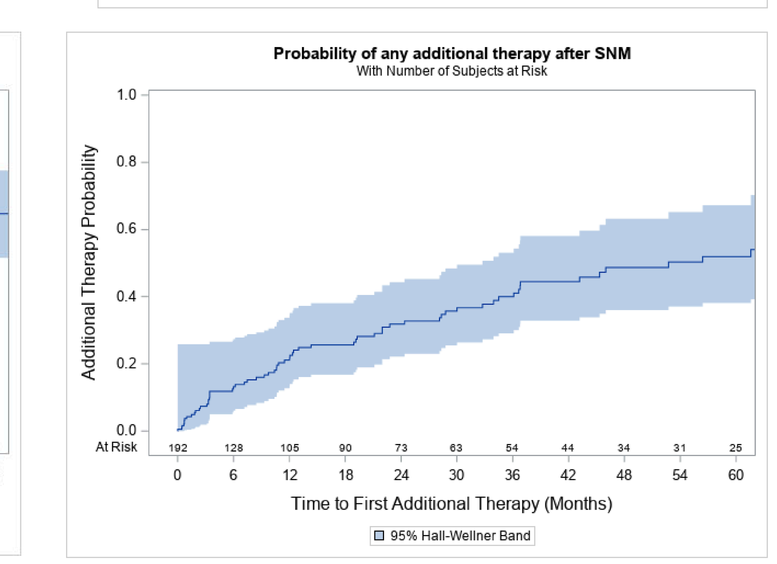

Conclusions

- **Clinicians and patients are frustrated by the current OAB care paradigm.**
- **Transparency in treatment goals and decisional priorities may improve patient centered care.**
- **Real-world MIT use within a contemporary LUGPA and UM cohorts is 9-10% at 1 year and 13-17% at 3 years.** Patients wait years for therapy, most never get them.
- **MIT is rarely a definitive endpoint, and is a therapeutic tool in a chronic syndrome.** Nearly half of patients require additional therapy within 3 years
- **Implications for transitioning from step therapy to a treat-to-target paradigm that offers patient centered care through a transparent, symptom severity and goal-based approach.**

References

1. Sitto HM, Brodsky CN, Wittmann D, et al. Patient and physician decision-making dynamics in overactive bladder care: A mixed methods study. Neurourol Urodyn. 2024. doi:10.1002/nau.25416
2. Li AN, Sridhar R, Sui W, Seibel C, Goldfischer E, Dowling RA, Ippolito GM. Incidence of and time to MIT among patients with idiopathic OAB. AUA Annual Meeting; 2026. Abstract #26-3009.
3. Zheng Y, Daignault-Newton S, Barboglio-Romo P, et al. PD33-05 Natural history of idiopathic OAB after sacral neuromodulation. AUA Annual Meeting; 2023.
4. Cameron AP, Chung DE, Dielubanza EJ, et al. AUA/SUFU Guideline on the diagnosis and treatment of idiopathic OAB. J Urol. 2024;212(1):11-20.

ECIS-12

Efficient Stepwise Differentiation of Human iPSCs into Long-Lived Leydig-Like Cells with Enhanced Testosterone Production for Potential Late-onset hypogonadism Therapy

Sato K.[1,2], Aoi T.[2], Miyake H.[1]

1) Division of Urology, Graduate School of Medicine, Kobe University, Kobe, Japan
2) Division of Stem Cell Medicine, Graduate School of Medicine, Kobe University, Kobe, Japan

Background

Late-onset hypogonadism results from age-associated testosterone decline and remains dependent on testosterone replacement therapy, which provides only transient effects. Cell-based therapy using human induced pluripotent stem cell (iPSC)-derived Leydig-like cells (LLCs) represents a promising alternative, but conventional differentiation protocols show limited efficiency, insufficient steroidogenic activity, and short cellular lifespan.

Objective

This study aimed to develop a stepwise differentiation protocol that improves Leydig lineage commitment, enhances steroidogenic maturation, and generates LLCs with stable long-term testosterone secretion suitable for therapeutic applications.

New Regenerative Therapy for Hypogonadism.

human iPSCs

Testosterone-secreting Leydig-like cells: LLCs

Patients with Hypogonadism

Stepwise differentiation protocol of hiPSCs into Leydig-like cells (LLCs)

＊NR5A1: Master regulator for Leydig cell differentiation

Achieved a 22-fold increase in testosterone production over the conventional protocol

Method for Forced Expression of NR5A1
Tet-On System
Tet-Off System

Testosterone (ng/mL)
600
400
200
0
Conventional
Improved

LLCs generated by the improved protocol survived for more than 16 weeks.

Tet-Off (Improved)
Tet-On (Improved)
Tet-On (Conventional)

Testosterone (ng/ml)
600
400
200
0
0 5 10 15
Weeks of Differentiation

scRNA-seq analysis revealed that the transcriptomic profiles of LLCs are highly similar to those of primary Leydig cells.

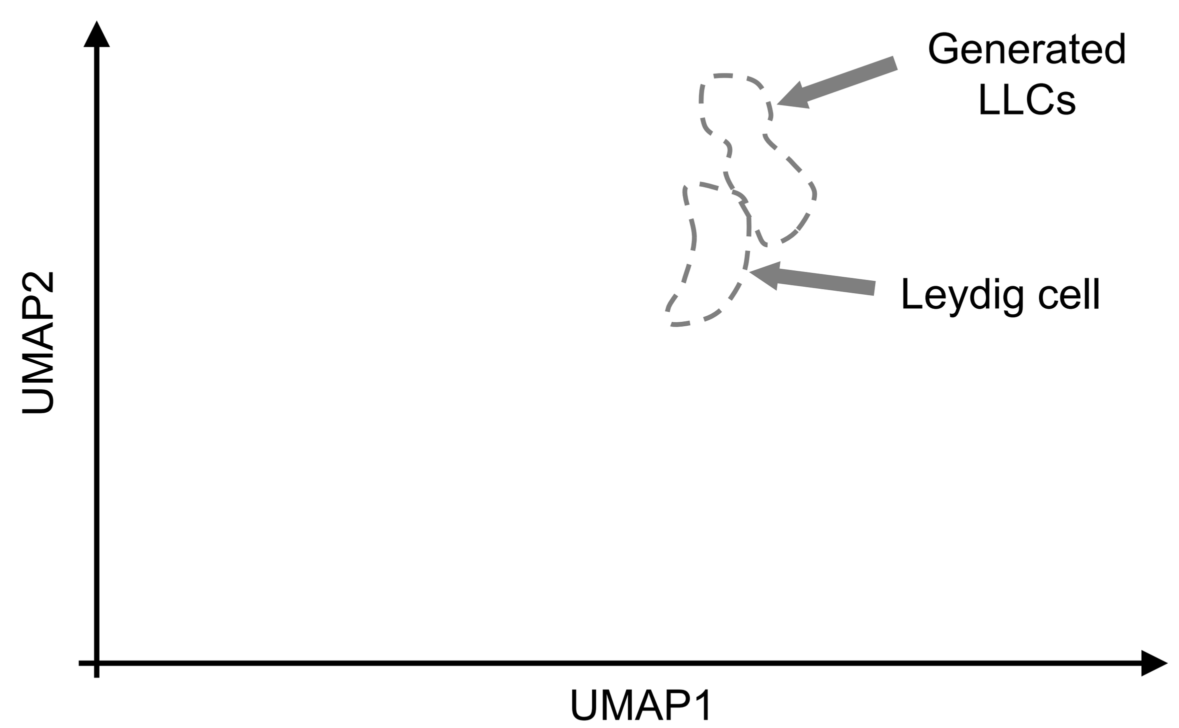

Achieved high differentiation efficiency : >99% of cells positive for Leydig cell marker s

HSD17B3
LHCGR
CYP17A1
STAR
normal IgG
Hoechst (nuclear)

Transplantation of LLCs into immunodeficient mice: Cell engraftment and elevation of serum testosterone

Luciferase
Transplantation
Control

Testosterone (ng/mL)
0.10
0.05
0.00
Transplant Control

The findings presented in this study were published in:
Sato et al., "Efficient differentiation of human iPSCs into Leydig-like cells capable of long-term stable secretion of testosterone," *Stem Cell Reports*, 2025.

We have no conflicts of interest related to this presentation.

Lineberger Comprehensive Cancer Center

Dissecting the spatial architecture of plasmacytoid urothelial carcinoma to inform therapeutic strategies

Kathryn H. Gessner[1,2,3], Siyao Liu[1], Mi Zhou[1], Jeffrey S. Damrauer[1,5], David Corcoran[1,3], Sara E. Wobker[4], William Y. Kim[1,5]
University of North Carolina Lineberger Cancer Center[1], Departments of Urology[2], Genetics[3], Pathology[4], Medicine[5]; Chapel Hill, NC

Background

- Plasmacytoid urothelial carcinoma (PUC) is a rare and aggressive histologic subtype of bladder cancer
- Histologically, this variant is defined by dyscohesive cells with scant cytoplasm and eccentric nuclei, reminiscent of plasma cells.
- PUC is frequently identified as a mixed variant with conventional urothelial carcinoma (CUC).
- PUC demonstrates a poor response to standard chemotherapy.
- Patients with PUC demonstrate a lower median overall survival compared to patients with CUC (24 vs 154 months, p < 0.01, Diamantopoulous *et al.*)
- Loss of E-cadherin is the canonical molecular alteration in PUC (Al-Ahmadie *et al.*, 2016).
- In other solid tumors, epithelial to mesenchymal transition is associated with alterations in the tumor microenvironment (TME).

Hypothesis

We hypothesize E-cadherin loss in PUC promotes an altered TME, creating therapeutic vulnerabilities.

Acknowledgements

This project was supported by the Bladder Cancer Advocacy Network, the North Carolina University Cancer Research Fund, the UNC Physician Scientist Training Program, and the National Institutes of Health (UNC Oncology K12 2K12CA120780).

Contact

kathryn_gessner@med.unc.edu
www.gessnerlab.com

Unpublished data. Do not post.

Results

H&E (left) and immunohistochemistry for E-cadherin (right) confirm mixed CUC + PUC histology with loss of E-cadherin in PUC region.

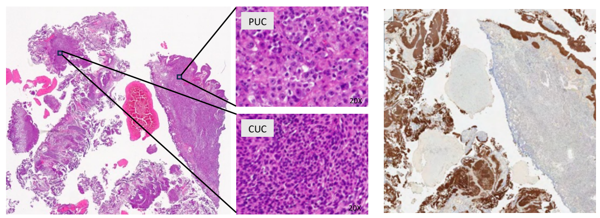

Precise mapping of cell types across mixed PUC + CUC tumor.

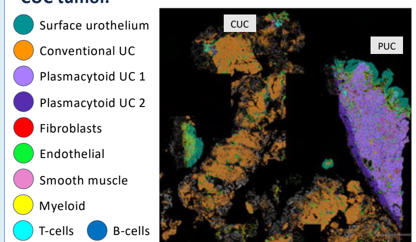

PUC shows loss of CDH1 and increased mesenchymal gene expression vs. CUC

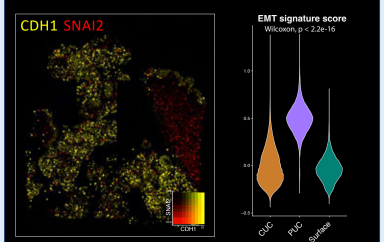

PUC demonstrates increased immune infiltration vs CUC

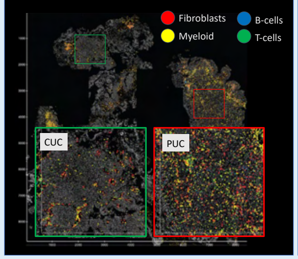

Neighborhood analysis identifies PUC-specific cell co-localization

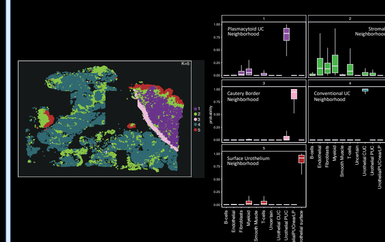

Subclustering of urothelial cells in snRNAseq data identifies distinct transcriptomic clusters enriched in PUC

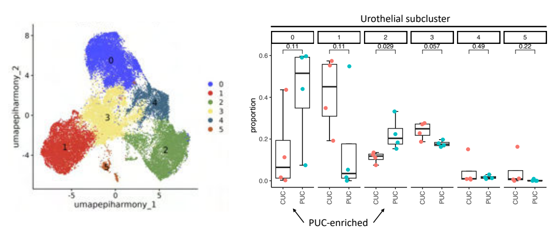

PUC demonstrates increased tumor cell - macrophage signaling

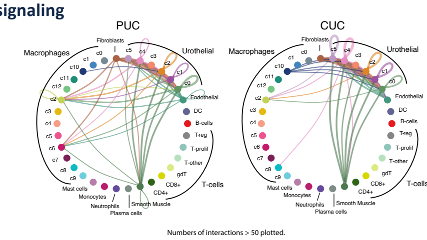

Conclusions

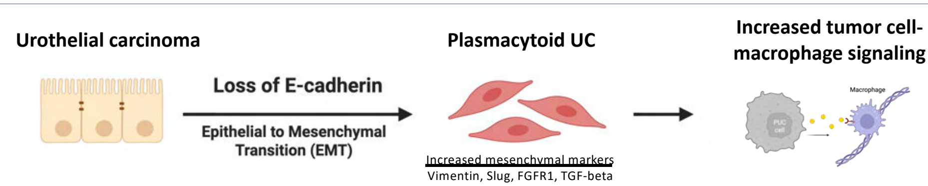

We hypothesize that this leads to immune evasion, metastasis, and therapeutic resistance.

Methodology

10X Genomics Xenium Spatial Transcriptomics performed on 4 FFPE tumors (2 PUC, 1 CUC, 1 CUC + PUC).

Gene panel: 477 total genes
377 multi-tissue and cancer, 100 custom

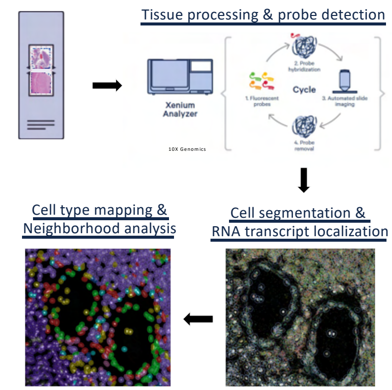

Neighborhood analysis on mixed PUC + CUC tumor performed using HoodScanR.

10X Genomics Single Nuclear RNA sequencing (snRNAseq) on 4 CUC, 4 PUC, and 4 mixed tumors. Data was integrated using Harmony and cell types assigned by canonical markers. CellChat used for cell communication analysis.

Future Directions

What mechanisms are driving the TME differences and macrophage signaling?

What molecular pathways are involved in tumor cell - macrophage crosstalk?

Can we target the TME to improve therapeutic efficacy and clinical outcomes for patients with PUC?

Development of a preclinical model of PUC to interrogate novel mechanistic and therapeutic vulnerabilities.

AUA 2026 Washington, DC

A wicked learning environment: calibration failure in surgical expertise

Ashwin Ramaswamy MD MPP, Runzhuo Ma MD,, Michael A. Gorin MD, Alexis E. Te MD, Steven A. Kaplan MD, Jim C. Hu MD MPH, Andrew J. Hung MD

INTRODUCTION

Surgeon-to-surgeon variation in functional recovery after radical prostatectomy ranges from **8-49%** at a single high-volume center, even after adjusting for patient factors.

Expertise calibrates against feedback. In surgery, feedback is delayed, noisy, and tangled with patient biology making radical prostatectomy a potentially **"wicked" learning environment** where experts may never converge on what works.

We asked whether 32 internationally recognized surgeons share a coherent understanding of nerve-sparing technique when **viewing identical operative footage**.

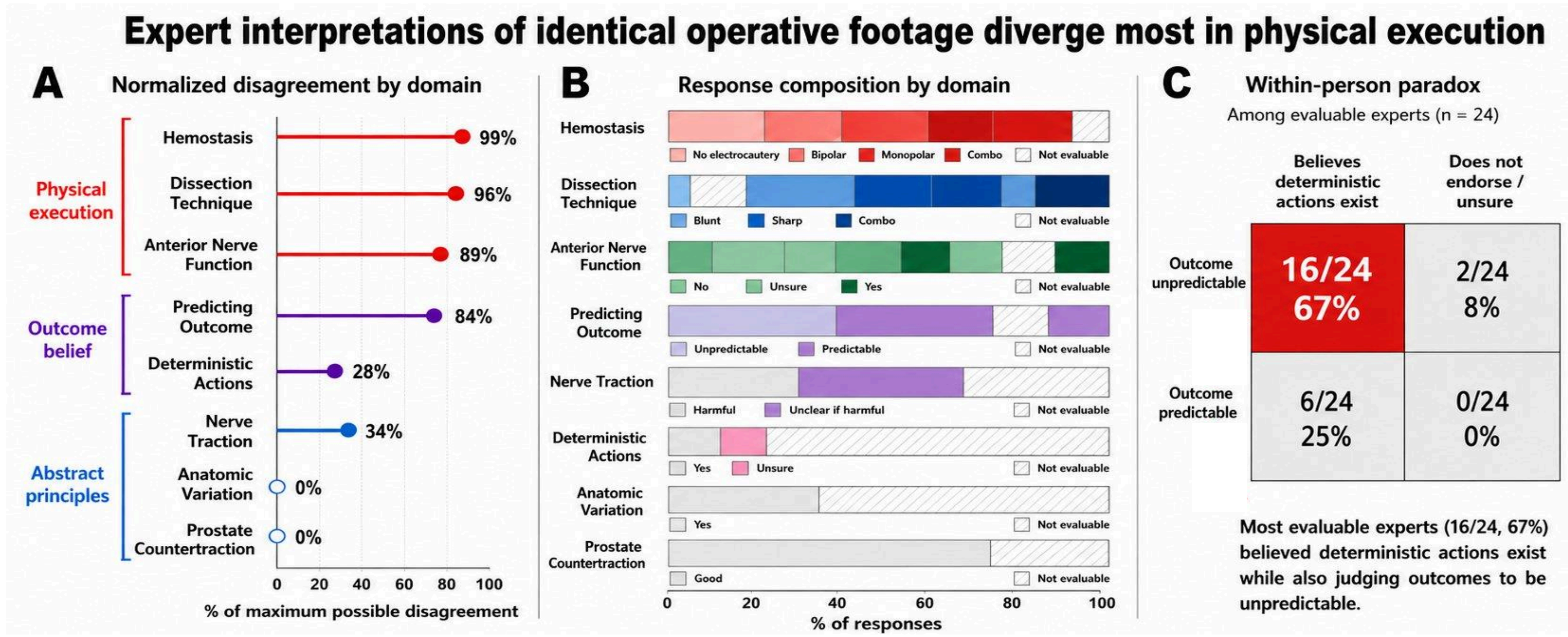

METHODS

Design. Controlled stimulus-evaluation experiment. 32 surgeons reviewed identical, footage of the nerve-sparing step of RARP

Sampling. Multistage purposeful sampling (criterion + maximum-variation + intensity + snowball). Eligibility: ≥5 yrs post-training, regular RP practice, academic appointment.

Coding. Free-form play-by-play commentary & standardized timestamped prompts. 23 hrs of footage coded line-by-line in NVivo. 25% double-coded; 96% raw agreement, κ = 0.77–0.94.

Quantification. Simpson's Diversity Index (D), normalized to % of theoretical maximum for cross-domain comparison. Prespecified: consensus D ≤ 0.20; divergence D ≥ 0.50.

RESULTS

Cohort. 32 surgeons, 24 institutions, 9 countries. Median 16 yrs post-training. 75% Professor/Chair.

Pairwise agreement collapsed along the abstraction gradient. Surgical principles: 79% (256/325) vs. surgical execution: 7% (24/351).

Consensus on principles (D ≤ 0.18). Anatomic variation, countertraction, and traction-as-harmful (91%); yet 83% said traction is "unavoidable."

Near-maximal divergence on execution (D = 0.62-0.68; 89-99% of theoretical max). Anterior nerve, sharp/blunt, electrocautery.

Within-person paradox. 92% said maneuvers determine recovery; 70% said outcomes cannot be predicted from it. **67% (16/24)** endorsed both.

CONCLUSIONS

Field-level calibration failure. Despite shared abstract principles, expert judgment on physical execution diverged at 89-99% of the theoretical maximum.

Clinical implications. Wide surgeon-to-surgeon-level outcome variation may reflect different operational definitions of optimal technique rather than differences in skill. Existing technical quality metrics do not resolve this divergence.

AI implications. Supervised models trained on near-maximally contested expert annotations risk encoding disagreement rather than resolving it. Outcome-anchored learning that bypasses contested labels warrants prioritization.

ACKNOWLEDGEMENTS. Urology Care Foundation, Robert J. Krane Resident Research Award
DISCLOSURES. The authors declare no competing interests.

COLUMBIA
Columbia University
Department of Urology

A Tumoroid Assay for Predicting Intravesical Therapy Response in Low-Grade Non-Muscle Invasive Bladder Cancer

AUA 2026
Washington, DC

Benjamin I. Joffe, John R. Christin, Jingqiang Wang, Clementine Le Coz, Nancy Wei, Caroline Laplaca, G. Joel DeCastro, Christopher B. Anderson, James M. McKiernan, Michael M. Shen, **Andrew T. Lenis**
Department of Urology, Columbia University Irving Medical Center, New York, NY

BACKGROUND

- Low-grade non-muscle invasive bladder cancer (LG NMIBC) has a high risk of recurrence despite current treatments.
- Multiple adjuvant intravesical chemotherapy options are available, but limited data exists to guide selection for a specific tumor and patient.
- Patient-derived organoids (PDOs) are three-dimensional culture models that replicate the histology, genomics, and drug responses of the parental tumors.
- **We utilized established PDOs and short-term patient-derived tumoroids (PDTs) to test an *in vitro* response assay to chemotherapy agents frequently used for LG NMIBC.**

METHODS

- Established PDOs and fresh PDTs were treated with serial dilutions (0.125uM to 10uM) of chemotherapy agents and left to incubate over five days.
- On day five, a cell viability assay (CellTiter-Glo, Promega) was performed to create dose response curves for each agent.
- Area under the curve (AUC) was calculated with lower numbers representing better drug efficacy.
- Response was defined as achieving growth inhibition of 50% at any drug dose.

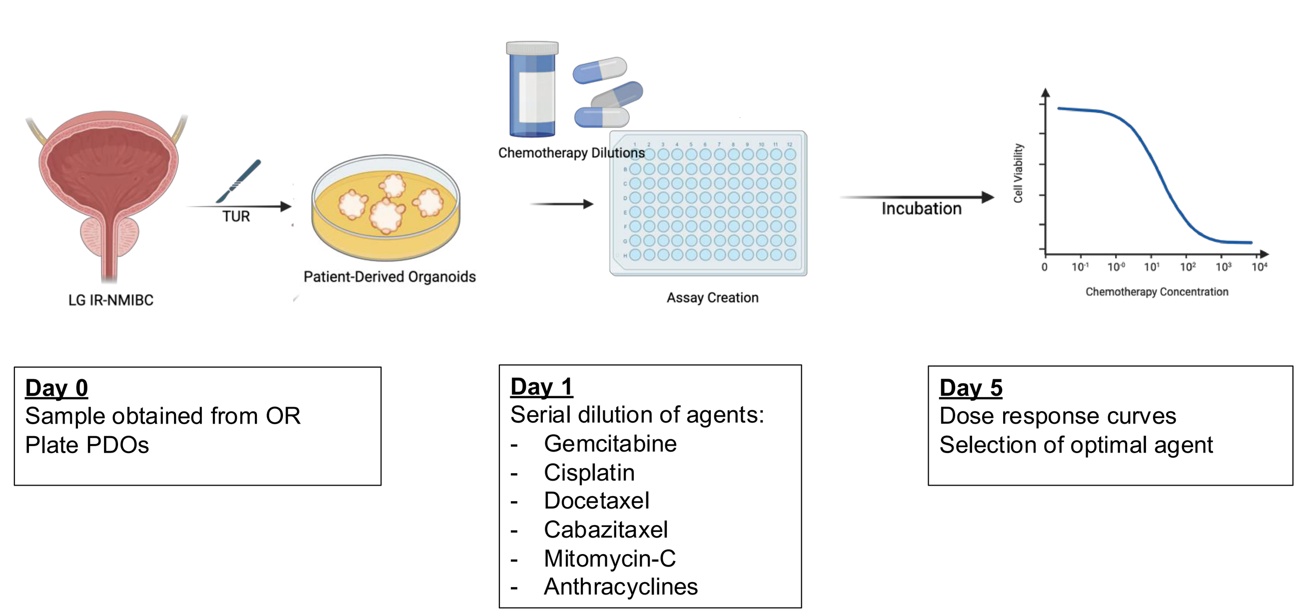

- In the prospective cohort (n=17), *in vitro* response data was correlated with clinical responses to adjuvant chemotherapy.
- To investigate mechanisms of response and resistance, bulk RNA sequencing was performed on parental tumor tissue and correlated with response to various chemotherapy agents.
- The cohort was 76% male, median age 75 years, 52% LG with a component of HG, and the median follow up was 10 months.

RESULTS

Area under the curve, growth inhibition 50% responses, and percent of samples with response in fresh PDTs (n=17) treated on Day 1 after obtaining the sample. Notably, gemcitabine was effective in only 50% of samples tested.

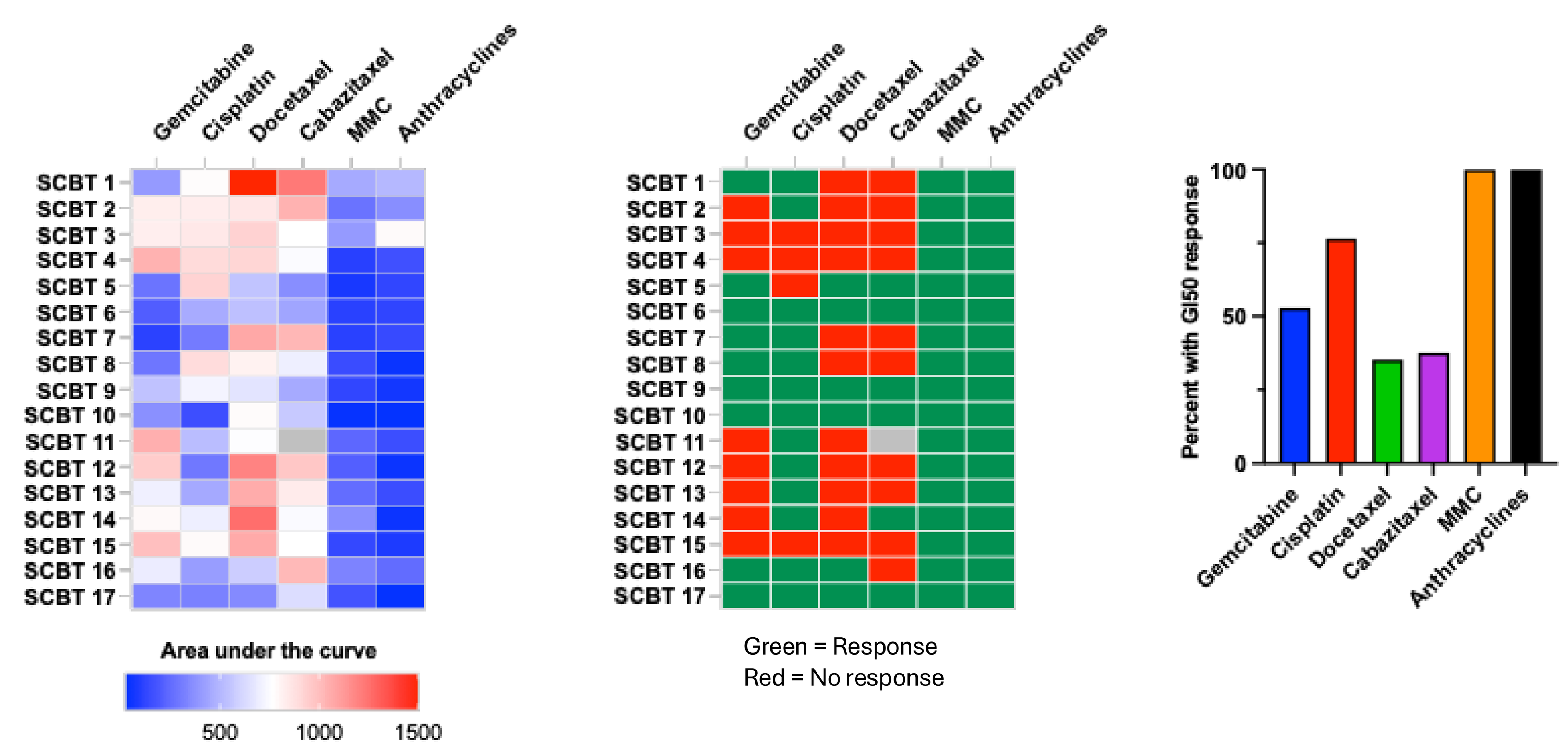

Swimmer's plot of n=17 patient outcomes and their corresponding in vitro responses. Correlation noted between in vitro gemcitabine responses and clinical outcomes in patients treated with gemcitabine-based adjuvant therapy.

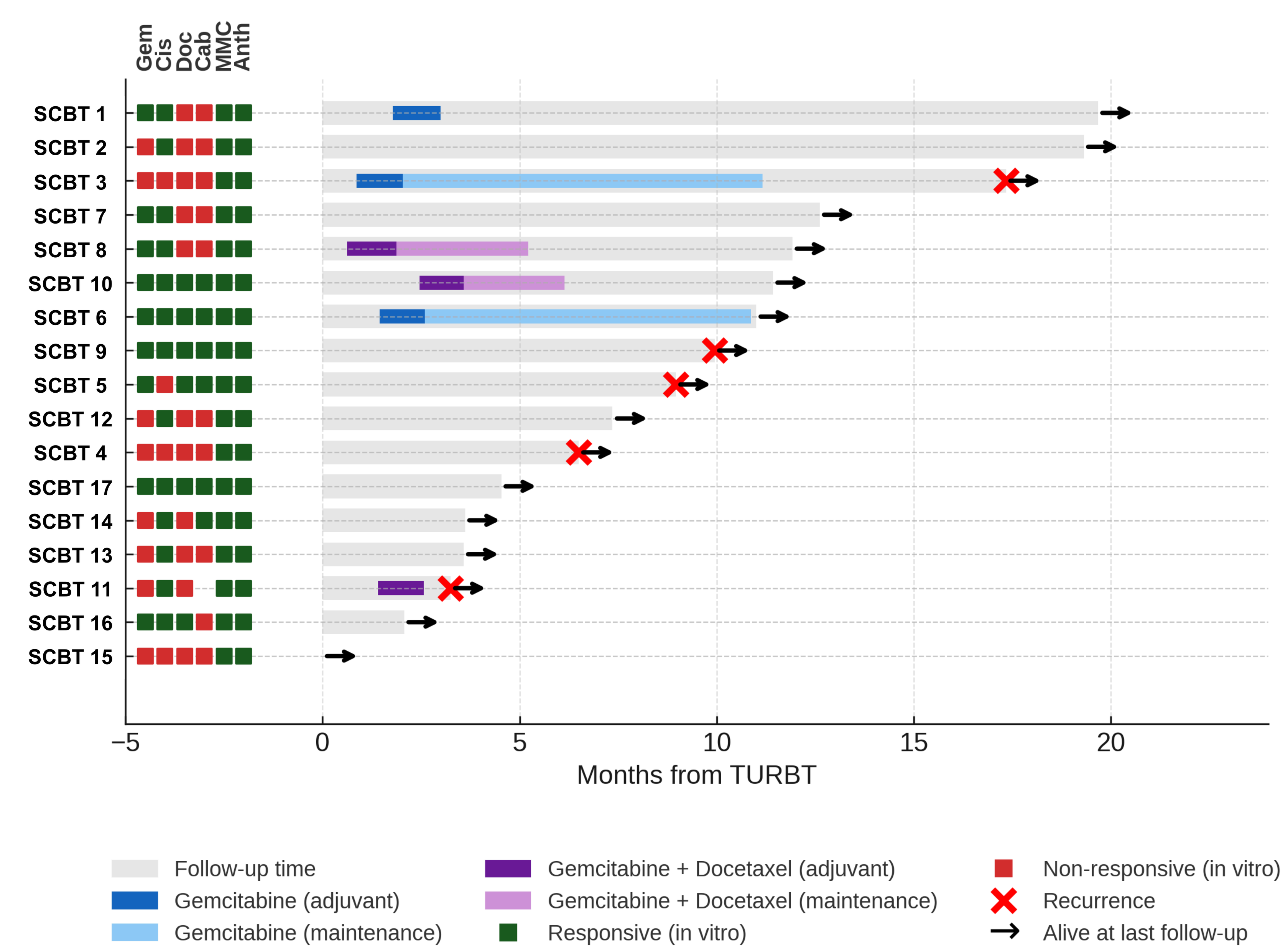

The in vitro assay performed similarly on established PDOs from patients with LG NMIBC (data not shown)

Validation studies were performed testing samples at different passages with similar results. Intra- and inter-operator variability was also tested and found to have a minimal impact on results (data not shown).

Bulk RNA sequencing identified interferon alpha and gamma response pathways enriched in gemcitabine resistant tumors, among others.

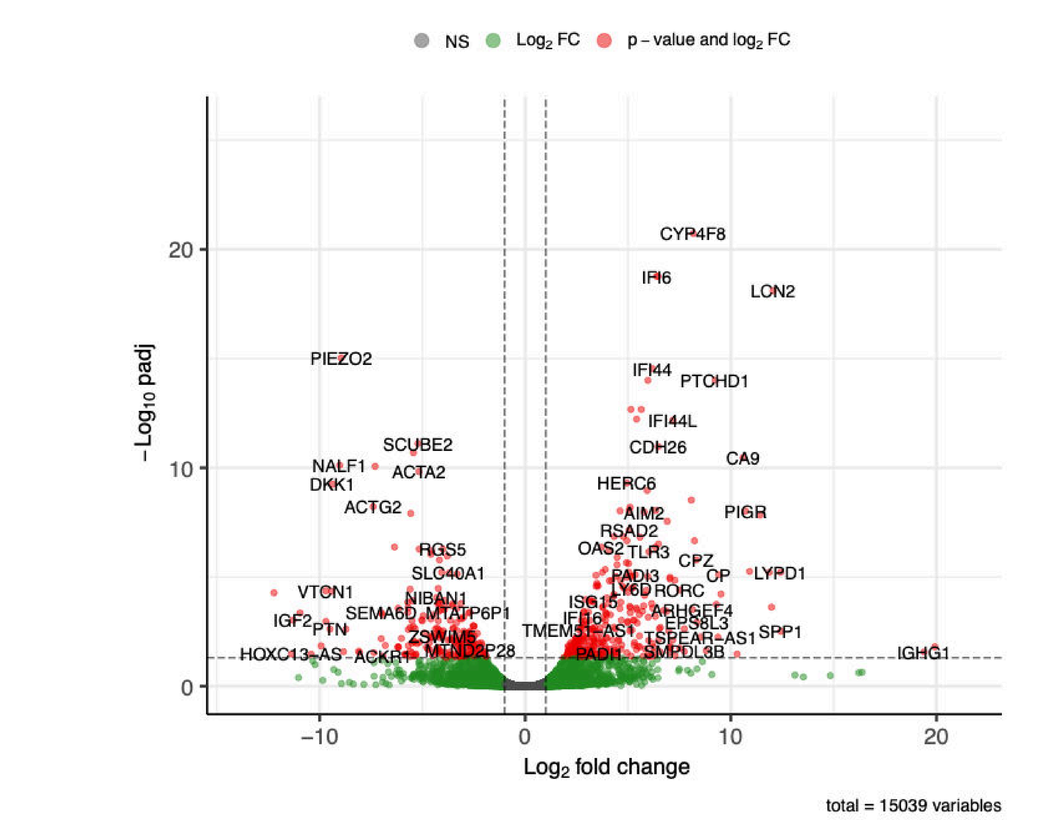

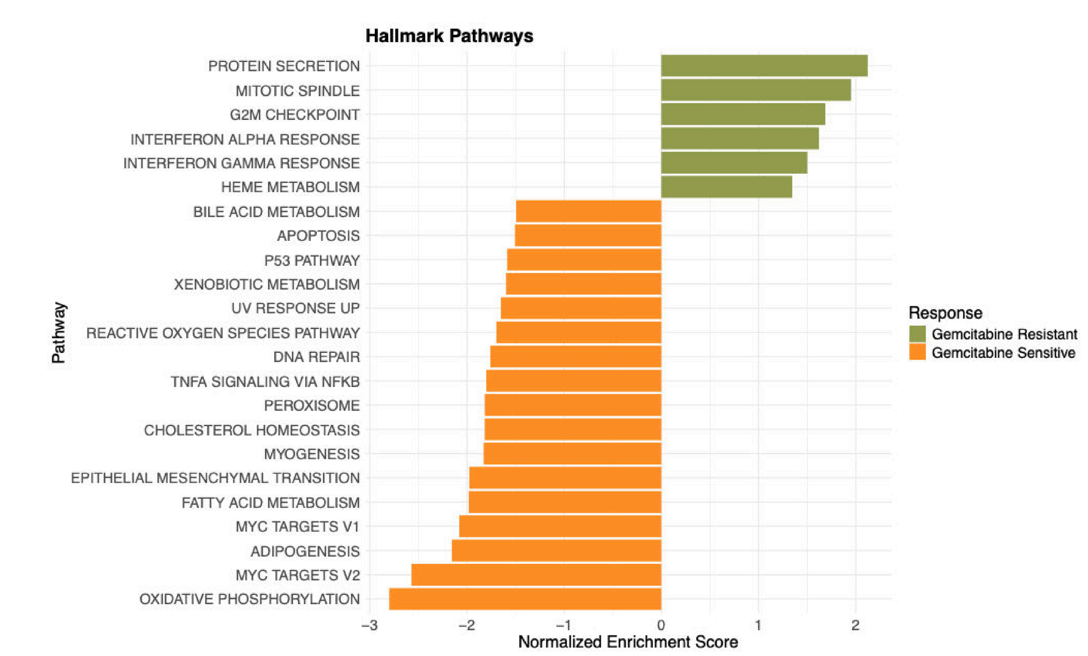

CONCLUSIONS

- An *in vitro* assay to test chemotherapy efficacy can be performed in a clinically relevant time frame.
- Gemcitabine, which is commonly used in the US, demonstrates variable responses *in vitro*.
- Gemcitabine *in vitro* responses correspond to clinical responses in this small cohort.
- Further studies are warranted to determine if PDT-guided therapy improves clinical outcomes.

Supported by:
Clinical Trialist Early Career Development Scholars Award (PI: ATL)
Herbert Irving Comprehensive Cancer Center, Columbia University Irving Medical Center, New York, NY
Award Number: PG010968

AUA 2026 Washington, DC

PERSONALIZING PREVENTION AND OPTIMIZING NON-ANTIBIOTIC THERAPIES IN CHILDREN AT RISK FOR URINARY TRACT INFECTION

Lauren E. Corona, MD[a]
[a]Department of Urology, Vanderbilt University Medical Center, Nashville, TN

Why Pediatric UTI Prevention Needs Rethinking

- **Antibiotic prophylaxis for UTI prevention is overused and harmful**: Modest, risk-dependent benefit with no reduction in renal scarring and equal risk of antimicrobial resistance.
- **Non-antibiotic prophylaxis** has emerging evidence without resistance risk (**Table 1**), but is not integrated into routine care.
- **Heterogenous at-risk patients make personalized prevention challenging**: UTI risk varies by patient factors (e.g., VUR, BBD, UTI history), but EHR data lack sufficient granularity to support individualized, evidence-based prophylaxis.
- Decisions are complex for **clinicians and families (Figure).** Contemporary guidelines recommend shared decision-making prior to use.

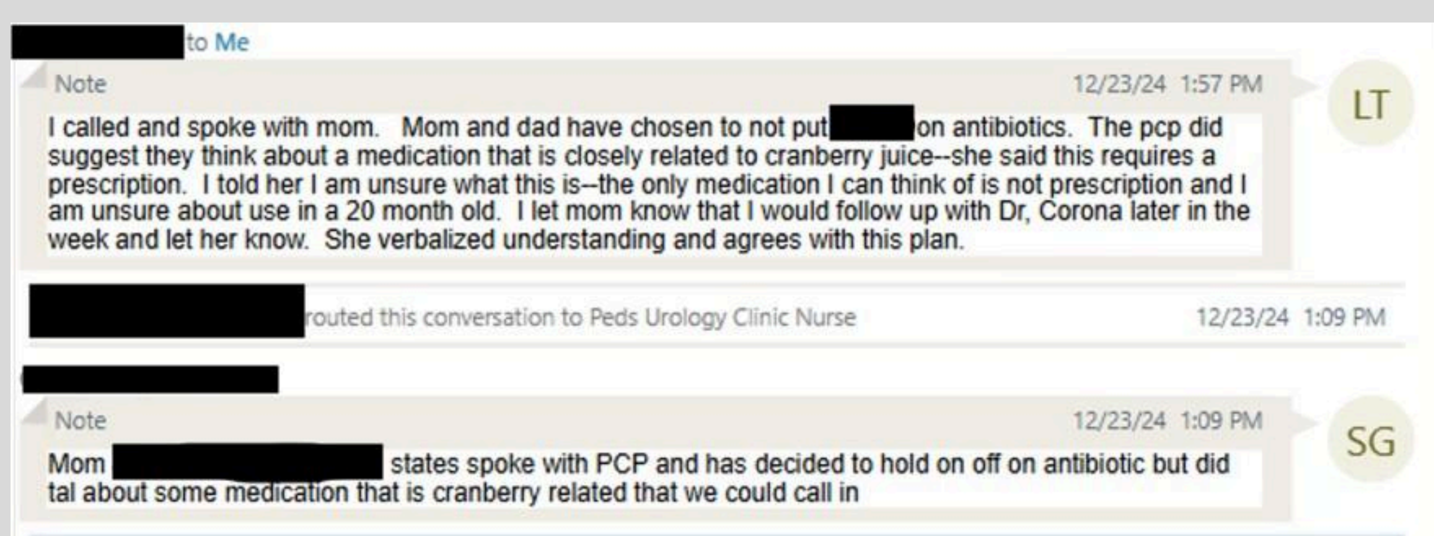
[redacted] to Me

Note 12/23/24 1:57 PM LT

I called and spoke with mom. Mom and dad have chosen to not put [redacted] on antibiotics. The pcp did suggest they think about a medication that is closely related to cranberry juice--she said this requires a prescription. I told her I am unsure what this is--the only medication I can think of is not prescription and I am unsure about use in a 20 month old. I let mom know that I would follow up with Dr, Corona later in the week and let her know. She verbalized understanding and agrees with this plan.

[redacted] routed this conversation to Peds Urology Clinic Nurse 12/23/24 1:09 PM

[redacted]

Note 12/23/24 1:09 PM SG

Mom [redacted] states spoke with PCP and has decided to hold on off on antibiotic but did tal about some medication that is cranberry related that we could call in

Figure. Example of caregiver-initiated inquiry regarding non-antibiotic UTI prevention documented in the EHR

Project aims and long-term goal:
EHR-phenotyping + decision support
-Develop validated EHR-based risk stratification
-Create shared, EHR-integrated tools to support prevention decisions in routine workflows
→ Targeted, patient-centered, antibiotic-responsible UTI prevention at scale

<ins>**Information holder input and co-design**</ins>:
-Adolescent/young adult patients
-Caregivers
-Clinicians (urology, ID, nephrology, primary care)
-Clinical pharmacists
-Nurses
-Researchers

Current Pharmacologic Prevention Landscape

Table 1. Current pharmacologic UTI prevention landscape: evidence in children, number needed to treat, and limitations.

<ins>Option</ins>	<ins>Pediatric Evidence Level</ins>	<ins>NNT to prevent 1 UTI</ins> (estimated, pediatric)	<ins>Limitations</ins>
Antibiotic prophylaxis	<ins>High</ins> (multiple large RCTs)	7-21* (depending on baseline risk)	• Antimicrobial resistance (individual + population) • Microbiome disruption • No prevention of renal scarring • Adherence
Proanthyocyanidin (Cranberry)	<ins>Moderate</ins> (5 pediatric RCTs)	~4* (based on RR 0.4, 40% baseline recurrence rate)	• Formulation/dose heterogeneity • Adherence • Costs
Probiotics	<ins>Low</ins> (small pediatric RCTs)	~5* (based on RR 0.50, 40% baseline recurrence rate)	• Small sample sizes, variable results • Strain heterogeneity • Adherence • Costs
D-Mannose 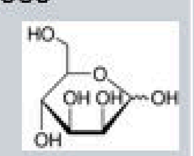	<ins>Very low</ins> (no pediatric RCTs)	Not calculable in children	• Largest adult RCT negative • Adherence • Costs
Methenamine Hippurate	<ins>Very low</ins> (no pediatric efficacy trials or RCTs)	Not calculable in children	• FDA-approved >=6 years, but no pediatric efficacy data • Adherence

NNT: Number needed to treat; RR: Relative risk; RCT: Randomized controlled trial.
*Based on estimates derived from pooled relative risks

Key Gaps:
-Variable use across providers
-Limited comparative effectiveness data
-Poor integration into clinical workflows
-No structure for shared decision support

Help shape this work!
Scan to provide feedback (1-2 min)

Personalizing Prevention and Optimizing Non-Antibiotic Prophylaxis for Prevention of UTI

Interested in collaborating or participating?
Provide your contact information in the survey.

Toward Personalized, Patient-Centered UTI Prevention

Step One: EHR-Based Phenotyping

Table 2. Guideline-informed risk groups (representative examples)

<ins>Low</ins>	<ins>Intermediate</ins>	<ins>High</ins>
-No prior UTIs -No BBD -No or low-grade VUR	-Prior UTIs with BBD and normal anatomy -High-grade VUR with no prior UTIs	-Recurrent febrile UTIs -Prior febrile UTI with high-grade VUR

BBD: bowel bladder dysfunction; VUR: vesicoureteral reflux

Table 3. Data elements and phenotypes

Data elements		Phenotyping risk factors	
Structured	Unstructured	Functional	Anatomic
-*Diagnosis Codes*: ICD-10 codes identifying risk factors -*Medications*: Antibiotic prescriptions detailing drug name, dosage, and duration -*Laboratory Results*: -Urinalysis: Point-of-care and microscopic -Urine (and other) Cultures including antimicrobial resistance	-*Clinical Notes*: Narrative documentation of diagnoses, risk factors -*Imaging Reports*: Interpretations from renal bladder ultrasounds, voiding cystourethrograms, functional studies	-*Previous UTI history* (frequency, febrile status, organism) -Bowel bladder dysfunction -Constipation -Status of toilet training	-Hydronephrosis + severity -Ureteral dilation + severity -Circumcision status -Vesicoureteral reflux + severity -Sex -Additional anatomic abnormalities (outlet obstruction, neurogenic bladder, renal scarring)

Step Two: Decision Support + Infrastructure
- Clinician-facing clinical decision support
- Patient-facing education
- Infrastructure for future CER

Impact and Next Steps

- Enable personalized, patient-centered UTI prevention
- Improve antimicrobial stewardship
- Support shared decision making
- Embed care within a learning health system
- Foundation for future CER

@lecorona
Lauren.corona@vumc.org

UCI Health
Department of Urology
University of California, Irvine
BRUCE M. GAO, MD

Electromotive Drug Administration as a Mechanistic Platform for Deep Urothelial Drug Delivery

Bruce M. Gao[1], Victor Pham[1], Seyedamirvala Saadat[1], Seyed Amiryaghoub M. Lavasani[1], Aymon Ali[1], Erika Martinez-Carcamo[1], Olga Derbeneva[1], Felix Grün[2], Sohrab N. Ali[1], Pengbo Jiang[1], Roshan M. Patel[1], Jaime Landman[1], Ralph V. Clayman[1], Yi Xi Wu[1]

[1]Department of Urology, University of California, Irvine, USA
[2]Department of Chemistry, University of California, Irvine, USA

Central Claim

EMDA enables localized urinary tract drug delivery by converting the urothelium from a barrier into a controllable transport interface.

We validate this platform through a bench-to-tissue pathway: candidate molecule screening, in vivo porcine delivery, physiologic response, and MALDI-MSI confirmation of intramural deposition.

1. Define the Delivery Problem

The Problem

The urothelial barrier protects the urinary tract, but limits local drug delivery.

- Urothelium resists molecular absorption
- Local therapy is constrained by poor tissue penetration
- A controllable method is needed to move drugs across intact urothelium

What is EMDA?

Electromotive drug administration uses a localized electric field to actively drive ionizable drugs into urinary tract tissue.

- Enhances transport beyond passive diffusion alone
- Uses iontophoresis and electroosmosis to move charged molecules
- Converts the urothelium into a controllable interface for local delivery

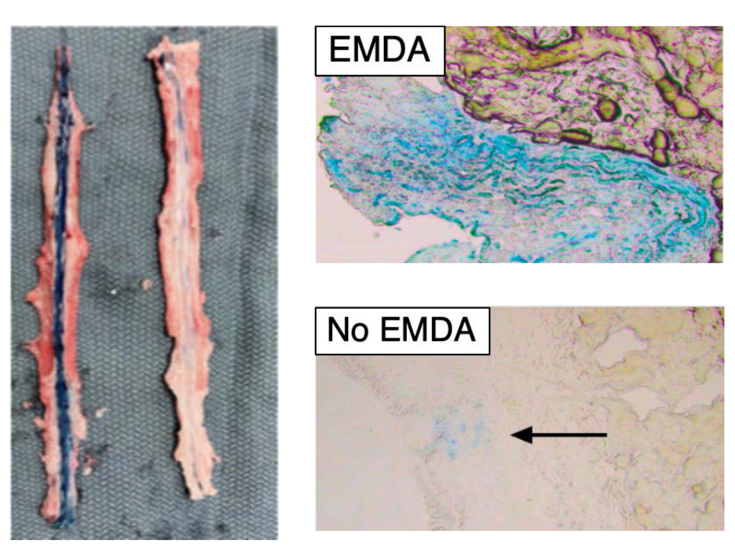

Figure 1. Pilot study of EMDA Methylene Blue delivery to the porcine ureter. Left ureter (+ EMDA) shows deep staining; the right control ureter shows scant staining. Light microscopy demonstrates dense staining of methylene blue with EMDA and minimal staining of methylene blue without EMDA (arrow).

The Strategy

Build EMDA as a stepwise platform for localized urinary tract drug delivery.

- Screen ionizable candidate drugs at the bench
- Deliver optimized candidates in vivo
- Measure physiologic response
- Confirm intramural deposition with MALDI-MSI
- Extend the workflow toward therapeutic molecule screening

2. Screen Candidate Molecules

Identify EMDA-compatible molecules before animal testing.

- Alfuzosin was selected as a functional probe because ureteral relaxation provides a measurable in vivo endpoint
- Benchtop EMDA assays tested whether applied current and diluent concentration alter alfuzosin transport

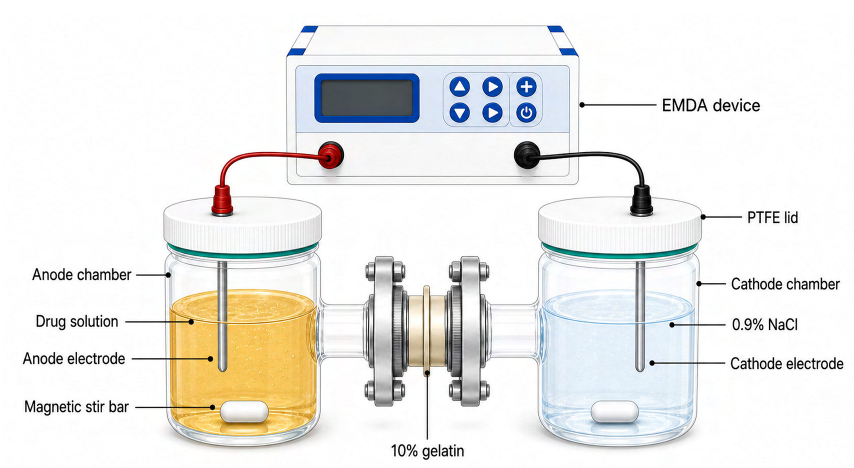

Figure 2. Benchtop EMDA setup used to screen alfuzosin transport under controlled current and diluent conditions.

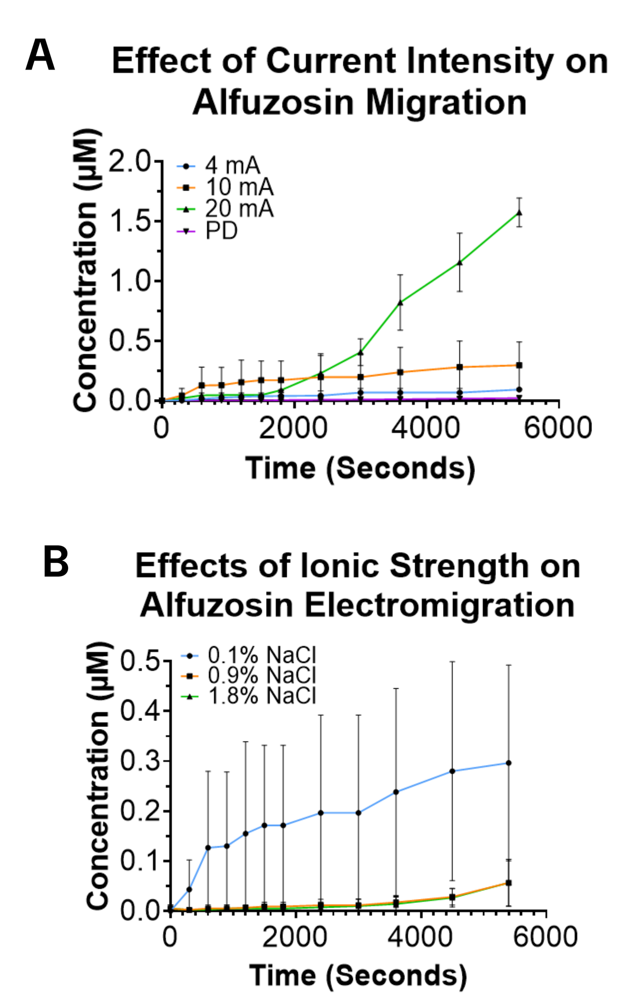

Figure 3. Effect of electrical current and ionic strength on alfuzosin electromigration. (A) Time-dependent migration profile of alfuzosin under varying applied currents (4, 10, and 20 mA) compared with passive diffusion (PD) control conditions. Increasing current intensity enhanced alfuzosin electromigration, with 20 mA producing the greatest cumulative drug transport. (B) Effect of NaCl concentration on the electromigration of alfuzosin. Increasing ionic strength reduced alfuzosin transport efficiency, with 0.1% NaCl showing the greatest electromigratory transport compared with 0.9% and 1.8% NaCl. Data are presented as mean ± SD.

3. Deliver & Measure In Vivo

Validate optimized EMDA delivery in a porcine model.

- In 18 juvenile female Yorkshire pigs, baseline ureteral diameter was measured using sequential dilators and a UCI force-sensor system standardized to 3.5 N
- Ureters were randomized to EMDA-alfuzosin, passive alfuzosin, EMDA-saline, or passive saline (n = 6/group)
- EMDA was delivered locally at 10 mA for 20 min
- Ureteral diameter was re-measured at 3.5 N immediately and at 20 min to quantify post-treatment dilation

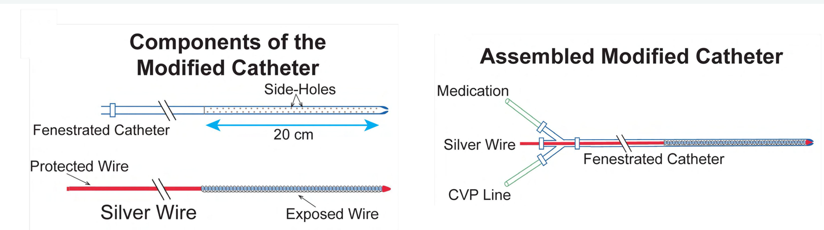

Figure 4. Modified ureteral EMDA catheter design incorporating a fenestrated drug-delivery lumen and silver wire electrode to co-localize medication exposure and electrical current for targeted ureteral wall delivery.

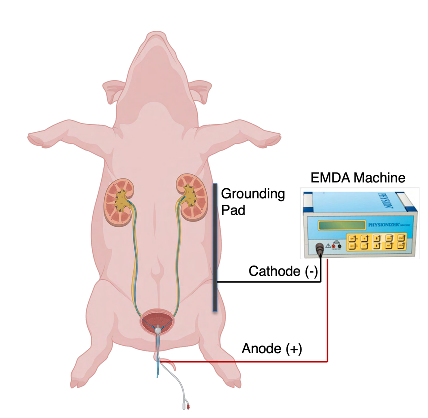

Figure 5. In vivo porcine EMDA setup demonstrating bilateral ureteral access, catheter-based drug delivery, and localized current application for upper urinary tract drug transport.

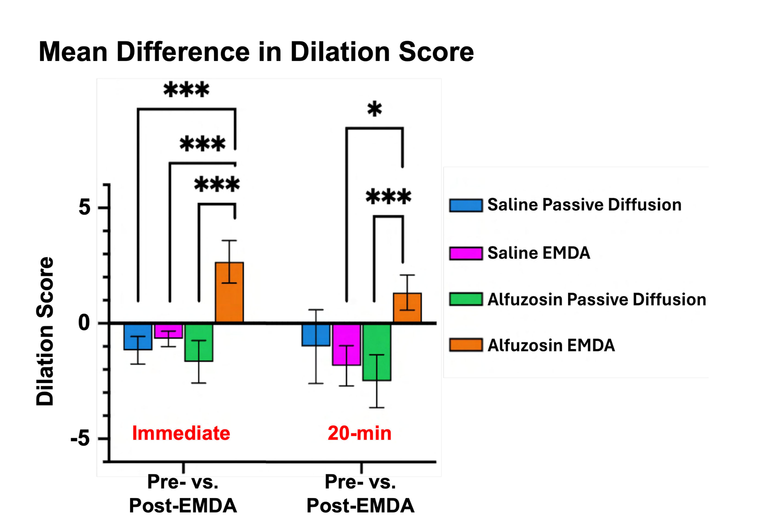

Figure 6. EMDA-alfuzosin significantly increased ureteral dilation score compared with passive alfuzosin and saline controls immediately after treatment and remained increased at 20 min.

- EMDA-alfuzosin increased ureteral dilation score versus passive alfuzosin, EMDA-saline, and passive saline immediately after treatment (+2.67 vs. -1.67, -0.67, and -1.17; $p \leq 0.001$)
- At 20 min, EMDA-alfuzosin maintained a moderate increase in ureteral size compared with passive alfuzosin and EMDA-saline (+1.33 vs. -2.50 and -1.83; p = 0.001 and 0.016)

4. Confirm Tissue Deposition

Confirm tissue-level drug delivery with MALDI-MSI.

- MALDI-MSI tested whether physiologic relaxation corresponded to intramural drug deposition
- Alfuzosin was detected at 390.4 m/z in ureteral tissue
- EMDA-alfuzosin produced an 12x higher intramural signal than passive exposure
- Signal localized within ureteral tissue compartments relevant to smooth-muscle relaxation

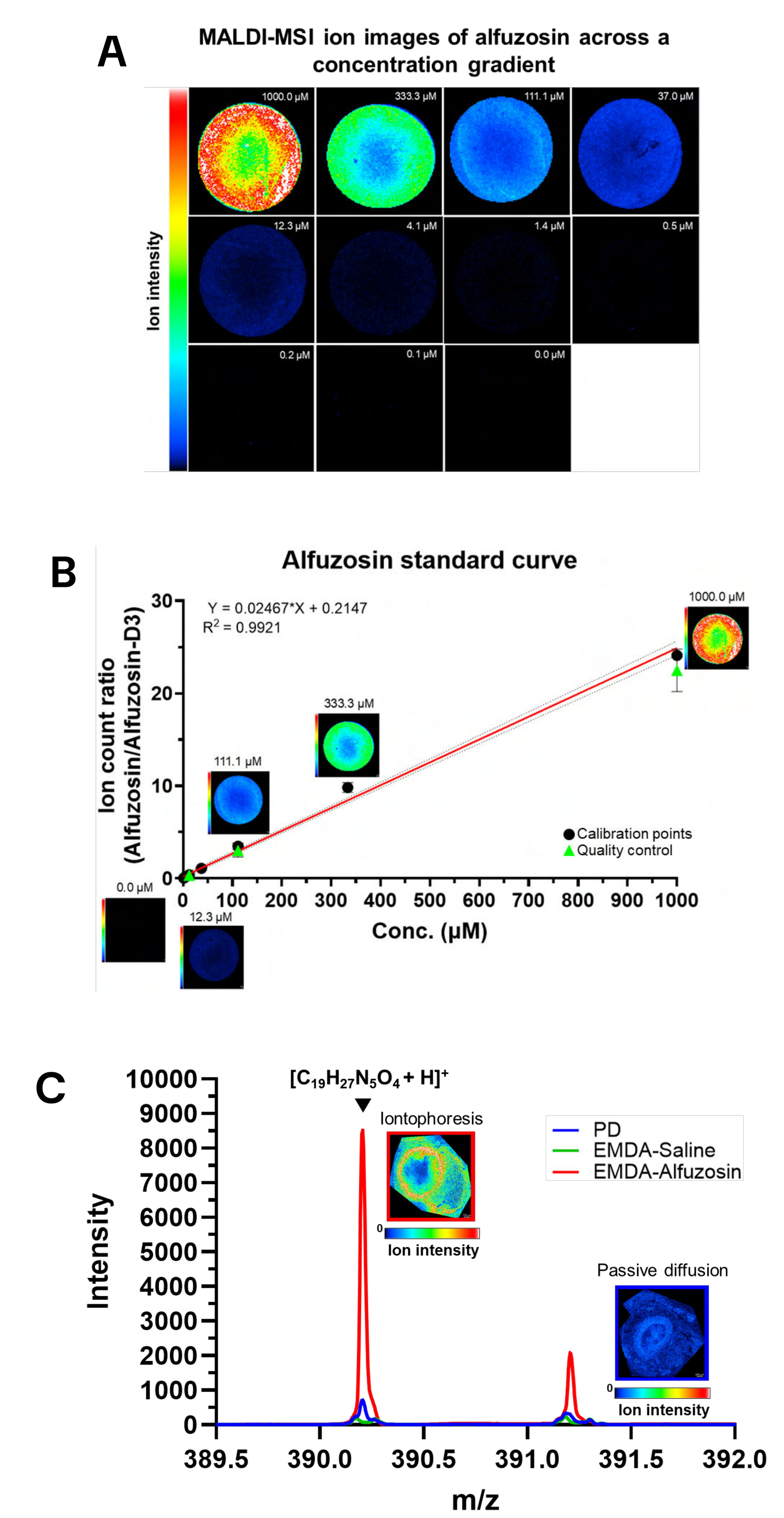

Figure 7. MALDI-MSI validation and visualization of alfuzosin in tissue.
(A) MALDI_MSI ion images of calibration standards generated by spotting known concentrations of alfuzosin and alfuzosin-D7 internal standard into homogenized ureteral tissue.
(B) standard curve for alfuzosin quantification using the alfuzosin/Alfuzosin-D7 ion count ratio, demonstrating strong linearity across concentrations (R^2 = 0.9921). Data are presented as mean ± SD.
(C) MALDI-MSI spectra and ion maps following passive diffusion (PD), EMDA-saline, and EMDA-alfuzosin treatment. EMDA-mediated delivery resulted in higher alfuzosin signal intensity and broader tissue distribution than controls.

5. Build the Therapeutic Pipeline

Extend the EMDA workflow to future therapeutic candidates.

- Alfuzosin establishes proof of concept using a molecule with a measurable physiologic endpoint
- The same bench-to-tissue workflow can be applied to other ionizable therapies
- Chemotherapy screening can prioritize candidate molecules before animal testing
- This creates a scalable pipeline for bladder and upper tract drug delivery

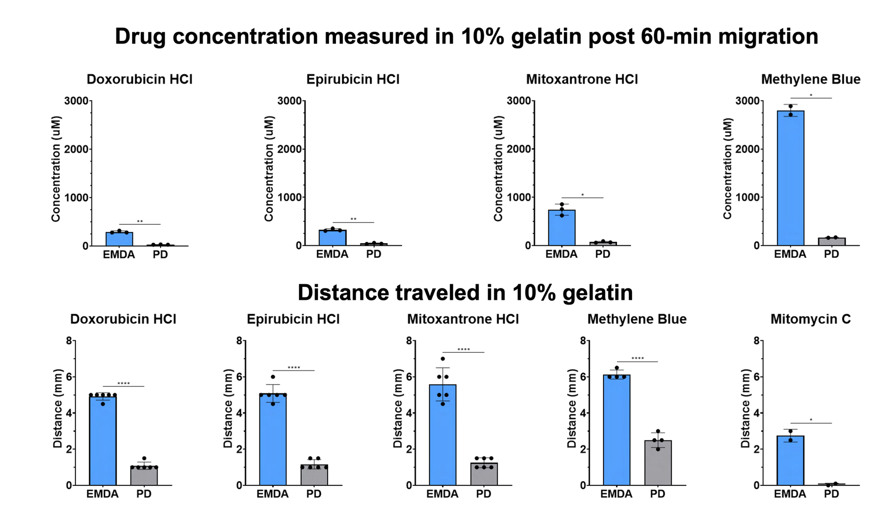

Figure 8. Benchtop chemotherapy screening demonstrates how EMDA can compare candidate molecules and prioritize future agents for localized bladder and upper tract delivery. In vivo study pends.

Conclusion

EMDA establishes a validated bench-to-tissue pathway for localized urinary tract drug delivery.

Using alfuzosin as a functional probe, we linked candidate screening, in vivo delivery, physiologic response, and MALDI-MSI confirmation of intramural deposition. This platform supports future disease-specific EMDA applications, including bladder and upper tract chemotherapy.

Disclosures

The project described was supported by the National Center for Advancing Translational Sciences, National Institutes of Health, through Grant UL1 TR001414. The content is solely the responsibility of the authors and does not necessarily represent the official views of the NIH.

A Contemporary Analysis of Radiation-Induced Genitourinary Toxicity Following Prostate Cancer Treatment

Bridget L. Findlay, MD[1]; Katherine A. Bews, MS[2]; Kristine T. Hanson, MPH[2]; Elizabeth B. Habermann, PhD[2]; Nikolas Moring, MD[3]; J. Nicholas Warner, MD[3]; Katherine T. Anderson, MD[3]; Boyd R. Viers, MD[3]

[1]Department of Urology, Mayo Clinic, Phoenix, AZ; [2]Robert D. and Patricia E. Kern Center for the Science of Health Care Delivery, Rochester, MN; [3]Department of Urology, Mayo Clinic, Rochester, MN

BACKGROUND

- Genitourinary (GU) toxicity from pelvic radiation (RT) can range from bothersome lower urinary tract symptoms and hematuria to end organ dysfunction
- 28% of patients with primary RT for prostate cancer experience GU toxicity within 10 years of treatment
- 20-30% of patients with GU injury will undergo a urologic procedure within 10 years of diagnosis

OBJECTIVES

- To evaluate the incidence of GU toxicity following radiation therapy for prostate cancer
- To describe primary interventions to manage urologic injury

METHODS

- Retrospective review of men ≥18 years undergoing RT for prostate cancer at large tertiary medical center between 2008-2023
- **Exclusion:**
  - Other solid organ malignancies including colorectal, gynecologic, or other urologic malignancies 10 years prior to index RT
- Kaplan Meier time-to-event analysis assessed incidence of radiation injury diagnosis and radiation injury treatment at 2,10, and 15 years, as well as median time to each outcome

RESULTS

Figure 1. Kaplan-Meier time-to-event analysis of freedom from radiation injury following index radiation treatment

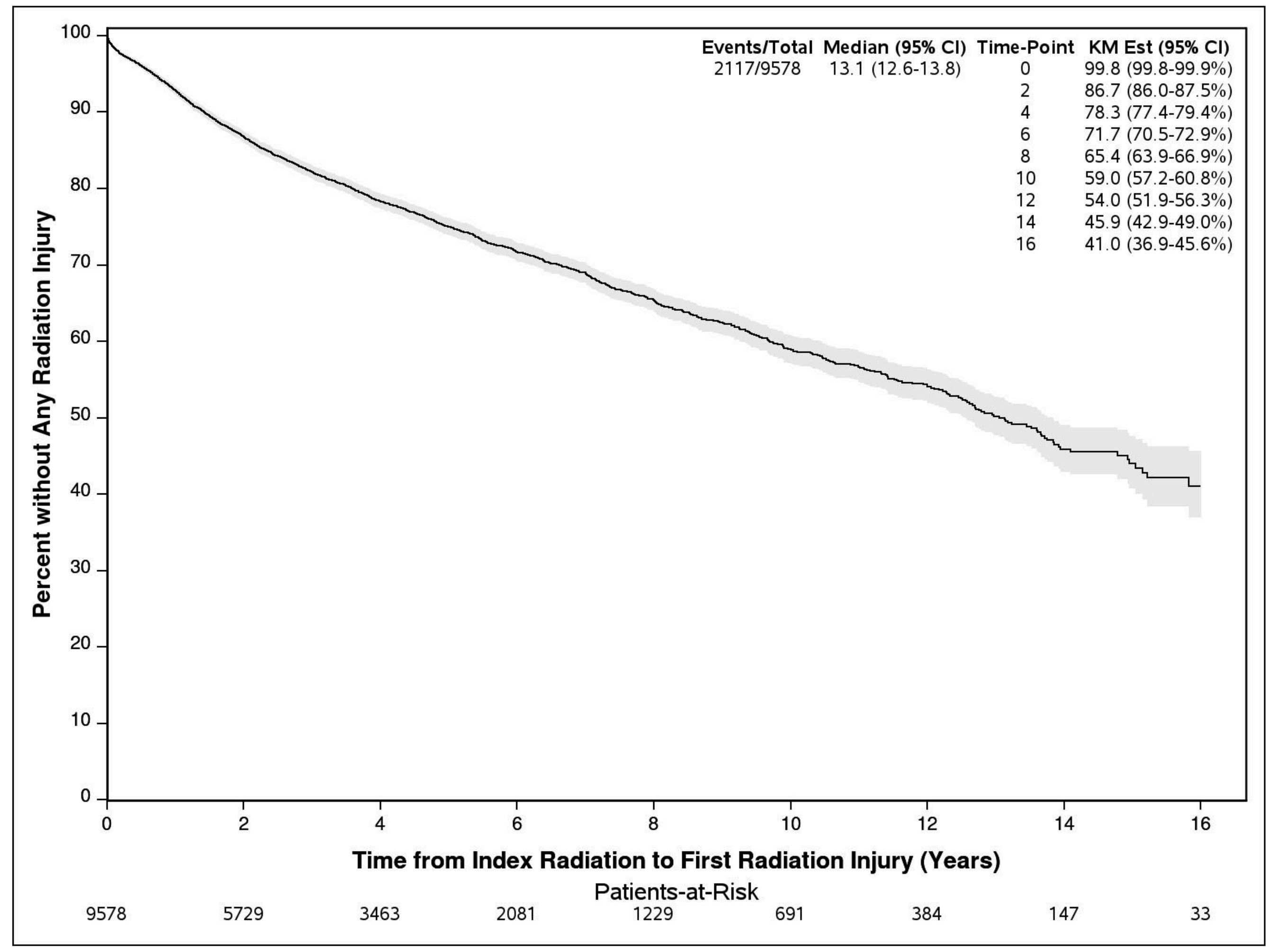

Median time to injury from index radiation:

- <u>Radiation cystitis/cystitis/hematuria</u>: 2.0 years (IQR 0.92-4.5)
- <u>Bladder neck obstruction/urethral stricture</u>: 1.7 years (IQR 0.52-4.1)
- <u>Incontinence</u>: 1.8 years (IQR 0.71-3.8)
- <u>Ureteral stricture</u>: 1.1 years (IQR 0.31-5.5)
- <u>Fistula</u>: 1.5 years (IQR 0.57-3.5)

Figure 2. Kaplan-Meier time-to-event analysis of time from radiation injury to first treatment in years colored by the radiation injury types

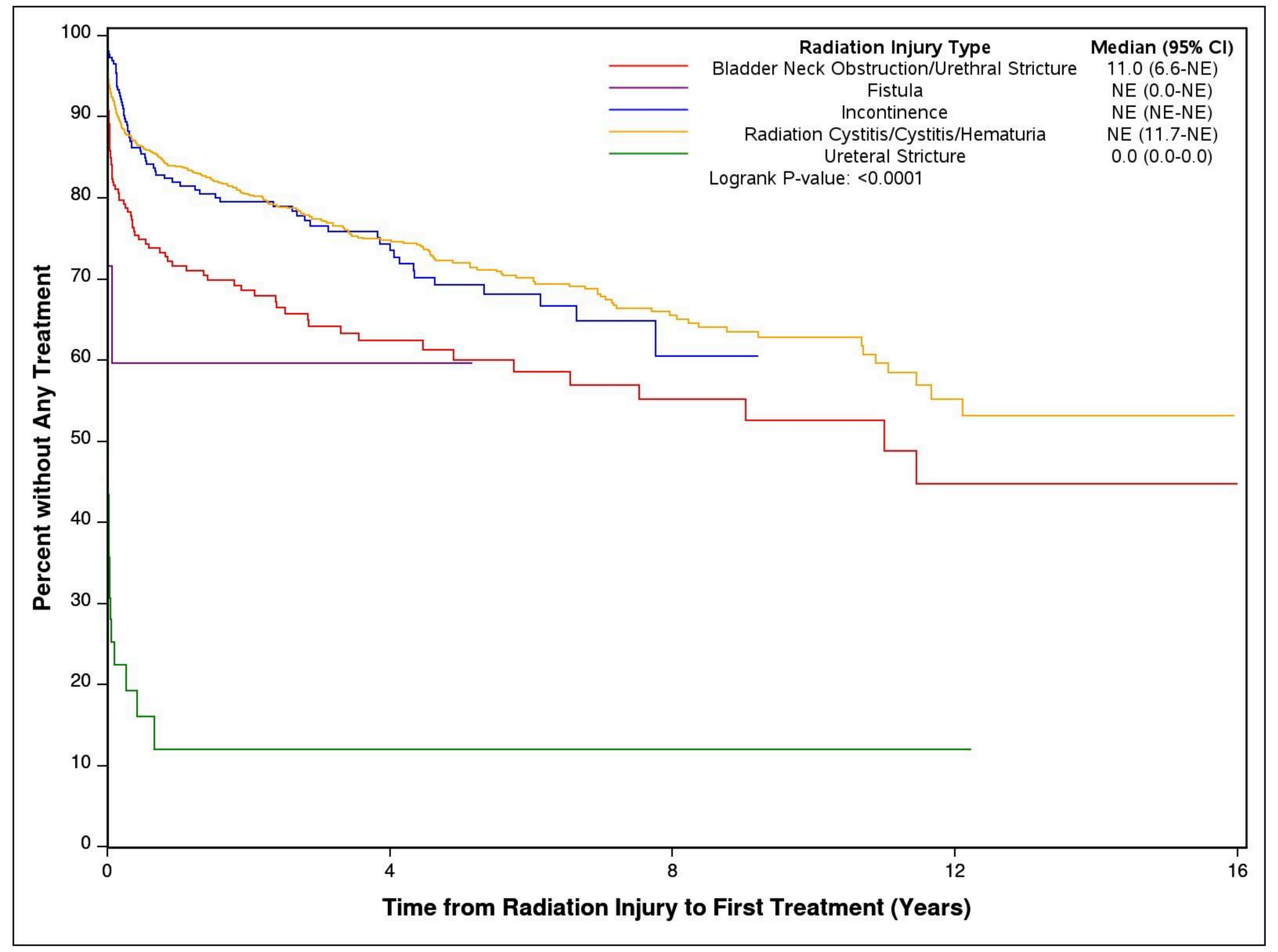

Cumulative incidence of patients undergoing treatment for GU injury:

- <u>2-years:</u> 23% (95% CI 21-25%)
- <u>10-years:</u> 42% (39-46%)
- <u>15 years:</u> 49% (95% CI 43-56%)

Median time to first treatment from injury diagnosis: 75 days (IQR 6-623)

Most common first treatment: catheterization (42%)

CONCLUSIONS

- **Genitourinary toxicity is prevalent within 10 years of prostate cancer radiation, with 23% of patients undergoing treatment within 2 years of diagnosis**
- **Although radiation cystitis/cystitis/hematuria was the most common injury type, HBOT was an underutilized treatment in this cohort**

Table 1. Cohort Demographics at Time of Index Radiation

	Total (N=9578)
Age at Radiation	
Median (IQR)	70 (65, 75)
Prostatectomy 10 years prior to index radiation, n (%)	
Yes	850 (8.9%)
Total Elixhauser	
Median (IQR)	1.0 (0.0, 3.0)
Diabetes, n (%)	
Yes	793 (8.3%)
Race, n (%)	
White	9167 (95.7%)
Black or African American	153 (1.6%)
Choose Not to Disclose/Unknown	101 (1.1%)
Other	157 (1.6%)

HBOT within 10 years of injury: 6.2% (95% CI 4.7-8.1%)

- 39% (31/79) of patients who underwent HBOT had additional treatment for radiation injury with **median time to retreatment** of 63 days (IQR 16-465)
  - Catheterization: 55% (n=17)
  - Nephrostomy tube placement: 16% (n=5)
  - Bladder irrigation: 6.5% (n=2)
- **None of the patients who underwent HBOT required bladder embolization or cystectomy during the follow-up period**

@BLFindlay @MayoUrology

Development of a Modernized AI-Ready Radical Prostatectomy Database to Inform Point of Care Decision Making

Alex Brame, Taxiarchis Botsis PhD, Eva Biswas PhD, Lap Sum Chan PhD, Matthew Kane, Rana Harb, Tamara Lotan MD, Angelo DeMarzo MD, PhD, Catherine Marshall MD, MPH, Eddie Imada PhD, Jun Luo PhD, Swaroop Vedula PhD, Patrick Walsh MD, Nilanjan Chatterjee PhD, Arun Rai MD, MBA

The James Buchanan Brady Urological Institute, Johns Hopkins University School of Medicine, Baltimore, MD, USA

Introduction

- The Brady Urological Institute maintains a world-class prospective database of over **30,000 men** who have undergone radical prostatectomy since the 1980s. This registry has been foundational for clinical risk stratification tools like the Partin and Han Tables.
- The legacy data storage platform relies on manual data entry, which limits its capacity for real-time or large-scale AI-driven analysis.
- This project aims to systematically modernize this database into a secure, interoperable **REDCap framework**.
- The ultimate goal is to create **AI-driven clinical decision support systems** that provide personalized prostate cancer management

Results

- **Modernized Registry**: Successful migration of 30,163 patients into a cloud-compatible, standardized REDCap environment
- **Automated Data Flow:** Validation of automated scripts for real-time EHR data population, significantly reducing manual abstraction burden
- **Predictive Performance**: Initial work by our group demonstrates that survival modeling using the database has achieved IPCW C-indices between 0.85 and 0.90, demonstrating high discrimination for predicting PSA recurrence
- **Patient Interface**: Implementation of a scalable PRO system that allows patients to electronically contribute long-term functional and laboratory data

Acknowledgments

This research has been made possible by the Patrick C. Walsh Prostate Cancer Research Fund. This work was nominated for ECIS2026 by Dr. Arthur Smith on behalf of the Society for Endourology.

Materials and Methods

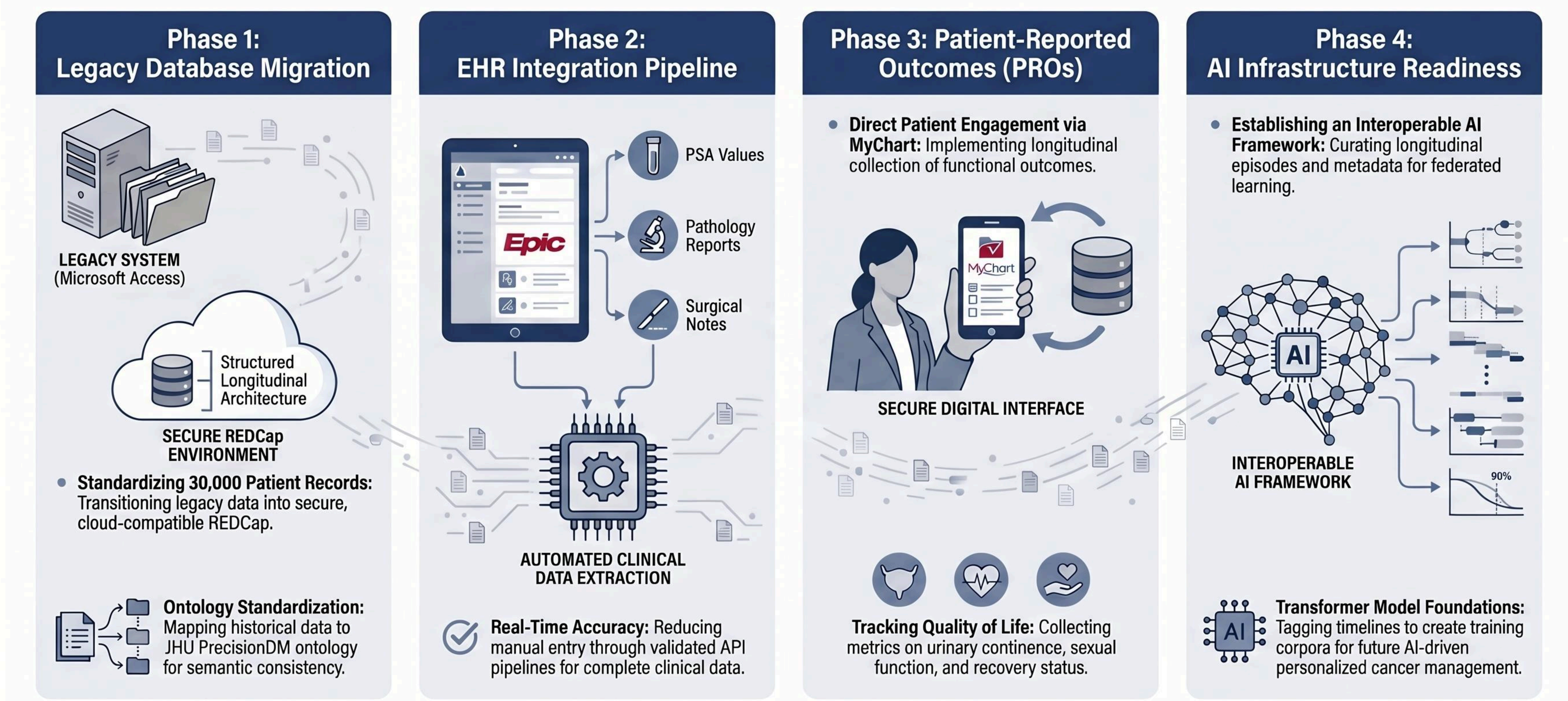

Discussion

- Modernizing to a standardized REDCap using JHU PrecisionDM ontology ensures data follows **FAIR (Findable, Accessible, Interoperable, and Reusable) principles**, which is a prerequisite for advanced machine learning.
- Current results show that non-parametric models (like Random Survival Forests) offer slightly higher accuracy, parametric models (like CoxPH) are currently recommended for clinical use due to their better interpretability of specific predictors.
- Based on data quality, transformer models are uniquely suited because they can analyze complex relationships across decades of patient history regardless of their position in the sequence, overcoming the limitations of older recurrent neural networks (RNNs).
- This infrastructure enables **federated learning efforts** through multi-institutional collaborations

Conclusion and Future Work

- Digital transformation of the radical prostatectomy outcomes database is a critical step toward **AI-driven precision urology**.
- By integrating automated EHR extraction and patient-reported outcomes, we create an intelligent framework capable of supporting **real-time clinical decision support**. This work provides the essential groundwork for a future transformer-based model aimed at **personalized prostate cancer prognostication**, ultimately empowering both clinicians and patients to make better-informed treatment decisions
- Currently, we are performing statistical analysis to establish weighting in preparation for transformer model construction

AUA 2026
Washington, DC

Abstract 21: Randomized Single-Blinded Trial of Patient Reported Experiences with Sparing External Oblique Fascia Vs Standard Inguinal Orchiectomy (PRESERVE Trial)

Muhannad Alsyouf, Jersey-Kate Castillo, Alan Cupino, Antoin Douglawi, Martin Hofmann, Herbert Ruckle, Aditya Bagrodia, Robert Hamilton, Nirmish Singla, Eric Umbreit, Premal Patel, Scott Eggener, Anne Schuckman, Hooman Djaladat, Siamak Daneshmand, Brian Hu

Primary institution: Loma Linda University Health, Loma Linda, California

INTRODUCTION

- Radical inguinal orchiectomy is the standard surgical approach for patients with testicular malignancy.
- Classically, the procedure involves incising the external oblique fascia (EOF) to expose and ligate the spermatic cord, a step that carries a risk of injuring the ilioinguinal nerve.
- A fascia-sparing modification has been described and avoids this step and potentially minimized surgical morbidity.
- The high rate of opioid prescription following orchiectomy in this young patient population highlights the critical need to reduce postoperative pain.
- **Purpose**: The PRESERVE trial aims to evaluate the difference in patient-reported outcomes between the standard inguinal orchiectomy and the EOF-sparing modification.

METHODS

- The PRESERVE trial is a multi-institutional, randomized, single-blinded clinical trial, with a total enrollment goal of 80 participants.
- Participants undergoing orchiectomy are randomized to:
  - **Arm 1** (Standard radical inguinal orchiectomy with external oblique fascia incision)
  - **Arm 2** (External oblique fascia sparing orchiectomy).
- Randomization is performed using permutated block randomization based on tumor size (≤ or >5 cm).
- Exclusion criteria: cT4, regular opioid use, history of illicit substance use, orchiectomy performed through incision other than standard (hockey stick incision).

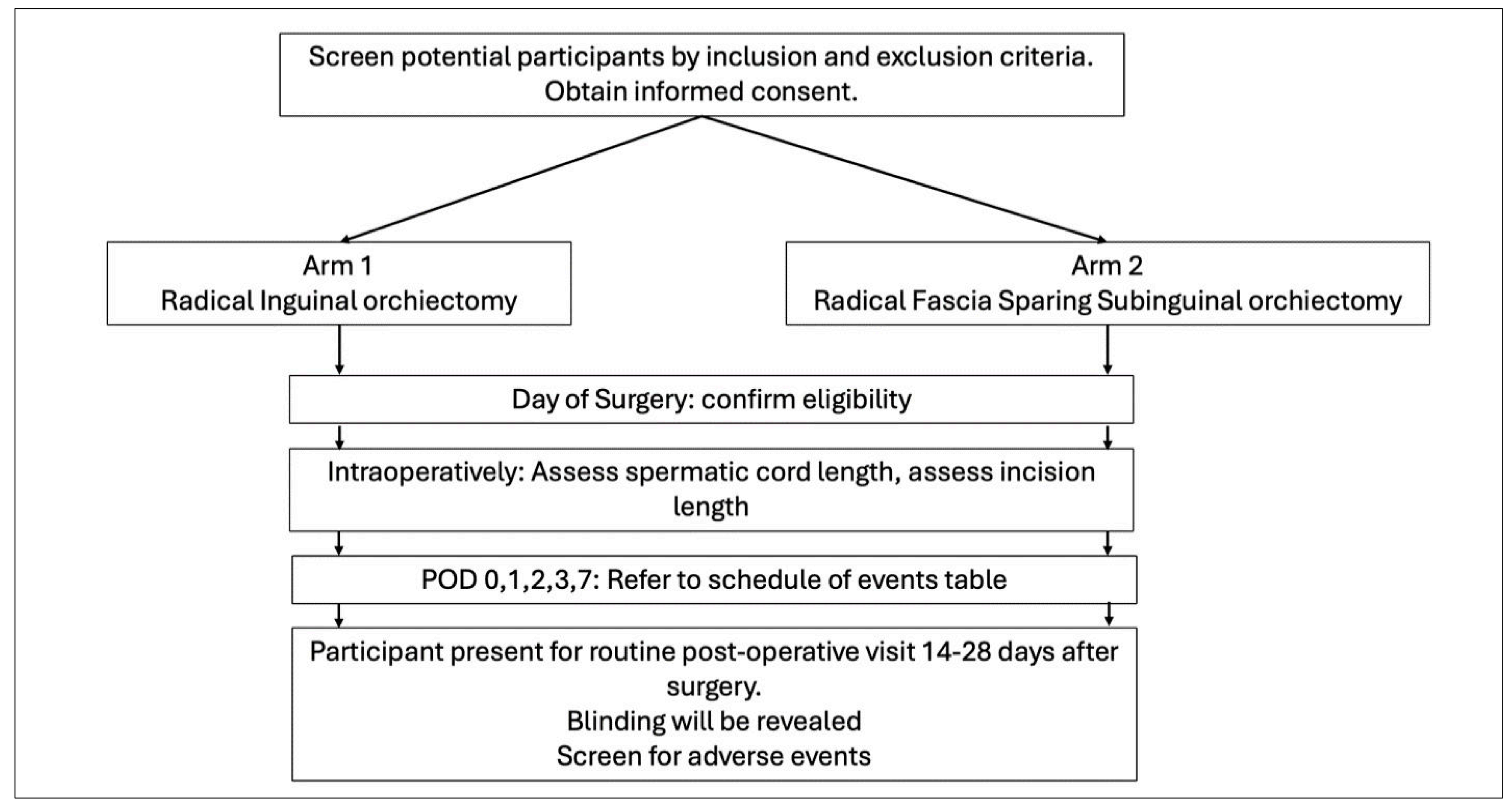

Figure 1: Trial Procedures and Scheduled

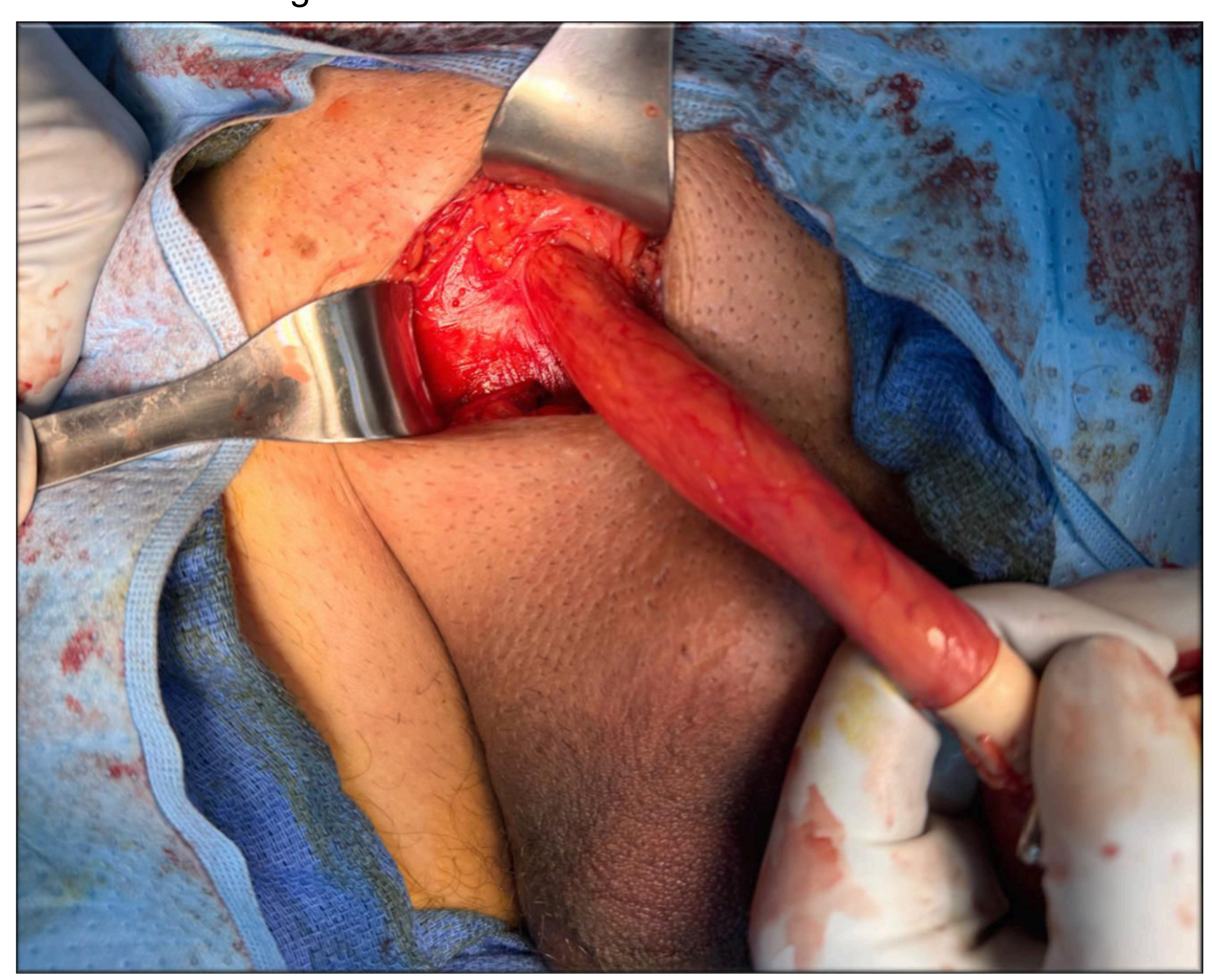

Figure 2: Operative picture demonstrating EOF orchiectomy with spermatic cord dissected without incising the external oblique fascia

ENDPOINTS

- **Primary:** To measure the difference in Pain Score, as measured by the Short Form Inguinal Pain Questionnaire (sf-IPQ), at postoperative day 7.
- **Secondary:** Neuropathic pain, opioid usage, incision length, spermatic cord length, complications.

RESULTS

- **16 patients** have been enrolled and randomized in the trial.
- An adaptive statistical approach with interim power analysis performed at 25 patients to adjust final enrolment number.
- Anticipated enrolment institutions:
  - University of Southern California
  - University of Toronto
  - University of California, San Diego
  - University of California, Los Angeles
  - UT San Antonio
  - Johns Hopkins University
  - University of Manitoba

CONCLUSIONS

The PRESERVE trial will provide evidence of whether the fascia sparing modification to radical orchiectomy improves postoperative pain and patient reported outcomes.

ACKNOWLEDGEMENTS

We thank all participating institutions for their support.

DISCLOSURES

None

LOMA LINDA UNIVERSITY
MEDICAL CENTER

Link to ClinicalTrials.gov

Imaging-Guided Sentinel Lymph Node Staging in Prostate Cancer

AUA 2026
Washington, DC

Toward SLN-only staging: integrating molecular imaging and AI for precision nodal decision-making

Javier Pérez Ardavín MD, PhD.   Hospital Universitari i Politèchnic La Fe. Valencia. Spain

INTRODUCTION

Accurate nodal staging directly influences prognosis and adjuvant treatment in prostate cancer (PCa). Extended pelvic lymph node dissection (ePLND) remains the reference standard but carries significant morbidity and leads to overtreatment in node-negative patients. Imaging-guided sentinel lymph node (SLN) biopsy — using Tc-99m SPECT/CT and near-infrared ICG fluorescence — offers a selective alternative that preserves staging accuracy while dramatically reducing surgical burden.

METHODS

We present a two-cohort prospective experience: a mature series (n=106) with long-term oncological validation, and an evolving SLN-only protocol (n=21) incorporating ICG fluorescence with AI-enhanced image processing.

Cohort 1 n=106
· Tc-99m + SPECT/CT
· Median follow-up 80.8 months
· SLN vs ePLND comparison

Cohort 2 n=21
· PET-CT + ICG fluorescence + Tc-99m · SLN-only protocol (no completion ePLND)
· Follow-up 12 months ongoing

Risk profile Cohort 2: ISUP 3–4 (86%), intermediate/high risk (100%), PSA mean 15.5 ng/mL

RESULTS

COHORT 1 · LONG-TERM VALIDATION (N=106)

A. DETECTION AND STAGING ACCURACY

96.2% SLN detection rate	**100%** Patient-level sensitivity & NPV	**91%** Node-level sensitivity
99.8% Node-level NPV	**24.5%** Nodal metastasis rate	**78%** SLN outside ePLND template

B. NODES REMOVED: SLN-GUIDED VS EPLND

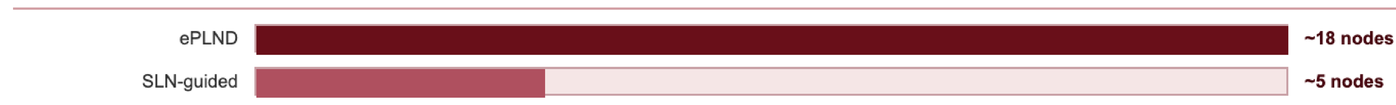

77% reduction in nodes removed (p<0.001)

C. ONCOLOGICAL OUTCOMES

Endpoint	Result
SLN positivity as predictor of BCR	OR 3.89 (95% CI 1.13–13.38)
Log-rank significance	p < 0.001
SLN nodes outside ePLND template	78% of positive cases

SLN biopsy → OSNA intraop. → Positive (5/21) → Extended dissection of positive territory
→ Negative (16/21) → SLN-only · no further dissection

COHORT 2 · SLN-ONLY PROTOCOL (N=21) PRELIMINARY

A. PRIMARY ENDPOINTS

100% SLN detection (21/21)	**23.8%** Nodal positivity (5/21)	**3.7** Mean sentinel nodes
5.7 Mean total nodes removed	**19%** Management change (4/21)	**2.2 d** Mean hospital stay

B. OSNA INTRAOPERATIVE PATHOLOGY

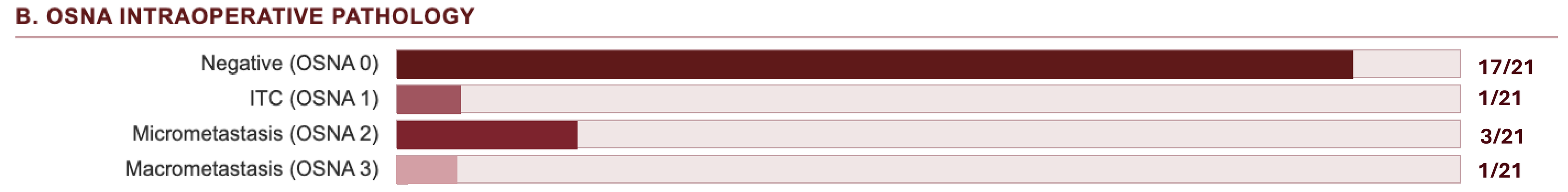

C. 12-MONTH ONCOLOGICAL OUTCOMES

Event	SLN status	OSNA	Nature
Persistence (×2)	SLN+	Micrometastasis	BCR
Recurrence (×1)	SLN+	Micrometastasis	BCR
Recurrence (×1)	SLN−	Negative	Local fossa
Persistence (×1)	SLN−	Negative	Systemic BCR
No evidence of disease	SLN−	Negative	16/21

No false-negative nodal staging identified. SLN-negative events represent local prostatic fossa recurrence or systemic BCR unrelated to nodal staging failure.

ICG FLUORESCENCE + AI-assisted fluorescence enhancement PROOF OF CONCEPT

A. NIR FLUORESCENCE IMAGING — REPRESENTATIVE CASES

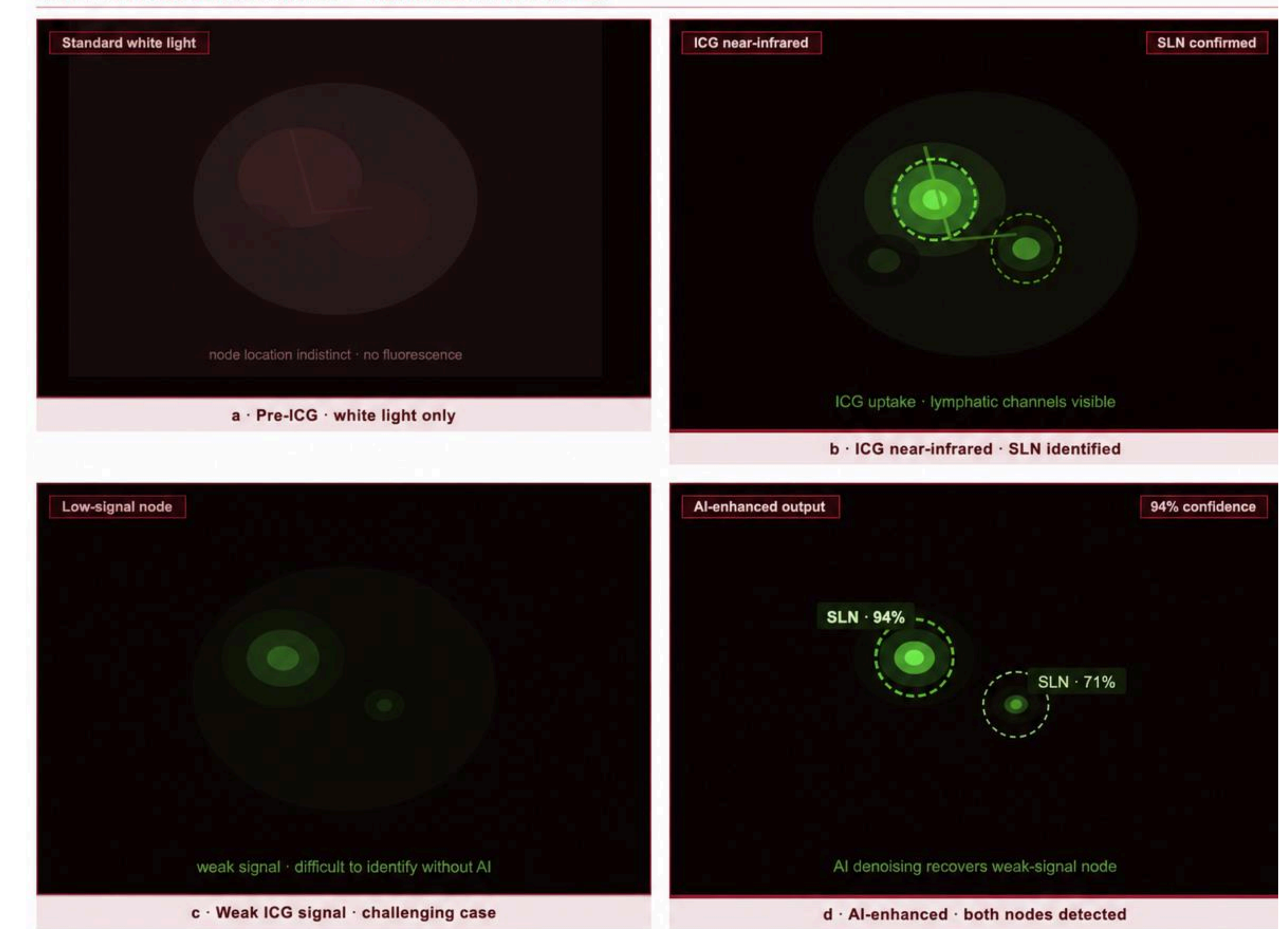

a · Pre-ICG · white light only
b · ICG near-infrared · SLN identified
c · Weak ICG signal · challenging case
d · AI-enhanced · both nodes detected

B. ICG DETECTION RESULTS · COHORT 2 (N=21)

Parameter	Result
SLN detection with ICG + Tc-99m	21/21 (100%)
Nodal positivity confirmed by OSNA	4/21 (19%)
Mean ICG-positive nodes per patient	3.0 (range 0–8)
Nodes outside ePLND template detected by ICG	4 patients (19%)
System used	Firefly · da Vinci robotic platform

ICG near-infrared fluorescence enables real-time intraoperative visualization of lymphatic channels and sentinel nodes. AI-based denoising and contrast enhancement is under active development to improve detection of low-signal nodes in challenging anatomical fields. Proof of concept — intended to assist, not replace, intraoperative surgeon judgment.

SLN DISTRIBUTION — COHORT 2

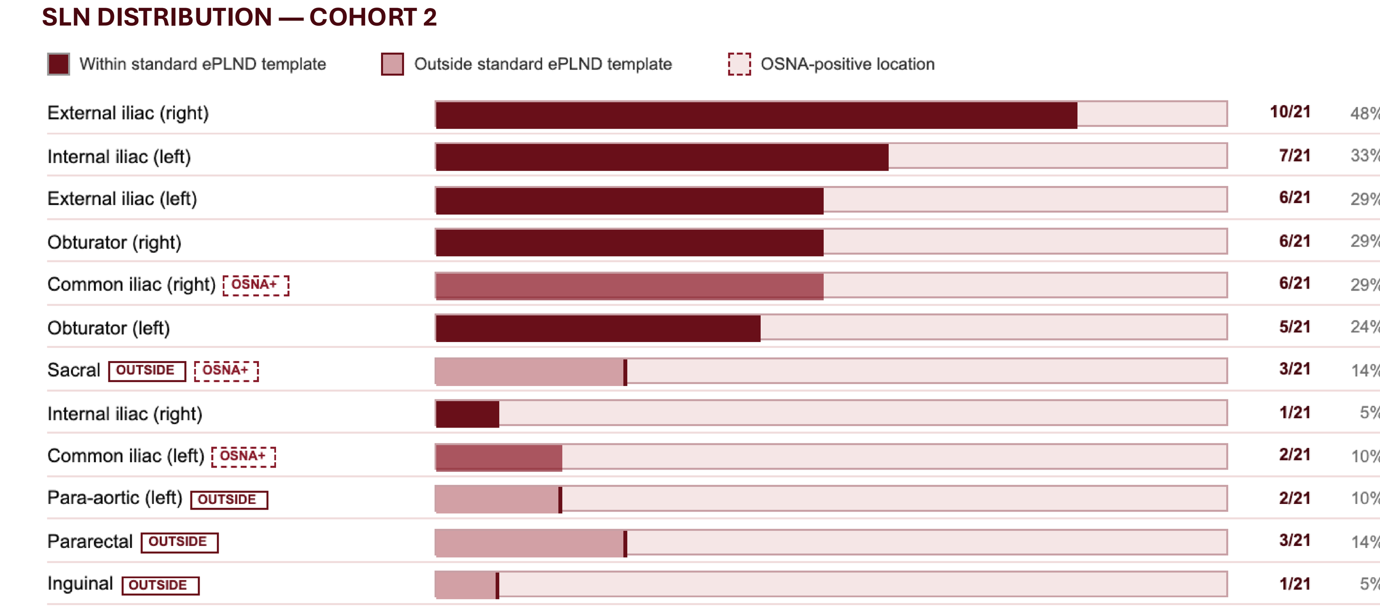

19% of patients (4/21) had ≥1 SLN outside the standard ePLND template (sacral, pararectal, inguinal, para-aortic). These nodes would have been missed by conventional dissection alone.

OSNA-positive locations: external iliac R ×2 · common iliac R ×1 · sacral ×1 · external iliac L ×1 · common iliac L ×1

CONCLUSIONS

- SLN staging shows high diagnostic accuracy with long-term validation and reduces surgical burden by >70% vs ePLND
-AI-assisted ICG enhancement and PSMA-PET integration represent the next step toward precision, patient-centred staging — currently under active investigation.
- SLN staging shows high diagnostic accuracy and significantly reduces surgical burden. Preliminary data from SLN-only protocols are promising, but longer follow-up is required before replacing ePLND.

ACKNOWLEDGEMENTS

I thank the Urology Department at Hospital La Fe particularly, Dr. Martínez-Sarmiento, Dr. Vera-Donoso and Dr. Monserrat.

DISCLOSURES

I have no disclosures to report.

AUA 2026
Washington, DC

Micro-Ultrasound as a complementary imaging modality for clinically significant PCa detection in active surveillance: A prospective clinical trial

Roldan Testillano R., Covarrubias C., Anidjar M., Sanchez-Salas R.

INTRODUCTION & OBJECTIVES

Active surveillance (AS) → standard strategy for low-fav intermediate risk PCa.

MRI central role in patient selection and follow-up. However:

- False-negative rates up to 20%.
- Limited access, cost, and inter-observer variability.

Micro-ultrasound (**mUS**) high-resolution imaging modality -- PRI-MUS scoring system → identify csPCa missed by mpMRI. **Rapid, office-based alternative**.

*No study assessed mUS diagnostic performance in men with negative or stable mpMRI during AS.

Objective: **evaluate mUS detecting csPCa** in patients with negative or stable mpMRI.

RESULTS

The study protocol in under ethical review. Recruitment is planned to start in 2026.

McGill UNIVERSITY

Visit Number	Visit 1	Visit 2	Visit 3
Tests	Screening & Eligibility Assessment	6-month follow up	12-month follow up/ End of Study
PSA	X	X	X
mUS[1]		X	X
mpMRI			X
Image guided prostate biopsy[1]			X

1. Image-fusion guided prostate biopsies will be done using the mUS.

ACKNOWLEDGEMENTS & DISCLOSURES

This study is supported by the *Bayer–CUASF–CUOG Research Award in Prostate Cancer* (Canadian Urological Association).

MATERIALS & METHODS

This is a prospective, single-arm, two-stage Phase II diagnostic study.

Population: **20-30 men on AS** with a negative (PI-RADS ≤2) or stable mpMRI.

Procedures:
All undergo mUS. Lesions PRI-MUS ≥3 will be targeted under mUS guidance + a 12-core systematic biopsy.

Endpoints:

- **Primary**: Sensitivity and specificity of mUS for csPCa detection on AS patients.
- **Secondary**: Incremental csPCa yield vs mpMRI, FP rate, PV in disease progression, and biopsy complications.

CONCLUSIONS

The study should provide evidence on the role of mUS as a complementary tool in AS.

We hypothesize mUS could enhance **csPCa detection**, **reduce MRI dependency**, and **improve accessibility** by combining imaging and biopsy in a single outpatient setting.

Liquid Biopsy-based Monitoring of Bladder Cancer Recurrence Using Somatic Mutation-derived Mutated Proteins in Urine Extracellular Vesicles

AUA 2026 Washington, DC

Yuji Hakozaki[1], Kazuma Sugimoto[1,2], Yuta Yamada[1], Haruki Kume[1], Koji Ueda[2]
1. Department of Urology, Graduate School of Medicine, The University of Tokyo
2. Division of Analytical Biochemistry, Cancer Precision Medicine Center, Japanese Foundation for Cancer Research

INTRODUCTION

Intravesical recurrence is common in bladder cancer. Urinary cytology is the only biomarker in routine use, but its sensitivity, particularly for low-grade tumors, is limited.

We have demonstrated that urinary extracellular vesicles (uEVs) contain somatic mutation-derived proteins (Front. Oncol., 2026). In this study, we aimed to investigate the utility of mutant proteins present in uEVs.

Objective

Development of a novel technique to detect proteins derived from somatic mutations in urinary extracellular vesicles.

METHODS

Tumor tissues, cultured tissue-derived EVs, and uEVs were collected from 28 patients with bladder cancer. Whole-exome sequencing was performed to generate patient-specific mutation databases.

Deep proteomic profiling by LC/MS was conducted for each specimen type, followed by a proteogenomic pipeline to identify somatic mutant proteins.

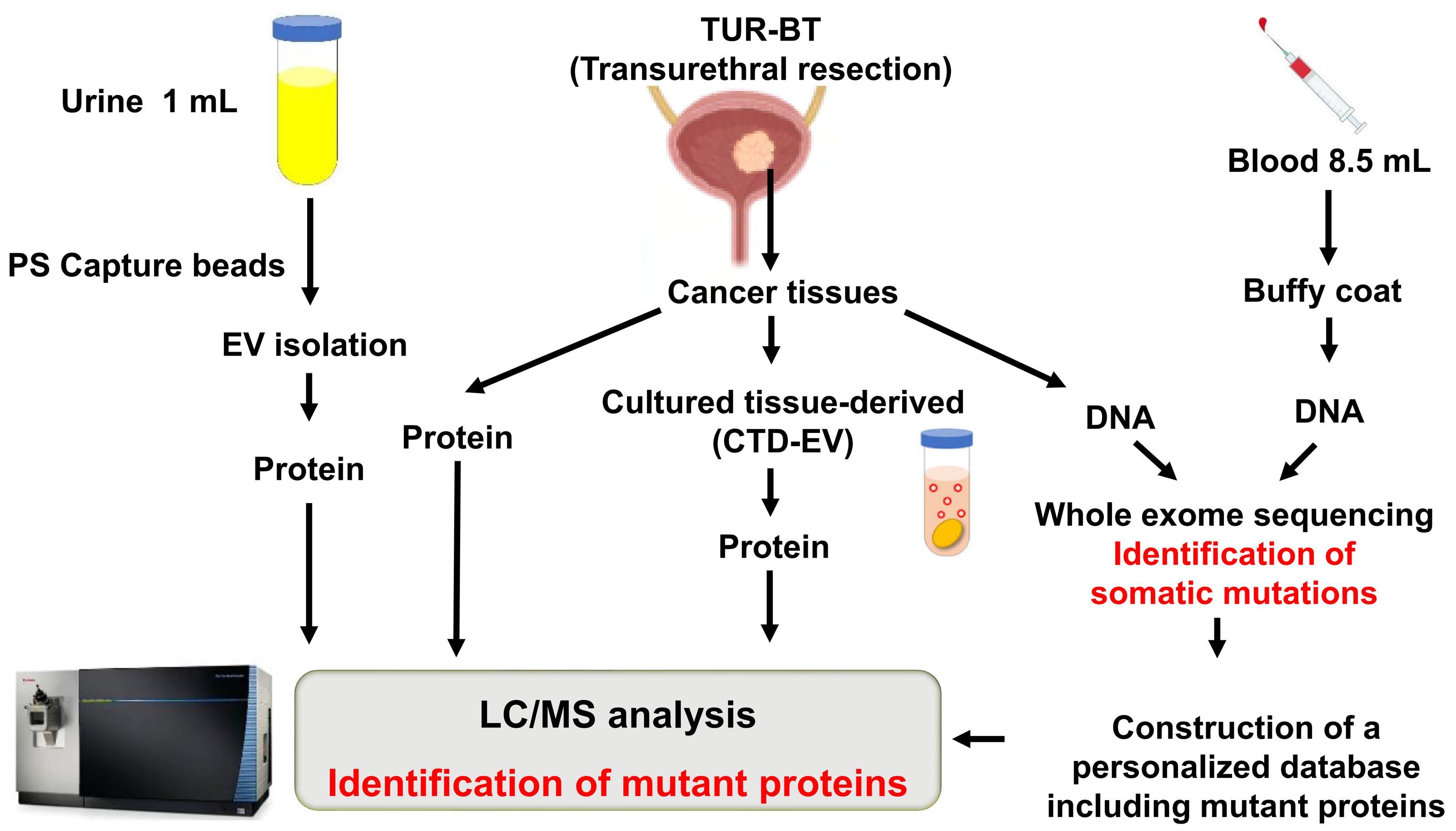

RESULTS

We identified 10,814, 10,727, and 8,378 proteins from cancer tissues, CTD-EVs, and uEVs, respectively.

Patient characteristics

Characteristics	N = 28
Age	74 (72-79)
Sex (M / F)	22(79%) / 6(21%)
T stage (Ta / T1 / ≧T2)	15 (54%) / 9 (32%) / 4 (14%)
CIS (y / n)	4 (14%) / 24 (86%)
Grade (LG / HG)	6 (21%) / 22 (79%)
Variant Histology (y / n)	7 (25%) / 21 (75%)
Tumor diameter (mm)	20 (13-28)
Multiple lesions (y / n)	16 (57%) / 12 (43%)
Urinary cytology at diagnosis (Ⅰ or Ⅱ / Ⅲ / Ⅳ or Ⅴ)	4 (14%) /13 (46%) /11 (40%)

Landscape of mutations

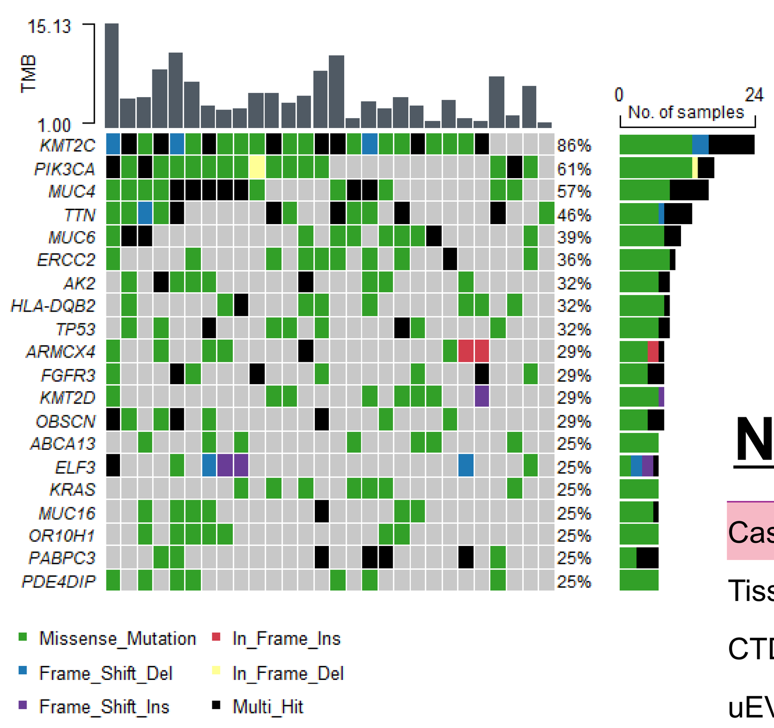

Identified mutant proteins

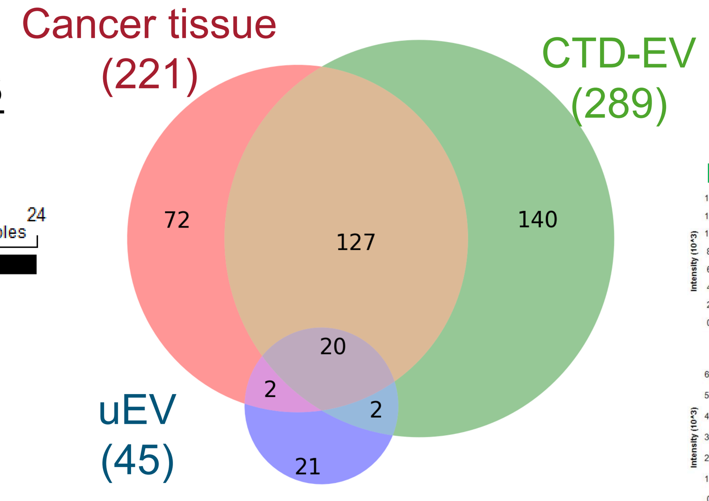

Detection of recurrence

UC, pTa, low-grade, 8 mm, single lesion

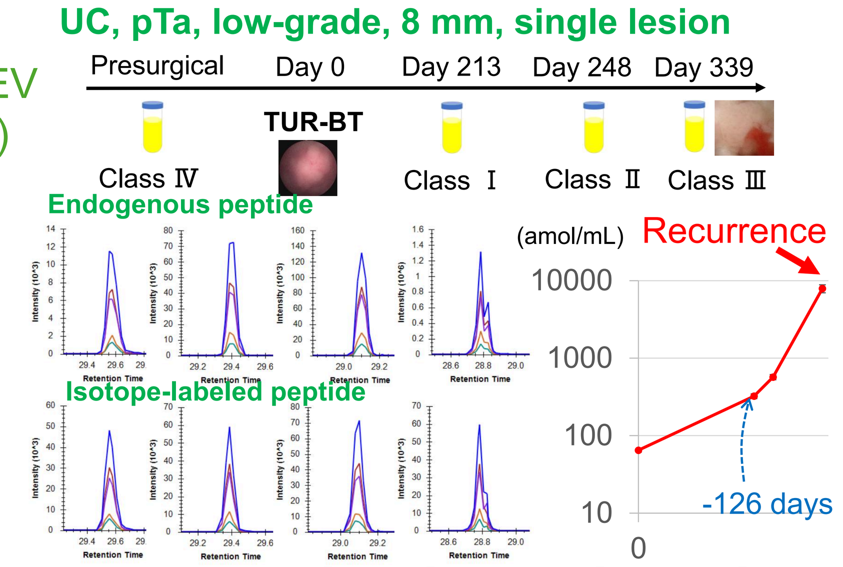

Number of identified mutant proteins in each patient

Case ID	1	2	3	4	5	6	7	8	9	10	11	12	13	14	15	16	17	18	19	20	21	22	23	24	25	26	27	28
Tissue	20	4	8	0	8	4	5	6	2	25	3	8	0	3	23	3	16	3	5	14	8	3	2	14	6	15	6	7
CTD-EV	15	0	6	0	10	4	4	3	1	19	1	4	0	5	34	6	30	19	9	16	19	6	2	34	9	16	7	11
uEV	1	0	3	0	0	2	1	0	0	2	0	0	0	0	0	0	8	1	0	1	1	2	2	5	2	9	4	1

CONCLUSIONS

We identified mutant proteins arising from cancer-acquired somatic mutations in uEVs. Theoretically, these mutant proteins can be detected only from cancer cells (100% specificity).

Somatic mutations can be identified by a proteogenomics approach using urinary EVs. This is the first report that comprehensively investigates mutant proteins in the liquid biopsy technique.

Detection of mutant proteins from urinary EVs has the potential to be a new strategy for recurrence monitoring, cancer screening, and predicting prognosis.

Mutant proteins can be detected in urinary EVs.

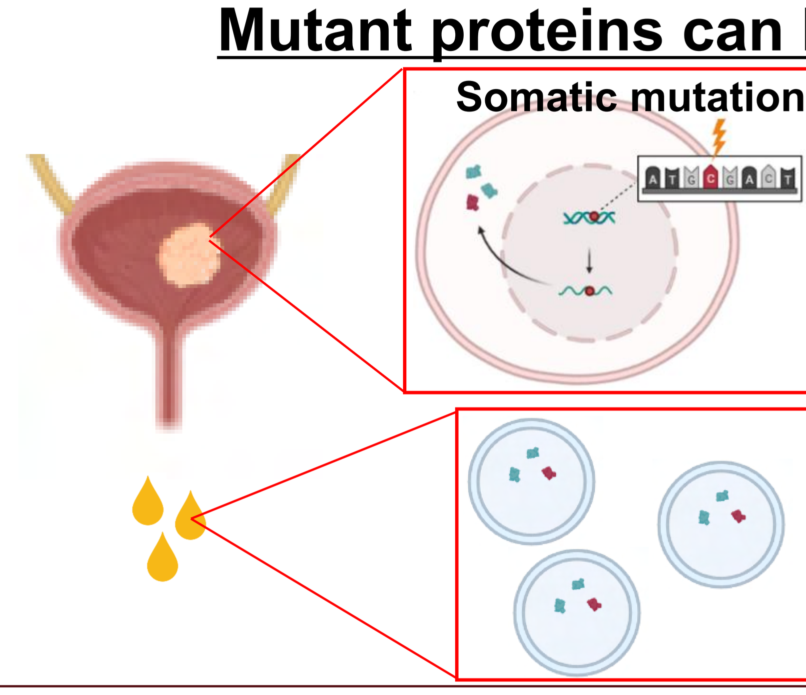

Recurrence monitoring

Cancer screening

De novo sequencing is necessary to predict mutant proteins without genetic information.

Predicting prognosis

Mutant proteins from KRAS proteins are attractive targets.

ACKNOWLEDGEMENTS

This work was supported by a grant from the Project for Promotion of Cancer Research and Therapeutic Evolution (P-PROMOTE) in Japan Agency for Medical Research and Development (AMED) (23ama221412h0002) and Japan Society for the Promotion of Science KAKENHI (24K19683).

DISCLOSURES

I have no conflict of interest to disclose.